UCRL-52185

ELECTROSTATIC BOUNCE MODES IN MIRROR PLASMAS

W. M. Sharp

March 3, 1977

Prepared for U.S. Energy Research & Development Administration under contract No. W-7405-Eng-48

Printed in the United States of America
Available from
National Technical Information Service
U.S. Department of Commerce
5285 Port Royal Road
Springfield, VA 22161
Price: Printed Copy $; Microfiche $3.00

Page Range	Domestic Price	Page Range	Domestic Price
001–025	$ 3.50	326–350	10.00
026–050	4.00	351–375	10.50
051–075	4.50	376–400	10.75
076–100	5.00	401–425	11.00
101–125	5.50	426–450	11.75
126–150	6.00	451–475	12.00
151–175	6.75	476–500	12.50
176–200	7.50	501–525	12.75
201–225	7.75	526–550	13.00
226–250	8.00	551–575	13.50
251–275	9.00	576–600	13.75
276–300	9.25	601–up	*
301–325	9.75		

*Add $2.50 for each additional 100 page increment from 601 to 1,000 pages; add $4.50 for each additional 100 page increment over 1,000 pages.

Distribution Category
UC-20

LAWRENCE LIVERMORE LABORATORY
University of California Livermore, California 94550

UCRL-52185

ELECTROSTATIC BOUNCE MODES IN MIRROR PLASMAS

W. M. Sharp

MS. date: March 2, 1977

CONTENTS

ELECTROSTATIC BOUNCE MODES IN MIRROR PLASMAS

ABSTRACT

Electrostatic bounce modes are standing waves that occur in a mirror plasma when the relative spread in electron bounce frequencies is small. The modes can be destabilized by an ion distribution with a peaked perpendicular energy, and experimental data suggest that this mechanism was the principal cause of instability in certain low-density mirror experimen .

After a review of theoretical work on electrostatic waves in mirror plasmas, a general matrix eigenvalue equation for the wave potential is derived which accounts accurately for electron histories and which includes the ion response. A computer program for calculating the plasma eigenmodes and the associated threshold densities for instability and maximum growth rates is then described.

Strong resonances at harmonics of the electron bounce frequency are found when that frequency is well defined. These resonances result from phase correlations between electrons on successive transits through the plasma, and they are weakened and shifted in frequency when the mirror force and spatial variation of the ambipolar potential spread the bounce frequencies. The effects of plasma and field parameters on the eigenmodes are discussed.

The threshold densities for unstable bounce modes expected in the Baseball I and Baseball II devices are compared with experimental values. The good agreement between theoretical and experimental thresholds in Baseball II makes bounce modes the most likely cause of instabilities in that device. In Baseball I, the most unstable modes expected from the theory have threshold densities consistently below observed values. The discrepancy probably results from idealizations in the model that reduce wave damping.

1. Introduction

DESCRIPTION OF BOUNCE MODES

Electrostatic bounce modes are oscillations of a quasineutral plasma arising from the periodic nature of trapped particle orbits. Whenever the bounce frequencies of particles in confining electrostatic and magnetostatic fields have small spread, then the particles retain substantial phase coherence on successive transits and can support standing wave modes. Electrons in typical hot-ion mirror plasmas meet this coherence requirement because they are confined principally by an electrostatic potential that is approximately quadratic. Bounce modes can have wavelengths comparable with scale lengths of the confining fields, and they are distinguished by the strong plasma response at frequencies near harmonics of the mean bounce frequency.

In certain low-density mirror plasmas, electron bounce modes can be destabilized by the ions. Ions can couple effectively to waves that have frequencies near harmonics of the ion gyrofrequency and have wavelengths perpendicular to the magnetic field that are about twice typical ion gyroradii. If the ion perpendicular energy distribution is peaked, then the free energy associated with this anisotropy can be transferred to the wave, and instability occurs when this ion drive exceeds electron Landau damping.

Unstable electron bounce modes are a likely cause of instabilities observed in low-density mirror experiments. These oscillations occur during plasma buildup by neutral beams when the electron Debye length becomes less than typical ion gyroradii. Since they have frequencies near low harmonics of the ion gyrofrequency, the instabilities have been attributed to electron plasma waves driven by free energy from the anisotropic ion distribution. Even though instability threshold measurements in early devices such as Baseball I (BBI)[1] and Phoenix II[2] seemed to support this model, the validity of early theoretical work on the modes was questionable because the infinite medium equations and Wentzel-Krammer-Brillouin (WKB) formalism used were not generally applicable to these devices. Also, instability threshold densities in the Baseball II (BBII) experiment were well below theoretical predictions and were more strongly affected by changes in plasma length and the buildup procedure than expected from theory.[3] The bounce mode mechanism is a more plausible explanation of the observed instabilities because it is based on a more accurate description of electron motion and requires no assumptions about parallel wavelength or wave reflection.

The present research studies electrostatic bounce modes in typical low-density hot-ion mirror plasmas and examines the adequacy of the proposed instability mechanism as an explanation of BBI and BBII findings.

SURVEY OF PREVIOUS WORK

Plasmas can support a great variety of cooperative electromagnetic disturbances. Growing disturbances, termed instabilities, are of particular concern in confined plasmas because they can disrupt a plasma in times that are short compared with collisional relaxation times. Two broad categories of instabilities are normally distinguished: Magnetohydrodynamic (MHD) instabilities[4] are bulk plasma disturbances with wavelengths much larger than ion gyroradii and frequencies well below the electron plasma frequency or typical ion gyrofrequencies. They gain energy by distorting the plasma as a whole and are suppressed when the plasma is confined in a magnetostatic field near a field strength minimum.[5] Microinstabilities,[6,7] in contrast, gain energy from anisotropies in the velocity space distributions of particles or from inhomogeneities in density and temperature. Since microinstabilities can be localized and often involve only a small group of resonant particles, they normally result in turbulence or enhanced diffusion, rather than in movement of the plasma as a whole. In present mirror experiments using MHD-stable confining fields, microinstabilities impose the principal limit on plasma confinement.

In the theoretical study of microinstabilities, a plasma is conveniently described by time-dependent particle distribution functions $F_\alpha(\underset{\sim}{x},\underset{\sim}{v},t)$ that give the density of particles of each species α at location $\underset{\sim}{x}$ having velocity $\underset{\sim}{v}$. Macroscopic quantities such as number and current densities and mean energy can be obtained as appropriate moments of the distribution functions, and the resulting plasma fields are given by Maxwell's equations. When wave growth occurs on a time scale that is short compared with characteristic collision times, the change in F_α due to collisions may be ignored. Particles then interact only through the macroscopic plasma fields, and F_α can be shown by Liouville's theorem to be constant along particle trajectories. Mathematically, this fact is expressed by the Vlasov equation

$$\frac{d}{dt} F_\alpha(\underset{\sim}{x},\underset{\sim}{v},t) \equiv \left(\frac{\partial}{\partial t} + \underset{\sim}{v} \cdot \frac{\partial}{\partial \underset{\sim}{x}} + \frac{d\underset{\sim}{v}}{dt} \cdot \frac{\partial}{\partial \underset{\sim}{v}}\right) F_\alpha(\underset{\sim}{x},\underset{\sim}{v},t) = 0 \ . \qquad (1)$$

If a magnetostatic field $\underset{\sim}{B}(\underset{\sim}{x})$ is the only external field, then the electric force results entirely from the self-consistent plasma potential $\Phi(\underset{\sim}{x},t)$, and the velocity derivative in Eq. (1) is

$$\frac{d\underset{\sim}{v}}{dt} = \frac{q_\alpha}{m_\alpha}\left[-\underset{\sim}{\nabla}\Phi(\underset{\sim}{x},t) + \frac{\underset{\sim}{v} \times \underset{\sim}{B}(\underset{\sim}{x})}{c}\right] . \tag{2}$$

Here notation summarized in Appendix A is used, and Φ is given by Poisson's equation

$$-\nabla^2\Phi(\underset{\sim}{x},t) = 4\pi \sum_\alpha q_\alpha N_\alpha(\underset{\sim}{x},t) , \tag{3}$$

with the sum taken over all species α and the number density of each species given by

$$N_\alpha(\underset{\sim}{x},t) = N_\alpha(\underset{\sim}{x}_0,t) \int d^3v\, F_\alpha(\underset{\sim}{x},\underset{\sim}{v},t) . \tag{4}$$

In Eq. (4), F_α has been normalized so the velocity integral is unity at an arbitrary point x_0. Whenever the fields seen by a particle over a gyration period are nearly constant, total particle energy $E = m_\alpha v^2 + q_\alpha\Phi$ and magnetic moment $\mu = m_\alpha v_\perp^2 / 2B$ may be treated as constants of the motion,[8] where $v \equiv |\underset{\sim}{v}|$, $B \equiv |\underset{\sim}{B}|$, and $v_\perp \equiv |\underset{\sim}{v} \times \underset{\sim}{B}|/B$. Any time-independent solution of Eq. (1) can then be shown to be a function of E and μ *only*,[5] and a set of such distribution functions for all species together with the corresponding potential Φ satisfying Poisson's equation, Eq. (3), constitutes a self-consistent plasma equilibrium state.

Electrostatic waves, characterized by a time-dependent perturbing potential $\phi(\underset{\sim}{x},t)$, are the main source of microinstabilities when plasma pressure is small compared with the magnetic pressure $B^2/8\pi$.[6] If the equilibrium plasma potential and distribution functions are denoted by $\Phi^0(\underset{\sim}{x})$ and $F_\alpha^0(\underset{\sim}{x},\underset{\sim}{v})$, then a self-consistent set of equations for ϕ is obtained by substituting $F_\alpha(\underset{\sim}{x},\underset{\sim}{v},t) = F_\alpha^0(\underset{\sim}{x},\underset{\sim}{v}) + f_\alpha(\underset{\sim}{x},\underset{\sim}{v},t)$ and $\Phi(\underset{\sim}{x},t) = \Phi^0(\underset{\sim}{x}) + \phi(\underset{\sim}{x},t)$ into Eqs. (1) through (4) and subtracting off the unperturbed expressions. Assuming that ϕ is small enough that products of perturbed quantities are negligible, the following linearized equations result:

$$\frac{df_\alpha}{dt}(\underset{\sim}{x},\underset{\sim}{v},t) = \frac{q_\alpha}{m_\alpha}\nabla\phi(\underset{\sim}{x},\underset{\sim}{v},t)\cdot\frac{\partial F_\alpha^0}{\partial \underset{\sim}{v}}(\underset{\sim}{x},\underset{\sim}{v}) \ , \tag{5}$$

and

$$\nabla^2\phi(\underset{\sim}{x},t) = -4\pi\sum_\alpha q_\alpha n_\alpha(\underset{\sim}{x},t) \ , \tag{6}$$

where the perturbed number density for species α is

$$n_\alpha(\underset{\sim}{x},t) = N_\alpha(\underset{\sim}{x}_0)\int d^3v\ f_\alpha(\underset{\sim}{x},\underset{\sim}{v},t) \ . \tag{7}$$

An expression for f_α in Eq. (7) is found by formally integrating Eq. (5):

$$f_\alpha(\underset{\sim}{x},\underset{\sim}{v},t) = \frac{q_\alpha}{m_\alpha}\int_{-\infty}^{t} dt'\,\nabla\phi[\underset{\sim}{x}_\alpha(t';\underset{\sim}{x},\underset{\sim}{v},t)]\cdot\frac{\partial F_\alpha^0[\underset{\sim}{x}_\alpha(t';\underset{\sim}{x},\underset{\sim}{v},t),\underset{\sim}{v}_\alpha(t';\underset{\sim}{x},\underset{\sim}{v},t)]}{\partial \underset{\sim}{v}} \ . \tag{8}$$

Here $f_\alpha(\underset{\sim}{x},\underset{\sim}{v},t)$ is assumed to vanish as $t \to -\infty$, and in the linear approximation the unperturbed particle trajectories $\underset{\sim}{x}_\alpha(t';\underset{\sim}{x},\underset{\sim}{v},t)$ and $\underset{\sim}{v}_\alpha(t';\underset{\sim}{x},\underset{\sim}{v},t)$ intersecting phase point $(\underset{\sim}{x},\underset{\sim}{v})$ at time t is used in calculating ϕ and F_α^0 at $t' < t$. In principle, Eq. (6) with Eqs. (7) and (8) describe the development of any disturbance so long as f_α and $q_\alpha\phi$ remain small compared respectively with F_α and the unperturbed forces.

The initial work on electrostatic microinstabilities treated waves in unbounded uniform plasmas. The customary approach to examining Vlasov plasmas was developed by Landau[10] and Bernstein[11] and was applied specifically to electrostatic modes by Harris[12,13]: A Fourier-Laplace transform is used to reduce Eq. (6) to an integral equation, and appropriate approximations to electron and ion orbits for $t' < t$ are made to allow the time integral in Eq. (8) to be evaluated. The dispersion equation that results is in general a transcendental relation between the propagation vector $\underset{\sim}{k}$ for a particular plane-wave mode and the frequency ω. Since these plane waves have a space-time dependence $\exp(i\underset{\sim}{k}\cdot\underset{\sim}{x} - i\omega t)$, they grow in time whenever $\gamma \equiv \mathrm{Im}(\omega) > 0$. So long as the fields seen by a particle over a gyroperiod vary slowly enough that E and μ may be considered constant, the orbit in a magnetized plasma is well described by a guiding center approximation. The time-averaged position of guiding center moves mainly along a flux line with in general some

crossfield drift, while the particle gyrates about this center with an angular frequency $\Omega_\alpha = q_\alpha B/m_\alpha c$ and a gyroradius $a_\alpha = v_\perp/\Omega_\alpha$. In a uniformly magnetized plasma, electron and ion guiding centers move with constant velocity along flux lines and have constant gyrofrequencies. The orbit integration in Eq. (8) is readily performed in this case and leads to a dispersion relation[13]

$$1 + \sum_\alpha \frac{\omega_{p\alpha}^2}{|k|^2} \sum_{j=-\infty}^{\infty} \int_{-\infty}^{\infty} d^3v \frac{J_j^2\left(\frac{k_\perp v_\perp}{\Omega_\alpha}\right)}{\omega - k_\parallel v_\parallel - j\Omega_\alpha} \left(\frac{j\Omega_\alpha}{v_\perp}\frac{\partial}{\partial v_\perp} + k_\parallel \frac{\partial}{\partial v_\parallel}\right) F_\alpha^0(v_\perp, v_\parallel) = 0 \ , \qquad (9)$$

where J_j is a Bessel function of the first kind, and $\omega_{p\alpha} = (4\pi N_\alpha q_\alpha^2/m_\alpha)^{1/2}$ is the plasma frequency for species α. Hereafter, subscripts $\parallel$ and $\perp$ denote vector components respectively along and perpendicular to the local magnetostatic field.

In plasmas confined by magnetic fields with open field lines, end losses cause a depletion of regions of velocity space, referred to as loss cones, where for a mirror ratio R, $v_\parallel^2/v_\perp^2 > R - 1$. The resulting anisotropy in the velocity distributions, along with the unavoidable spatial inhomogeneities due to confinement, acts as sources of free energy for the class of instabilities called loss-cone modes. A review of electrostatic microinstabilities by Hall *et al.*[14] showed that ions could couple effectively with an electrostatic wave provided that the perpendicular wavelength is comparable with a_i and the wave frequency is near some gyrofrequency harmonic $j\Omega_i$. In this case, ions drift in phase relative to the wave toward a phase stable point, and near this phase point, ions on average lose energy to the wave when

$$\int_0^\infty \frac{dv_\perp}{v_\perp} \frac{\partial F_i^0(v_\perp, v_\parallel)}{\partial v_\perp} J_j^2\left(\frac{k_\perp v_\perp}{\Omega_i}\right) > 0 \ . \qquad (10)$$

This condition indicates that the perpendicular ion velocity distribution must be nonmonotonic for instability to occur and gives the requirement for a sharply peaked distribution that $k_\perp a_i \geq 1.85$. In addition, Post and Rosenbluth[15] and others[16,17] showed that systems with loss-cone distributions could support instabilities with $|k_\perp| >> |k_\parallel|$ and $\omega \approx j\Omega_i$ even when $k_\perp a_i >> 1$. Although accurate analytic expressions for the plasma densities at which these ion-driven modes should become unstable are somewhat complicated, a simple

estimate based on Eq. (9) was given by Damm et al.[1] For effectively stationary ions, the real part of Eq. (9) reduces in the case $|k_\perp| >> |k_\parallel|$ and $\omega << \Omega_e$ to

$$\frac{\omega^2}{k_\parallel^2} \simeq \frac{\omega_{pe}^2}{k_\perp^2} , \tag{11}$$

Electron Landau damping is accounted for in Eq. (9) by the imaginary contribution from the singularity at $v_\parallel = \omega/k_\parallel$ in the electron velocity integral. Because F_e drops off exponentially with velocity, this damping becomes ineffective when $\omega/k_\parallel$ is significantly greater than the electron thermal velocity V_e. The phase velocity condition

$$\frac{\omega}{k_\parallel} \gtrsim V_e \tag{12}$$

is therefore taken as an approximate requirement for instability, and from Eq. (11) instability occurs at the lowest density when the equality in Eq. (12) holds. Since electrons in a hot-ion mirror plasma are principally confined by the plasma potential Φ, the maximum potential energy barrier along a flux line is comparable to the electron energy $W_e = \frac{1}{2} m_e V_e^2$:

$$\psi_{max} \equiv -e\Phi \simeq W_e . \tag{13}$$

Combining Eqs. (11), (12), and (13) gives an approximate plasma density at the onset of instability. In terms of the dimensionless density parameter $\varepsilon \equiv (\omega_{pi}/\Omega_i)^2$, the minimum density at which instability can occur is

$$\varepsilon_{th} \simeq (k_\perp a_i)^2 \frac{\psi_{max}}{W_i} . \tag{14}$$

To test this model Damm et al. observed that the azimuthal component of $k_\perp$ can have only discrete values because an integral number of wavelengths must fit around a flux surface. For a flux surface with radius r, $k_\perp$ is then given by $k_\perp^2 = k_r^2 + (n/r)^2$, where k_r is the radial k component and n is a perpendicular mode number. The values of $k_\perp$ inferred from measured instability thresholds in the low-density Baseball I experiment were found to have a clear $k_\perp$ mode structure, and when optimum k_r and r were chosen for the data, ε_{th} for each

mode number showed the approximate linear dependence on ψ_{max}/W_i expected from Eq. (14).

Despite the qualitative agreement between theoretical instability predictions and BBI findings, the infinite medium formalism gives an incomplete description of electron-ion microinstabilities in confined plasmas. For a wave with finite $k_\parallel$ to affect plasma stability, it must either grow to appreciable strength during one transit of the plasma or reflect coherently enough at the ends that there is net growth during each transit. To treat such finite plasma effects as reflection, infinite-medium theory is commonly extended by adopting a WKB wave model.[18] When the bulk plasma properties have characteristic lengths that are long compared with a wavelength, a wave potential spatial dependence along a field line of the form

$$\phi(s)\ \exp\left[i\int^{s} ds'\ k_\parallel(s')\right] \tag{15}$$

may be used, with $k_\parallel$ determined at each point by an infinite-medium dispersion equation. Wave attenuation in this model is given by the factor $\exp\{-\int^{s} ds'\ \mathrm{Im}[k_\parallel(s')]\}$, and for reflection to occur the validity condition for a WKB representation[19]

$$\max\left(\frac{1}{k_\parallel^2}\frac{dk_\parallel}{ds}\ ,\ \frac{1}{k_\parallel^3}\frac{d^2k_\parallel}{ds^2}\right) \ll 1 \tag{16}$$

must be violated somewhere along a flux line. Early papers[20,21] suggested that waves generated near the center of a mirror plasma would be effectively Landau damped in the low-density mirror regions, where $\omega_{pe} \to 0$ and $k_\parallel \to \infty$. Berk[19] pointed out that this conclusion applies to a Maxwellian electron distribution, whereas actual distributions have a loss-cone character for electron energies exceeding ψ_{max} and vanish continuously near the loss boundary. His WKB analysis showed that a distribution cutting off abruptly at ψ_{max} leads to wave reflection, while one with a linear energy dependence for $E < \psi_{max}$ causes absorption. A similar treatment by Hamilton and Moir[22] using an analytic Fokker-Planck equation solution for the electron distribution and taking magnetic confinement into account, predicted wave reflection near Baseball I mirror points. Cordey[23] likewise carried out a WKB analysis of longitudinal electrostatic wave reflection in plasmas with a loss-cone ion

distribution and electrons confined either electrostatically or magnetically. He concluded that significant wave attenuation would occur when the magnetic field scale length L_B satisfied $L_B >> a_i V_e / V_i$.

One shortcoming of early work on wave reflection in mirrors was the use of a local dispersion relation obtained from an infinite-medium analysis. A series of papers[24,25,26] pointed out that the closed orbits of mirror-confined particles could add a strongly resonant contribution to the dispersion equation and result in nonlocal reflection of waves. Since all phase information in a collisionless plasma is retained by particles, long-term periodicities in particle motion can lead to regeneration of disturbances damped by phase mixing. Berk and Book[26] gave a clear physical description of the phenomenon: When a group of particles has phase space trajectories with the same bounce frequency ω_b, as they do in a quadratic electrostatic well, then any wave disturbance will be regenerated each time they return to that phase space configuration. The reactive term that this effect adds to the dispersion equation becomes infinite when the wave frequency coincides with an integral multiple of ω_b. Any velocity dependence of ω_b results in exact resonance occurring only for discrete values of $v_{\parallel}$, and the resonant dispersion equation term is replaced by its velocity space average. Nonlocal particle histories continue to make a significant contribution so long as the spread in bounce frequency $\Delta\omega_b = \langle |\omega_b - \langle \omega_b \rangle| \rangle$ is small enough to satisfy

$$\frac{\omega_b^2}{\omega \Delta\omega_b} >> 1 \ . \tag{17}$$

Berk and Book account for these regenerative effects in WKB formalism by including terms in the time integral of the perturbed Vlasov equation representing the accumulated perturbation of the particles on previous transits. This modified procedure gives good agreement with exact treatments for $k_\perp \approx 0$ waves in simple electron plasmas.

WKB formalism fails when wavelengths are comparable with scale lengths of macroscopic plasma or field quantities. An alternate approach to analyzing plasma waves in mirror devices is to directly solve the integral dispersion relation obtained from the perturbed Poisson equation for the normal modes of the system. Cordey[27] used this method to treat unstable electron-ion waves in a plasma confined by a quadratic electrostatic potential. Since he assumed $\omega/\omega_b << 1$ for electrons, bounce-frequency resonances were unimportant, and he

was able to use local expressions for the perturbed distribution functions in an asymptotic series solution of the dispersion equation. A long wavelength mode at the first harmonic of the ion gyrofrequency was found to become unstable at the lowest plasma density, while for constant $k_\perp$ higher threshold modes showed increasing maximum growth rates. When electron-bounce frequency resonances are significant, periodic orbits must be used when integrating the perturbed Vlasov equation for f_e. The several papers using this general method differ mainly in the detail and generality of their plasma models. An early treatment by Weibel[28] considered waves with $k_\perp = 0$ in a one-dimensional Maxwellian electron plasma confined by an infinite quadratically varying electrostatic potential. Particle trajectories in this case are sinusoidal, and when the wave electric field is represented by a Hermite series, the time integral in Eq. (8) can be exactly evaluated. Laplace transforming Poisson's equation then leads to a matrix eigenvalue equation that is solved iteratively. Harker[29] likewise examined parallel modes in a collisionless, one-dimensional electron plasma, but he used a Green's function technique to obtain an integral equation for the perturbed electric field in an arbitrary symmetric confining potential. The equation was specialized to quadratically varying potentials and solved numerically. Equations were derived by Kaufman for normal modes in an unmagnetized one-dimensional plasma[30] and a magnetized cylindrical plasma[31] using a Hamiltonian formalism, but he made no attempt to solve them. Beasley et al.[32] presented a more general analysis of electron-ion instabilities. They considered electrostatically confined Maxwellian electrons coupled to ions by a uniform magnetic field, and the separable ion distribution they used assumed a peaked $v_\perp$ distribution and a Gaussian number density variation along field lines to approximate the velocity and spatial nonuniformities found in mirror devices. Taking the plasma potential to vary quadratically, they expressed f_α as a Fourier series in harmonics of Ω_α and evaluated the coefficients by integrating over gyrophase. Fourier analyzing Poisson's equation over the plasma length then yielded a matrix eigenvalue equation for the Fourier components of the wave potential. This theoretical approach was extended by McCune[33] to slightly nonquadratic potential wells in a treatment of electron Landau damping in mirror plasmas, and Beasley et al.[34] applied the formalism to several loss-cone instabilities. In this work, spatial variation of Ω_i was included in integrating the ion Vlasov equation, and a radial density gradient was incorporated in the electron term to permit analysis of density-driven instabilities such as drift waves[35] and drift-cyclotron loss-cone modes.[36]

DESCRIPTION OF THE PRESENT WORK

Previous papers on electrostatic electron-ion instabilities idealize the plasma or the confining fields for the sake of mathematical tractability. Even the careful treatment by Beasley et al.[34] omits magnetic confinement of electrons and the loss-cone nature of F_e, and the Gaussian number density profile assumed is inconsistent with the unperturbed electron distribution function. Although the model does include important effects like electron bounce resonances and Landau damping, the simplifications limit the predictive value of the theory.

The treatment of electrostatic mirror plasma modes in the present research avoids several of the simplifications of earlier work. A matrix eigenvalue equation formalism similar to that of Beasley et al. is used to find the plasma normal modes, but arbitrary monotonic magnetic and electrostatic fields are allowed, and the distribution functions used are appropriate for a quasi-neutral mirror plasma. Perpendicular density and temperature gradients are neglected because only unstable modes specifically driven by the peaked-ion perpendicular energy distribution are of interest. In addition, the normal modes are calculated from the complete complex eigenvalue equation, whereas earlier work solved only the equation for undamped electron modes.

A derivation of the matrix eigenvalue equation for electrostatic mirror plasma modes is presented in Chapter 2 along with the methods used to solve the equation for marginally stable waves and to calculate instability threshold densities and maximum growth rates. The computer coding to carry out these calculations is also described. The model is used specifically to study normal modes in the parameter ranges where electron bounce resonance effects dominate the plasma response. Chapter 3 summarizes the numerical results. Important characteristics of the eigenmodes and the parametric dependences of instability thresholds and growth rates are discussed first, and then predictions of the model for instabilities in the BBI and BBII devices are compared with experimental values. A final chapter suggests further refinements and extensions of the model.

2. Bounce Mode Formalism

MODEL

Electrostatic bounce modes in a finite mirror plasma are obtained from an appropriate integro-differential eigenvalue equation for the electrostatic potential of small-amplitude waves. This equation is reduced to a matrix eigenvalue equation by Fourier analysis and solved numerically.

The physical situation considered retains important features of typical hot-ion mirror plasmas. Both the magnetic field strength B and electrostatic potential Φ are assumed to be monotonic functions of the distance s along flux lines, cutting off at the endpoints $\pm s_{max}$. Particles which reach either endpoint with a nonzero velocity in the direction of B are considered to escape confinement immediately. In terms of total electron energy E and magnetic moment μ, an appropriate electron distribution function is

$$F_e(E,\mu) = C_e(\mu B_{max} + \psi_{max} - E)\exp(-E/W_e) \quad . \tag{18}$$

This describes a distribution that is approximately thermalized at energies well below the cutoff value $E = \mu B_{max} + \psi_{max}$, but drops linearly to zero near the loss boundaries. Here B_{max} and ψ_{max} are the values of B and electrostatic potential energy $\psi = -e\Phi$ at s_{max}, and the normalization constant C_e is chosen to satisfy

$$N(s) = 4\pi \frac{N_0 B(s)}{m_e^2} \int_0^\infty d\mu \int_{\mu B(s)+\psi(s)}^{\mu B_{max}+\psi_{max}} dE \frac{F_e(E,\mu)}{|v_{e\parallel}(s;\,E,\mu)|} \quad , \tag{19}$$

where $v_{e\parallel} = 2(E - \mu B - \psi)^{1/2}/m_e$ is the parallel electron velocity, and the subscript 0 hereafter labels quantities at s = 0. Appendix B gives the analytic expression for C_e. Since the ions affect electron bounce modes principally by transferring free energy of the distribution to the waves, the anisotropy of the ion distribution rather than the specific form is the main concern guiding the choice of a model distribution function. A form with separable s, $v_\parallel$, and $v_\perp$ dependences like that used by Guest and Dory[16] is selected:

$$F_i(s,v_\parallel,v_\perp) = \frac{N(s)}{N_0} F_\parallel(v_\parallel) F_\perp(v_\perp^2) \quad , \tag{20}$$

where $F_{\parallel}$ and $F_{\perp}$ are unit normalized according to $2\int_0^\infty dv_{\parallel} F_{\parallel} = 1$ and $\pi\int_0^\infty dv_{\perp}^2 F_{\perp} = 1$. Since the equilibrium electron and ion number densities must be nearly equal to maintain quasi-neutrality, the electron expression Eq. (19) with F_e given by Eq. (18) is used for N in Eq. (20). Appendix B gives the analytic N expression. The separable form assumed for F_i is not a solution to the unperturbed Vlasov equation as a correct equilibrium distribution would be, but it permits important simplifications in calculating the ion response without sacrificing significant physical effects. The functions chosen for $F_{\perp}$ model two simple situations: At low density, a plasma decays principally by charge exchange with the background gas. In this case, an initially monoenergetic ion distribution such as that created by neutral-beam injection will remain peaked about some mean value $V_{\perp} \equiv \langle v_{\perp}^2 \rangle^{1/2}$, and a delta function

$$F_{\perp}(v_{\perp}^2) = \frac{1}{\pi}\,\delta(v_{\perp}^2 - V_{\perp}^2) \tag{21}$$

is an appropriate approximation. At higher densities, electron drag and ion-ion collisions can spread the perpendicular distribution during the plasma lifetime. A general broadened distribution

$$F_{\perp}(v_{\perp}^2) = \frac{4}{\pi V_{\perp}^4}\, v_{\perp}^2 \exp\left(-\frac{2v_{\perp}^2}{V_{\perp}^2}\right) \tag{22}$$

is then used. In practice, conditions such as the finite neutral-beam cross section, multiple energy components in the beam, and spreading of the distribution by electron drag and collisions during buildup result in more complicated ion distributions, but the effect of ions on plasma stability is still expected to be between the two extreme cases modeled by Eqs. (21) and (22). For the ion parallel velocity distribution, a Gaussian form

$$F_{\parallel}(v_{\parallel}) = \frac{1}{\pi^{1/2} V_{\parallel}} \exp\left(-\frac{v_{\parallel}^2}{V_{\parallel}^2}\right) \tag{23}$$

is normally chosen, where $V_{\parallel}^2 \equiv \langle v_{\parallel}^2 \rangle$ is the mean squared parallel velocity, and a ratio

$$\frac{V_{\parallel}^2}{V_{\perp}^2} = \frac{2(B_{max} - B_0)}{4B_{max} + B_0}\,, \tag{24}$$

derived in Appendix B for magnetically confined ions, is used.

Several assumptions about the plasma are introduced to simplify the model and to eliminate complicating physical effects:

- The equilibrium B and Φ fields are assumed symmetric about s = 0. It is shown in Appendix C that this choice leads to eigenmodes that are either even or odd functions of s. Even though magnetic field strength in minimum-B mirror fields is not exactly symmetric about the centerplane, the deviation along field lines near the mirror axis is small and should not significantly alter the plasma response.
- The number density and field gradients perpendicular to flux surfaces are ignored, so that finite gyroradius effects and gradient-driven instabilities such as drift waves do not appear. This assumption is justified in low-density plasmas when the ion gyroradius is small compared with characteristic lengths for N and B variation normal to flux surfaces.[35]
- The only azimuthal effect retained is the variation of $k_\perp$ along a field line as the cross section of the flux surface changes. When flux surfaces have approximate axial symmetry, the quantity $k_\perp^2/B$ is nearly independent of s.[37] Neither the fanning of field lines[38] nor the limitation of $k_\perp$ to discrete values resulting from azimuthal periodicity are incorporated into the numerical model. Since these simplifications allow electrostatic disturbances to be treated as plane waves perpendicular to field lines, the resulting wave equation involves only one spatial dimension.
- A pure hydrogenic plasma with H^+ ions only is assumed, and both electron and ions are treated as collisionless.
- A guiding center description of unperturbed particle motion is used for both species: E and μ are considered constant, and orbits are approximated by motion along a guiding flux line plus a circular gyration at the local gyrofrequency Ω_α. This description is acceptable when the variation of B over a gyroperiod is small. It follows that

$$\frac{a_\alpha}{B} \nabla_\perp B << 1$$

and

$$\frac{v_\parallel}{\Omega_\alpha B} \nabla_\parallel B << 1 \qquad (25)$$

must be satisfied for typical particles.

- Long parallel wavelength modes characterized by $k_\perp^2 >> \frac{1}{\phi}\frac{\partial^2\phi}{\partial s^2}$ are sought in particular because only such waves can couple effectively with the ions for the temperatures and magnetic fields found in typical mirror experiments. This choice allows the parallel derivative in the perturbed Poisson equation, Eq. (6), to be neglected for resonant modes. In addition, modes with $k_\perp = 0$ are treated to illustrate bounce resonance phenomena.

With these assumptions, a one-dimensional integral equation is readily derived for the wave potential Φ along a field line. Since E and μ are constants of the unperturbed motion, it is convenient to write the integrand of Eq. (25) as

$$\underset{\sim}{\nabla}\phi(\underset{\sim}{x}'_\alpha,t') \cdot \frac{\partial F_\alpha^0(\underset{\sim}{x}'_\alpha,\underset{\sim}{v}'_\alpha,t')}{\partial \underset{\sim}{v}_\alpha} = m_\alpha \frac{\partial F_\alpha(E,\mu)}{\partial E}\, \underset{\sim}{v}'_\alpha \cdot \underset{\sim}{\nabla}'\phi(\underset{\sim}{x}'_\alpha,t') + \frac{m_\alpha}{B(\underset{\sim}{x}'_\alpha)} \frac{\partial F_\alpha(E,\mu)}{\partial \mu}\, \underset{\sim}{v}'_{\alpha\perp} \cdot \underset{\sim}{\nabla}'\phi(\underset{\sim}{x}'_\alpha,t') \ , \tag{26}$$

where primed quantities are understood to be evaluated at time t' on the unperturbed trajectories $\underset{\sim}{x}_\alpha(t';\underset{\sim}{x},\underset{\sim}{v},t)$. Noting that

$$\frac{d\phi}{dt}(\underset{\sim}{x},t) = \frac{\partial\phi}{\partial t}(\underset{\sim}{x},t) + \underset{\sim}{v}\cdot\underset{\sim}{\nabla}\phi(\underset{\sim}{x},t) \ , \tag{27}$$

the distribution function perturbations from Eq. (25) can be rewritten

$$f_\alpha(\underset{\sim}{x},\underset{\sim}{v},t) = q_\alpha \frac{\partial F_\alpha(E,\mu)}{\partial E} \int_{-\infty}^{t} dt' \left[\frac{d\phi}{dt}(\underset{\sim}{x}'_\alpha,t) - \frac{\partial\phi}{\partial t}(\underset{\sim}{x}'_\alpha,t')\right] + q_\alpha \frac{\partial F_\alpha(E,\mu)}{\partial \mu} \int_{-\infty}^{t} dt' \frac{\underset{\sim}{v}'_{\alpha\perp}\cdot\underset{\sim}{\nabla}\phi(\underset{\sim}{x}'_\alpha,t')}{B(\underset{\sim}{x}'_\alpha)} \ . \tag{28}$$

An appropriate representation for ϕ is

$$\phi(\underset{\sim}{x},t) = \phi(s)\exp(i\underset{\sim}{k}_\perp\cdot\underset{\sim}{x}-i\omega t) \ . \tag{29}$$

This form permits accurate treatment of the wave along a field line but ignores the perpendicular wave structure. Since the gyroradius a_α is nearly constant

over a gyroperiod, both $\underset{\sim}{k}_\perp \cdot \underset{\sim}{x}_\alpha$ and $\underset{\sim}{k}_\perp \cdot \underset{\sim}{v}_\alpha$ can be written in terms of a gyration phase angle θ:

$$\begin{aligned} \underset{\sim}{k}_\perp \cdot \underset{\sim}{x}_\alpha &= k_\perp a_\alpha \sin\theta \ , \\ \underset{\sim}{k}_\perp \cdot \underset{\sim}{v}_\alpha &= k_\perp v_{\alpha\perp} \cos\theta \ . \end{aligned} \tag{30}$$

Here $k_\perp a_\alpha = (2\mu B/m_\alpha)^{1/2} k_\perp/\Omega_\alpha$ is an approximate constant of the motion due to the assumed constancy of μ and $k_\perp^2/B$ along guiding center trajectories. If f_α is written in the form $f_\alpha(s;E,\mu,\theta)\exp(-i\underset{\sim}{k}_\perp \cdot \underset{\sim}{x} - i\omega t)$, then Eq. (28) gives

$$\begin{aligned} f_\alpha^\pm(s;E,\mu,\theta) = q_\alpha \Bigg\{ & \phi(s) \frac{\partial F_\alpha(E,\mu)}{\partial E} + i\omega \frac{\partial F_\alpha(E,\mu)}{\partial E} \\ & \int_{-\infty}^{t} dt' \phi(s_\alpha^{\pm\prime}) \exp[ik_\perp a_\alpha(\sin\theta^{\pm\prime} - \sin\theta) - i\omega(t'-t)] + i \frac{\Omega_\alpha}{B} k_\perp a_\alpha \frac{\partial F_\alpha(E,\mu)}{\partial \mu} \\ & \int_{-\infty}^{t} dt' \cos\theta^{\pm\prime} \phi(s_\alpha^{\pm\prime}) \exp[ik_\perp a_\alpha(\sin\theta^{\pm\prime} - \sin\theta) - i\omega(t'-t)] \Bigg\} , \end{aligned} \tag{31}$$

where the $\pm$ superscripts designate quantities on positive and negative going trajectories at s. Using the Bessel function expansions[39]

$$\exp(ix\sin\theta) = \sum_{j=-\infty}^{\infty} J_j(x)\exp(ij\theta) \tag{32}$$

and

$$\cos\theta \exp(ix\sin\theta) = \sum_{j=-\infty}^{\infty} \frac{2j}{x} J_j(x)\exp(ij\theta) \ , \tag{32}$$

the time integrals in Eq. (31) may be consolidated to give

$$\begin{aligned} f_\alpha^\pm(s;E,\mu,\theta) = q_\alpha \Bigg\{ & \phi(s) \frac{\partial F_\alpha(E,\mu)}{\partial E} + i \sum_{j=-\infty}^{\infty} \sum_{m=-\infty}^{\infty} \left[\omega \frac{\partial F_\alpha(E,\mu)}{\partial E} + \frac{j\Omega_\alpha}{B} \frac{\partial F_\alpha(E,\mu)}{\partial \mu} \right] \\ & J_j(k_\perp a_\alpha) J_m(k_\perp a_\alpha) \int_{-\infty}^{t} dt' \phi(s_\alpha^{\pm\prime}) \exp[i(j-m)\theta] \exp[-ij\Delta^\pm\theta_\alpha(t',t) - i\omega(t'-t)] \Bigg\} , \end{aligned} \tag{33}$$

where

$$\Delta^{\pm}\theta_\alpha(t',t) \equiv \theta - \theta(s_\alpha^{\pm'}) = \int_{t'}^{t} dt''\Omega_\alpha(s_\alpha^{\pm''}) \ . \tag{34}$$

When Eq. (33) is integrated to give the number density perturbations, the integral over θ is nonzero only for $j = m$. The first-order Poisson equation, Eq. (6), then becomes

$$-k_1^2(s)\phi(s) = 4\pi \sum_\alpha q_\alpha n_\alpha(s) \ , \tag{35}$$

with n_α given by

$$\begin{aligned} n_\alpha(s) = \frac{2\pi q_\alpha N_0 B(s)}{m_\alpha^2} \int_0^\infty d\mu \int_{\mu B(s)+\psi(s)}^{\mu B_{max}+\psi_{max}} \frac{1}{|v_{\alpha_\parallel}(s;E,\mu)|} \Bigg\{ 2\frac{\partial F_\alpha(E,\mu)}{\partial E}\phi(s) \\ + i\sum_{j=-\infty}^{\infty}\left[\omega\frac{\partial F_\alpha(E,\mu)}{\partial E} + \frac{j\Omega_\alpha}{B}\frac{\partial F_\alpha(E,\mu)}{\partial \mu}\right] J_j^2(k_\perp a_\alpha) \\ \sum_{\pm}\int_{-\infty}^{t} dt'\,\phi(s_\alpha^{\pm'})\exp[-ij\Delta^{\pm}\theta_\alpha(t',t) - i\omega(t'-t)]\Bigg\} \ . \end{aligned} \tag{36}$$

Physically, the first term of Eq. (36) represents the species response to the local wave potential and is referred to as the adiabatic or nonresonant contribution. Information about the accumulated density perturbation over particle histories is contained in the resonant second term.

To solve Eq. (35), ϕ is first expressed as a Fourier series. Appropriate basis functions for representing ϕ on the interval $|s| < s_{max}$ are sinusoidal functions having the same parity as ϕ and satisfying the boundary condition $\phi(s_{max}) = 0$ implicit in Eq. (35). For odd ϕ, suitable functions are $\sin(m\pi s/s_{max})$ for positive integral m, while the set $\cos\left[\left(m-\frac{1}{2}\right)\pi s/s_{max}\right]$ is used for even ϕ. Both sets are complete for representing functions with the chosen symmetry and boundary value. The notation $sc(k_m s)$ is used hereafter to denote sine and cosine respectively for odd and even eigenfunctions, and k_m is defined

$$k_m \equiv \left(m + \frac{\sigma-1}{2}\right)\frac{\pi}{s_{max}} \ , \tag{37}$$

where σ is zero for even functions and unity for odd. With this notation, the Fourier series representation of ϕ is

$$\phi(s) = \sum_{m=1}^{\infty} \hat{\phi}_m \, sc(k_m s) \ , \tag{38}$$

where $\hat{\phi}_m$ is the Fourier transform of ϕ over the plasma length

$$\hat{\phi}_m \equiv \frac{2}{s_{max}} \int_0^{s_{max}} ds \ \phi(s) \ sc(k_m s) \ . \tag{39}$$

The perturbed Poisson equation, Eq. (35), is reduced to matrix form by first multiplying by B_0/B to remove the s dependence of $k_\perp^2$ and then Fourier transforming both sides in the manner of Eq. (39). The resulting matrix eigenvalue equation is

$$\sum_{m=1}^{\infty} (k_{\perp 0}^2 \lambda_{De0}^2 \, \delta_{mn} - R_{mn}^e - R_{mn}^i) \, \hat{\phi}_m = 0 \ , \tag{40}$$

where the response matrix R_{mn}^α for either species is

$$R_{mn}^\alpha = 8\pi \, q_\alpha \frac{\lambda_{De0}^2}{s_{max}} \int_0^{s_{max}} ds \ \hat{n}_m^\alpha(s) \ sc(k_n s) \ , \tag{41}$$

with

$$\hat{n}_m^\alpha(s) = 2\pi \frac{q_\alpha N_0 B_0}{m_\alpha^2} \int_0^\infty d\mu \int_{\mu B(s)+\psi(s)}^{\mu B_{max}+\psi_{max}} \frac{dE}{|v_{\alpha_\parallel}(s;E,\mu)|} \left\{ 2 \frac{\partial F_\alpha(E,\mu)}{\partial E} \, sc(k_m s) \right.$$

$$+ i \sum_{j=-\infty}^{\infty} \left[\omega \frac{\partial F_\alpha(E,\mu)}{\partial E} + \frac{j\Omega_\alpha}{B} \frac{\partial F_\alpha(E,\mu)}{\partial \mu} \right] J_j^2(k_\perp a_\alpha)$$

$$\left. \sum_{\pm} \int_{-\infty}^{t} dt' \, sc(k_m s_\alpha^\pm) \exp[-ij\Delta^\pm \theta_\alpha(t',t) - i\omega(t'-t)] \right\} . \tag{42}$$

Here the electron Debye length at the centerplane $\lambda_{De0} = (V_e^2/2\omega_{pe0}^2)^{1/2}$ has been introduced as a scaling factor to give a dimensionless eigenvalue $\lambda \equiv (k_{\perp 0}\lambda_{De0})^2$.

An equation analogous to Eq. (40) for parallel modes is derived by retaining the parallel derivative in the first-order Poisson equation, Eq. (6), while setting $k_\perp = 0$. Substituting the Fourier series, Eq. (38), for ϕ in the expression for n_α and again Fourier transforming Poisson's equation then leads to the eigenvalue equation

$$\sum_{m=1}^{\infty} \left(k_m^2 \lambda_{De0}^2 \delta_{mn} - R_{mn}^e - R_{mn}^i\right) \hat{\phi}_m = 0 \ . \tag{43}$$

A dimensionless eigenvalue equation with the same form as Eq. (40) is obtained by multiplying Eq. (43) by $(k_m s_{max})^{-2} \delta_{mn}$ and symmetrizing:

$$\sum_{m=1}^{\infty} \left[\frac{\lambda_{De0}^2}{s_{max}^2} \delta_{mn} - \frac{1}{2s_{max}^2}\left(\frac{1}{k_m^2} + \frac{1}{k_n^2}\right)\left(R_{mn}^e + R_{mn}^i\right)\right] \hat{\phi}_m = 0 \ . \tag{44}$$

The real eigenvalues $(\lambda_{De0}/s_{max})^2$ of Eq. (44) then determine for a device of length s_{max} the plasma densities at which parallel electrostatic modes satisfying the $\phi(s_{max}) = 0$ boundary condition can be supported.

For either finite $k_\perp$ modes or $k_\perp = 0$ modes, two forms of the appropriate matrix equation are used to determine the spatial profile and stability of the eigenmodes: An approximate form retaining only the real part of the electron response matrix is acceptable when electron Landau damping and the ion response are negligibly weak. In this case, these small effects are treated as perturbations of the undamped electron response in analyzing plasma stability. Otherwise, the damping term and the ion contribution must be retained when solving for eigenmodes, and the plasma density at marginal stability is determined by requiring that ω and $k_\perp$ for the modes be real. In either case, the matrices are truncated by discarding elements with indices above some maximum value M, and the remaining finite matrix eigenvalue equation is solved numerically. Maximum growth rates for waves with real $k_\perp$ are found by a perturbation procedure at low plasma densities and by direct search at higher densities.

DERIVATION OF THE ELECTRON RESPONSE MATRIX

Since mirror plasma bounce modes depend on electrons retaining phase coherence longer than a half bounce period, accurate trajectories must be used

in the electron orbit integral in Eq. (42). Orbits of adiabatic electrons are in general periodic with a velocity-dependent period ω_b given by the integral

$$\frac{\pi}{2\omega_b(E,\mu)} = \int_0^{s_{max}} \frac{ds}{|v_{e\parallel}(s;E,\mu)|} \ . \tag{45}$$

The perturbed potential along an electron trajectory is likewise periodic, and it is conveniently represented by a Fourier series in harmonics of ω_b. This representation gives a time dependence that can be exactly integrated and leads to an integral expression for R^e_{mn} that is suitable for numerical evaluation.

For electrons, the $\hat{n}^e_m$ expression, Eq. (42), is simplified by observing that typical electron gyroradii are small compared with perpendicular wavelengths for modes of interest. For a wave to gain energy from the ion distribution, most ions must satisfy the condition[14] $k_\perp a_i \geq 1.85$, and since

$$\frac{a_e}{a_i} \sim \left(\frac{m_e}{m_i}\frac{W_e}{W_i}\right)^{1/2} << 1 \ , \tag{46}$$

the Bessel function argument in Eq. (42) is small enough for modes of interest to permit a small argument expansion of J_j:[40]

$$J_0(k_\perp a_e) \approx 1$$

$$J_j(k_\perp a_e) \approx \frac{1}{j!}\left(\frac{k_\perp a_e}{2}\right)^j \quad \text{for } j > 0 \ . \tag{47}$$

Only the $j = 0$ term then contributes significantly to the sum in Eq. (42), and the expression reduces to

$$\hat{n}^e_m(s) = -\frac{2\pi e N_0 B_0}{m_e^2} \int_0^\infty d\mu \int_{\mu B(s)+\psi(s)}^{\mu B_{max}+\psi_{max}} dE \frac{1}{|v_{e\parallel}(s;E,\mu)|}\frac{\partial F_e(E,\mu)}{\partial E}\left[2\,sc(k_m s) + i\omega\int_{-\infty}^{t} dt' \left(sc[k_m s^+_e(t';E,\mu,t)] + sc[k_m s^-_e(t';E,\mu,t)]\right)\exp[-i\omega(t'-t)]\right] , \tag{48}$$

where both positive and negative going trajectories coincide with s when $t' = t$.

In terms of a trajectory $s_e(t;E,\mu)$ that satisfies the conditions $s_e(0;E,\mu) = 0$ and $v_{e\parallel}(0;E,\mu) > 0$, the trajectories in Eq. (48) may be written

$$\begin{aligned} s_e^+(t';E,\mu,t) &= s_e(t'-t_0;E,\mu) \\ s_e^-(t';E,\mu t) &= s_e(2t-t'-t_0;E,\mu) \ , \end{aligned} \tag{49}$$

where t_0 is the last time at which $s_e^+(t';E,\mu,t)$ crosses $s = 0$. Explicitly,

$$t_0(s;E,\mu) = t - \int_0^s \frac{ds'}{|v_{e\parallel}(s';E,\mu)|} \ . \tag{50}$$

Since $s_e(t;E,\mu)$ is an odd function of time, $sc(k_m s)$ along that path has the same symmetry in time as in position and so may be represented by an appropriate sine or cosine series of the form

$$sc[k_m s_e(t;E,\mu)] = \sum_{\ell=0}^{\infty} T_{\ell m}(E,\mu)\ sc[(2\ell+\sigma)\omega_b(E,\mu)t] \ , \tag{51}$$

where

$$T_{\ell m}(E,\mu) = \frac{4\omega_b(E,\mu)}{\pi} \int_0^{\pi/2\omega_b(E,\mu)} dt'\ sc[(2\ell+\sigma)\omega_b(E,\mu)t']\ sc[k_m s_e(t';E,\mu)] \ . \tag{52}$$

When $sc(k_m s_e^{\pm})$ in Eq. (48) are replaced by appropriate Fourier series using Eqs. (49) and (51), the time integral can be exactly evaluated:

$$\begin{aligned} &\int_{-\infty}^{t} dt' \left(sc[k_m s_e^+(t';E,\mu,t)] + sc[k_m s_e^-(t';E,\mu,t)] \right) \exp[-i\omega(t'-t)] \\ &\quad = \sum_{\ell=0}^{\infty} T_{\ell m}(E,\mu) \int_{-\infty}^{0} d\tau' \Big(sc[(2\ell+\sigma)\omega_b(E,\mu)(t-t_0+\tau)] + sc[(2\ell+\sigma)\omega_b(E,\mu) \\ &\qquad (t-t_0-\tau)] \Big) \exp(-i\omega\tau) \\ &\quad = 2i\omega \sum_{\ell=0}^{\infty} \frac{T_{\ell m}(E,\mu) sc[(2\ell+\sigma)\omega_b(E,\mu)(t-t_0)]}{\omega^2 - (2\ell+\sigma)^2 \omega_b^2(E,\mu)} \ . \end{aligned} \tag{53}$$

With Eq. (53), the $\hat{n}^e_m$ expression, Eq. (48), becomes

$$\hat{n}^e_m(s) = -\frac{4\pi e N_0 B_0}{m_e^2} \int_0^\infty d\mu \int_{\mu B(s)+\psi(s)}^{\mu B_{max}+\psi_{max}} dE \frac{1}{|v_{e\parallel}(s;E,\mu)|} \frac{\partial F_e(E,\mu)}{\partial E}$$

$$\times \left[sc(k_m s) - \sum_{\ell=0}^{\infty} \frac{\omega^2 T_{\ell m}(E,\mu)\, sc[2\ell+\sigma)\omega_b(E,\mu)(t-t_0)]}{\omega^2 - (2\ell+\sigma)^2 \omega_b^2(E,\mu)} \right] . \qquad (54)$$

The spatial integral, Eq. (41), giving R^e_{mn} is then rewritten using the relation

$$\int_0^{s_{max}} ds \int_0^\infty d\mu \int_{\mu B(s)+\psi(s)}^{\mu B_{max}+\psi_{max}} dE \frac{\mathcal{F}(s;E,\mu)}{|v_{e\parallel}(s;E,\mu)|} = \int_0^\infty d\mu \int_{\mu B_0}^{\mu B_{max}+\psi_{max}} dE$$

$$\int_0^{\pi/2\omega_b(E,\mu)} dt' \mathcal{F}[s_e(t';E,\mu);E,\mu] , \qquad (55)$$

where $\mathcal{F}$ represents an arbitrary continuous integrand. The final expression for the response matrix is

$$R^e_{mn} = \frac{\pi^2 v_e^2 B_0}{m_e s_{max}} \int_0^\infty d\mu \int_{\mu B_0}^{\mu B_{max}+\psi_{max}} dE \frac{1}{\omega_b(E,\mu)} \frac{\partial F_e(E,\mu)}{\partial E}$$

$$\left[S_{mn}(E,\mu) - \sum_{\ell=0}^{\infty} \frac{\omega^2}{\omega^2 - (2\ell+\sigma)^2 \omega_b^2(E,\mu)} T_{\ell m}(E,\mu) T_{\ell n}(E,\mu) \right] . \qquad (56)$$

Here the definition

$$S_{mn}(E,\mu) \equiv \frac{4\omega_b(E,\mu)}{\pi} \int_0^{\pi/2\omega_b(E,\mu)} dt' sc[k_m s_e(t';E,\mu)] sc[k_n s_e(t';E,\mu)] \qquad (57)$$

has been introduced, and Eqs. (50) and (52) have been used to reduce the second bracketed term.

The response matrix, Eq. (56), is put into a form better suited for numerical evaluation by a change of variables. When restoring forces on a particle vary linearly with position as in quadratically varying ψ and B fields, then particles execute simple harmonic motion

$$s(t;E,\mu) = s_t(E,\mu)\,\sin[\omega_b(E,\mu)t] \tag{58}$$

with turning point s_t defined by

$$E - \mu B(s_t) - \psi(s_t) = 0\ . \tag{59}$$

In Appendix D it is shown that the orbit integrals S_{mn} and T_{lm} in this case are expressible in terms of Bessel functions of the first kind depending only on s_t:

$$S_{mn}(E,\mu) = J_0[(k_m-k_n)s_t(E,\mu)] + (-1)^\sigma\, J_0[(k_m+k_n)s_t(E,\mu)] \tag{60}$$

$$T_{lm}(E,\mu) = 2\, J_{2\ell+\sigma}\,[k_m s_t(E,\mu)]\ . \tag{61}$$

Except in strongly anharmonic fields, Eqs. (60) and (61) remain good approximations of the orbit integrals, and when s_t is held constant, S_{mn} and T_{lm} are in general weakly dependent functions of μ. Because of this slow variation, it is convenient to rewrite the R^e_{mn} expression, Eq. (56), using the dimensionless turning point $\chi = s_t/s_{max}$ instead of E:

$$R^e_{mn} = \frac{\pi^2 V_e^2 B_0}{m_e s_{max}} \int_0^1 d\chi \int_0^\infty d\mu\, \frac{1}{\omega_b(\chi,\mu)} \frac{\partial F_e(\chi,\mu)}{\partial \chi} \left[S_{mn}(\chi,\mu) - \sum_{\ell=0}^{\infty} \frac{\omega^2}{\omega^2 - (2\ell+\sigma)^2\omega_b^2(\chi,\mu)}\, T_{lm}(\chi,\mu\quad T_{ln}(\chi,\mu) \right]\ , \tag{62}$$

where all functions of χ are obtained from E-dependent forms by the substitution $E = \mu B(\chi s_{max}) + \psi(\chi s_{max})$.

Since the strongest μ dependence of the integrand in Eq. (62) arises from F_e and from the resonant factor multiplying T_{lm}, a useful approximate expression for R^e_{mn} is obtained by using the Bessel function forms, Eqs. (60) and (61), for S_{mn} and T_{lm} and factoring them outside the μ integration

$$R^e_{mn} \approx \frac{\pi^2 V_e^2 B_0}{m_e s_{max}} \int_0^1 d\chi \left[\left(J_0[(\bar{k}_m-\bar{k}_n)\chi] + (-1)^\sigma J_0[(\bar{k}_m+\bar{k}_n)\chi] \right) I_1(\chi) - 4 \sum_{\ell=0}^{\infty} J_{2\ell+\sigma}(\bar{k}_m\chi) J_{2\ell+\sigma}(\bar{k}_n\chi) I_2(\chi) \right]\ , \tag{63}$$

where the μ integrals I_1 and I_2 are defined

$$I_1(\chi) = \int_0^\infty d\mu \, \frac{1}{\omega_b(\chi,\mu)} \frac{\partial F_e(\chi,\mu)}{\partial \chi} \quad , \tag{64}$$

and

$$I_2(\chi) = \int_0^\infty d\mu \, \frac{1}{\omega_b(\chi,\mu)} \frac{\omega^2}{\omega^2 - (2\ell+\sigma)^2} \frac{}{\omega_b^2(\chi,\mu)} \frac{\partial F_e(\chi,\mu)}{\partial \chi} \quad , \tag{65}$$

and $\bar{k}_m = k_m s_{max} = \left(m + \sigma \frac{1}{2}\right)\pi$ is the dimensionless parallel wave number for Fourier modes. The R^e_{mn} expression, Eq. (63), is exact for quadratically varying equilibrium fields and closely approximates Eq. (62) except for strongly anharmonic B or ψ.

For the special case of electrons in a uniform magnetic field confined by a quadratic electrostatic potential $\psi(s) = \psi_{max} s^2/s^2_{max}$, the bounce frequency from (D15) of Appendix D is

$$\omega_{b0} = \left(\frac{2}{m_e} \frac{\psi_{max}}{s^2_{max}}\right)^{1/2} \tag{66}$$

for all particles. The R^e_{mn} expression, Eq. (63), then reduces to

$$R^e_{mn} \approx \frac{\pi^2 v_e^4}{2\omega_{b0} s_{max}} \int_0^1 d\chi \, \frac{\partial \hat{F}_e(\chi)}{\partial \chi} \left[J_0[(\bar{k}_m - \bar{k}_n)\chi] + (-1)^\sigma J_0[(\bar{k}_m + \bar{k}_n)\chi] \right.$$
$$\left. -4 \sum_{\ell=0}^{\infty} \frac{\omega^2}{\omega^2 - (2\ell+\sigma)^2 \omega_{b0}^2} J_{2\ell+\sigma}(\bar{k}_m\chi) J_{2\ell+\sigma}(\bar{k}_n\chi) \right] \quad , \tag{67}$$

where

$$\hat{F}_e(\chi) \equiv \frac{B_0}{W_e} \int_0^\infty d\mu \, F_e(\chi,\mu) \quad . \tag{68}$$

In particular, Eq. (68) gives

$$\hat{F}_e(\chi) = C_e \psi_{max}(1-\chi^2) \exp\left(-\frac{\psi_{max}\chi^2}{W_e}\right) \tag{69}$$

for the cutoff Maxwellian distribution, Eq. (18).

DERIVATION OF THE ION RESPONSE MATRIX

The assumption that the ion distribution function is separable in $v_\parallel$ and $v_\perp$ makes it convenient to rewrite the perturbed number density integral in terms of the velocity components. Introducing the identities

$$dv_\parallel dv_\perp^2 = \frac{2B}{m_i v_\parallel} dE d\mu \tag{70}$$

$$\frac{\partial F_i}{\partial E} = \frac{1}{m_i v_\parallel} \frac{\partial F_i}{\partial v_\parallel} \tag{71}$$

and

$$\frac{\partial F_i}{\partial \mu} = \frac{B}{m_i} \left(- \frac{1}{v_\parallel} \frac{\partial F_i}{\partial v_\parallel} + 2 \frac{\partial F_i}{\partial v_i^2} \right), \tag{72}$$

the $\hat{n}_{mn}^i$ expression, Eq. (42), becomes

$$\hat{n}_{mn}^i(s) = \frac{2\pi q_i N_0}{m_i} \frac{B_0}{B(s)} \int_{v_{\perp \min}(s)}^{\infty} dv_\perp^2 \int_0^{v_{\parallel \max}(s)} dv_\parallel \left[\frac{1}{v_\parallel} \frac{\partial F_i}{\partial v_\parallel}(s, v_\parallel, v_\perp) \right] sc(k_m s)$$

$$+ \sum_{j=-\infty}^{\infty} \left[\frac{\omega - j\Omega_i(s)}{2v_\parallel} \frac{\partial F_i}{\partial v_\parallel}(s, v_\parallel, v_\perp) + j\Omega_i(s) \frac{\partial F_i}{\partial v_\perp^2}(s, v_\parallel, v_\perp) \right]$$

$$J_j^2 \left(\frac{k_\perp v_\perp}{\Omega_i} \right) I_{jm}(s, v_\parallel, v_\perp) \Bigg\} \tag{73}$$

where

$$v_{\perp \min}(s) = \left[\frac{2\psi(s)}{m_i} \right]^{1/2},$$

$$v_{\parallel \min}(s) = \left[v_\perp^2 \left(\frac{B_{max}}{B(s)} - 1 \right) + \frac{2}{m_i} \left(\psi_{max} - \psi(s) \right) \right]^{1/2},$$

and

$$I_{jm}(s,v_\parallel,v_\perp) = i \sum_{\pm} \int_{-\infty}^{t} dt' \; sc[k_m s_i^{\pm}(t';v_\parallel,v_\perp,t)] \exp[ij\Delta\theta_i^{\pm}(t',t)-i\omega(t'-t)]. \quad (74)$$

The $\hat{n}_{mn}^{i}$ expression is simplified by noting that magnetic confinement causes a relative spread in ion bounce frequencies $\Delta\omega_b/\langle\omega_b\rangle \sim 1$, so the condition for ion bounce resonances, Eq. (17), is not satisfied for frequencies near electron bounce harmonics. The phase factor in I_{lm} is then rapidly oscillating except near points of stationary phase $\omega \sim j\Omega_i$. This fact makes I_{jm} resonant at these frequencies, and the integral is approximately proportional to

$$\frac{2(\omega - j\Omega_i)}{(\omega - j\Omega_i)^2 - (k_m v_\parallel)^2} .$$

For the long parallel wavelength modes considered $\frac{k_m v_\parallel}{\Omega_i} \leq \frac{k_m v_\perp}{\Omega_i} \frac{B_{max}-B_0}{B_0} << \frac{k_\perp v_\perp}{\Omega_i}$ so all $\partial F_i/\partial v_\perp^2$ terms in the j summation are smaller than the resonant term by a factor of order $(k_m v_\parallel)^2/[j\Omega_i(\omega-j\Omega_i)]$. Also, since $1 = J_0^2 + 2\sum_{j=1}^{\infty} J_j^2$, the nonresonant $\partial F_i/\partial v_\parallel$ term in $\hat{n}_m^i$ is nearly cancelled by the $\partial F_i/\partial v_\parallel$ terms in the summation, leaving a term comparable in magnitude with the nonresonant $\partial F_i/\partial v_\perp^2$ terms. So long as the resonance condition $\omega \sim j\Omega_i$ is satisfied in the system for some j, these nonresonant terms may be neglected, and Eq. (73) reduces to

$$\hat{n}_m^i(s) \approx 2\pi \frac{q_i j\Omega_{i0} N(s)}{m_i} \int_{v_{\perp min}(s)}^{\infty} dv_\perp^2 \; \frac{\partial F_i(v_\perp^2)}{\partial} \; J_j^2\left(\frac{k_\perp v_\perp}{\Omega_i}\right)$$

$$\int_0^{v_{\parallel max}(s)} dv_\parallel \; F_\parallel(v_\parallel) \; I_{jm}(s,v_\parallel,v_\perp) . \quad (75)$$

An ion phase mixing time τ may be defined as the interval in which particle orbit perturbations lose phase coherence. Approximately τ is the duration $|t - t'|$ that makes the I_{jm} phase factor, averaged over the distribution, equal to unity.[19] Evaluating the phase factor for a quadratic B field with $\omega = j\Omega_{i0}$ gives $\tau = (3/v_\parallel^2\Delta\Omega)^{1/3}$ as an upper bound, where $\Delta\Omega \equiv \frac{1}{2}(\partial^2\Omega/\partial s^2)_{s=0}$.

Since the corresponding phase mixing length $V_{\parallel}\tau$ is smaller than the characteristic length for changes in $v_{\parallel}$, $L_v \equiv \left\langle \frac{1}{v_{\parallel}} \frac{\partial v_{\parallel}}{\partial s} \right\rangle^{-1} \sim \left(\frac{1}{B} \frac{dB}{ds} \right)^{-1}$, by a factor of order $(V_{\parallel}/V_e)^{1/3}$, a straight orbit approximation treating $v_{\parallel}$ as constant along trajectories is justified and removes the $v_{\perp}$ dependence of I_{jm}. The further observation that $W_i >> W_e \sim \psi_{max}$ in a hot-ion plasma allows all ψ terms in Eq. (75) to be discarded, and since the Gaussian $v_{\parallel}$ distribution, Eq. (23) is small for $v_{\parallel}^2 >> v_{\parallel}^2 \sim V_{\perp}^2(B_{max} - B_0)/B_0$, the $v_{\parallel}$ integration may be extended to infinity with little error. These approximations separate the $v_{\parallel}$ and $v_{\perp}$ integrals. Introducing the function

$$\Lambda_j \equiv \pi V_{\perp}^2 \int_0^{\infty} dv_{\perp}^2 \frac{\partial F_{\perp}(v_{\perp}^2)}{\partial v_{\perp}^2} \quad J_j^2 \left(\frac{k_{\perp} v_{\perp}}{\Omega_i} \right) \tag{76}$$

then allows the ion response matrix expression from Eq. (41) to be written

$$R_{mn}^i \approx \frac{2j\Lambda_j \Omega_{i0}}{s_{max}} \frac{W_e}{W_i} \int_0^{s_{max}} ds \frac{N(s)}{N_0} sc(k_n s) \int_0^{\infty} dv_{\parallel} F_{\parallel}(v_{\parallel}) I_{jm}(s, v_{\parallel}) , \tag{77}$$

where

$$I_{jm}(s, v_{\parallel}) = i \sum_{\pm} \int_{-\infty}^{t} dt' \; sc[k_m(s \pm v_{\parallel}(t'-t))] \exp[ij\Delta\theta_i^{\pm}(t', t) - i\omega(t'-t)] . \tag{78}$$

A simple approximation of R_{mn}^i follows from treating Ω_i as a constant over a phase mixing length. In this case,

$$\Delta\theta^{\pm}(t', t) \approx \Omega_i(s)(t-t') , \tag{79}$$

and the integral, Eq. (23), is readily evaluated

$$I_{jm}(s, v_{\parallel}) \approx -sc(k_m s) \sum_{\pm} \frac{1}{\omega - j\Omega_i(s) + k_m v_{\parallel}} . \tag{80}$$

For a Gaussian $F_{\parallel}$, the $v_{\parallel}$ integral in Eq. (77) may be rewritten in terms of the plasma dispersion function

$$R_{mn}^i \approx \frac{2j \Lambda_j \Omega_{i0}}{k_m V_{\parallel} s_{max}} \frac{W_e}{W_i} \int_0^{s_{max}} ds \frac{N(s)}{N_0} sc(k_m s) sc(k_n s) Z\left[\frac{\omega - j\Omega_i(s)}{k_n V_{\parallel}} \right] , \tag{81}$$

where Z for a complex argument z is defined[42]

$$Z(z) = \frac{1}{\pi^{1/2}} \int_{-\infty}^{\infty} dy \, \frac{\exp(-y^2)}{y - z} \, . \tag{82}$$

Symmetrizing Eq. (81) then gives

$$R^i_{mn} \approx -\frac{j\Lambda_i \Omega_{i0}}{s_{max}} \frac{W_e}{W_i} \int_0^{s_{max}} ds \, \frac{N(s)}{N_0} \, sc(k_m s) \, sc(k_n s)$$
$$\times \left\{ \frac{1}{k_m V_{\parallel}} \, Z\left[\frac{\omega - j\Omega_i(s)}{k_m V_{\parallel}}\right] + \frac{1}{k_n V_{\parallel}} \, Z\left[\frac{\omega - j\Omega_i(s)}{k_n V_{\parallel}}\right] \right\} . \tag{83}$$

The local approximation, Eq. (83), is invalid near s = 0 because the phase mixing length increases as $\nabla_{\parallel} B$ vanishes. When $\omega \approx j\Omega_{i0}$, Ω_i is expanded in a Taylor series about s = 0, and the quadratic term is retained in calculating $\Delta^{\pm}\theta$. Again treating $v_{\parallel}$ as constant then gives, instead of Eq. (79),

$$\Delta\theta^{\pm}(t',t) \approx \int_{t'}^{t} dt'' \, \{\Omega_{i0} + \Delta\Omega \, [s^2 \pm 2v_{\parallel} s(t''-t) + v_{\parallel}^2 (t''-t)^2]\}$$
$$\approx (t'-t) \, \{\Omega_{i0} + \Delta\Omega \, [s^2 \mp v_{\parallel} s(t'-t) + \frac{v_{\parallel}^2}{3} (t'-t)^2]\} \, . \tag{84}$$

Since $t' - t \approx -|s' - s|/v_{\parallel}$, the phase change $\Delta\theta^{\pm}$ may be written as a function of positions s and s':

$$\Delta\theta^{\pm}(s',s) \approx \frac{|s'-s|}{v_{\parallel}} \left\{ \Omega_{i0} + \Delta\Omega \left[\left(\frac{s'+s}{2} \right)^2 + \frac{(s'-s)^2}{12} \right] \right\} . \tag{85}$$

With Eq. (85), the time integration in Eq. (78), is rewritten as a spatial integral

$$I_{jm}(s,v_{\parallel}) = i \int_{-s_{max}}^{s_{max}} \frac{ds'}{v_{\parallel}} \, sc(k_m s') \, \exp\left[i \, \frac{|s'-s|}{v_{\parallel}} \left\{ \omega - j\Omega_{i0} - j\Delta\Omega \left[\left(\frac{s'+s}{2} \right)^2 + \frac{(s'-s)^2}{12} \right] \right\} \right] , \tag{86}$$

and for a Gaussian parallel distribution the R^i_{mn} expression, Eq. (77), becomes

$$R^i_{mn} \approx i\pi^{-1/2} \frac{j\Lambda_j \Omega_{i0}}{V_u s_{max}} \frac{W_e}{W_i} \int_0^\infty \frac{dv_u}{v_u} \exp\left(\frac{-v_u^2}{V_u^2}\right) \int_{-s_{max}}^{s_{max}} ds \frac{N(s)}{N_0} sc(k_n s) \int_{-s_{max}}^{s_{max}} ds' sc(k_m s')$$

$$\times \exp\left[i \frac{|s - s'|}{v_u} \left\{\omega - j\Omega_{i0} - j\Delta\Omega \left[\left(\frac{s'+s}{2}\right)^2 + \frac{(s'-s)^2}{12}\right]\right\}\right]. \qquad (87)$$

The unspecified functional form of N makes simplification of Eq. (87) difficult. However, an expression for R^i_{mn} that is suitable when $\omega \approx j\Omega_{i0}$ is obtained by taking $N/N_0 = 1$. This approximation is allowable because it uses the correct number density where the ions couple most strongly with the wave. The resulting expression is reduced to a single complex integral similar to that of Beasley et al.[34] or Baldwin et al.[37] by first introducing the variables

$$x = \frac{s' + s}{2}$$

and (88)

$$y = s' - s \ .$$

In terms of x and y, the product $sc(k_m s')sc(k_n s)$ is written

$$sc(k_m s')sc(k_n s) = \frac{1}{4} \left\{\exp\left[i(k_m - k_n)x + i\left(\frac{k_m + k_n}{2}\right) y\right]\right.$$
$$+ (-1)^\sigma \exp\left[i(k_m + k_n)x + i\left(\frac{k_m - k_n}{2}\right) y\right] + \exp\left[-i(k_m - k_n)x - i\left(\frac{k_m + k_n}{2}\right) y\right]$$
$$\left. + (-1)^\sigma \exp\left[-i(k_m + k_n)x - i\left(\frac{k_m - k_n}{2}\right) y\right]\right\} \ . \qquad (89)$$

Each term in Eq. (89) has the form $\exp(ik_1 x + ik_2 y)$ and makes a contribution to R^i_{mn} given formally by

$$I(k_1, k_2, j) = \frac{1}{\pi V_u} \int_0^\infty \frac{dv_u}{v_u} \exp\left(-\frac{v_u^2}{V_u^2}\right) \int_{-\infty}^{\infty} dx \int_{-\infty}^{\infty} dy$$
$$\exp\left[ik_1 x + ik_2 y + \frac{i|y|}{v_u} (C_1 - C_2 x^2 - C_3 y^2)\right] \qquad (90)$$

where the coefficients in the exponential argument are $C_1 = \omega - j\Omega_i$, $C_2 = j\Delta\Omega$, $C_3 = j\Delta\Omega/12$, and the former integration limits $\pm s_{max}$ have been extended to $\pm\infty$ to simplify evaluation. By using the relation

$$\int_{-\infty}^{\infty} dx\, \exp(-\alpha x - \beta x^2) = \left(\frac{\pi}{\beta}\right)^{1/2} \exp\left(\frac{\alpha^2}{4\beta}\right) \tag{91}$$

to carry out the x integration, Eq. (90) becomes

$$I(k_1,k_2,j) = \frac{1}{\pi V_n} \int_0^{\infty} \frac{dv_n}{v_n} \int_{-\infty}^{\infty} dy \left(\frac{\pi v_n}{iC_2|y|}\right)^{1/2} \exp\left(-\frac{v_n^2}{V_n^2}\right) \exp\left[ik_2 y - \frac{k_1^2 v_n}{4iC_2|y|} + \frac{i|y|}{v_n}(C_1 - C_3 y^2)\right] . \tag{92}$$

A second change of variables $z = y/v_n$ results in a v_n integral with the form of Eq. (91), which evaluates to

$$I(k_1,k_2,j) = \frac{1}{\pi V_n} \int_{-\infty}^{\infty} dz \int_0^{\infty} dv_n \left(\frac{\pi}{iC_2|z|}\right)^{1/2} \exp\left(-\frac{v_n^2}{V_n^2}\right) \exp\left[ik_2 v_n z - \frac{k_1^2}{4iC_2|z|} + i|z|(C_1 - C_3 v_n^2 z^2)\right]$$

$$= \int_0^{\infty} dz \frac{\exp\left[iC_1|z| - \frac{k_1^2}{4iC_2|z|} - \frac{k_2^2 V_n^2 z^2}{4(1+iC_3 V_n^2 z^3)}\right]}{(iC_2 z)^{1/2}\,(1+iC_3 V_n^2 z^3)^{1/2}} . \tag{93}$$

Since k_1 and k_2 enter Eq. (93) as squared quantities, the last two terms of Eq. (89) make the same contribution as the first two, and the resulting R_{mn}^i expression is

$$R_{mn}^i \approx \frac{i\pi^{1/2}}{2} \frac{jA_j\Omega_{i0}}{s_{max}} \frac{W_e}{W_i} [I(k_m-k_n, k_m+k_n, j) + (-1)^{\sigma} I(k_m+k_n, k_m-k_n, j)] , \tag{94}$$

with

$$I(k_1,k_2,j) = \int_0^{\infty} dz \frac{\exp\left[i(\omega - j\Omega_{i0})z - \frac{k_1^2}{4ij\Delta\Omega z} - \frac{k_2^2 V_n^2 z^2}{16(1+\frac{ij\Delta\Omega}{12} V_n^2 z^3)}\right]}{(ij\Delta\Omega z)^{1/2}\,(1+\frac{ij\Delta\Omega}{12} V_n^2 z^3)^{1/2}} . \tag{95}$$

The function $I(k_1,k_2,j)$ is evaluated as a contour integral in the complex z plane, with the path chosen to avoid singularities of the integrand.

A single expression for R^i_{mn} suitable when $j\Omega_{i0} \leq \omega < j\Omega_i(s_{max})$ is obtained by combining the local approximation, Eq. (83), and the quasi-local form, Eq. (94). If the resonance point s_{res} is defined by $\omega = j\Omega_i(s_{res})$, then Eq. (94) is valid for any $s_{res} < s_{max}$ provided that $N/N_0 = 1$, and Eq. (83) is acceptably accurate for resonances away from s = 0 for any N/N_0. It follows that setting $N/N_0 = 1$ in Eo. (83) should give a good approximation to Eq. (94) for $s_{res} > 0$. When $s_{res} = 0$, $N/N_0 \approx 1$ at the resonance point, and Eq. (94) is approximately valid. A suitable composite form may therefore be written symbolically as

$$R^i_{mn} \approx R^L_{mn}(N) - R^L_{mn}(1) + R^{QL}_{mn} , \tag{96}$$

where $R^L_{mn}(N)$ is the local approximation given by Eq. (83) using the correct number density, $R^L_{mn}(1)$ is the same integral with the change $N/N_0 \to 1$, and R^{QL}_{mn} is the quasi-local form, Eq. (94). For $s_{res} \approx 0$, the first two terms nearly cancel, while for off-center resonances the second two terms do. R^i_{mn} is then approximately R^{QL}_{mn} for $s_{res} \approx 0$ and R^L_{mn} elsewhere as desired. Written out explicitly, the hybrid form for R^i_{mn} is

$$R^i_{mn} \approx \frac{j\Lambda_j\Omega_{i0}}{s_{max}} \frac{W_e}{W_i} \left\{ \frac{i\pi 1/2}{2} \left[I(k_m-k_n,k_m+k_n,j) + (-1)^\sigma I(k_m+k_n,k_m-k_n,j) \right] + \left[II(k_m,k_n,j) + II(k_n,k_m,j) \right] \right\} , \tag{97}$$

where

$$II(k_m,k_n,j) \equiv \frac{1}{k_m V_{\parallel}} \int_0^\infty ds \left[\frac{N(s)}{N_0} - 1 \right] sc(k_m s)\, sc(k_n s)\, Z\left[\frac{\omega - j\Omega_i(s)}{k_m V_{\parallel}} \right] . \tag{98}$$

CALCULATION OF MARGINALLY STABLE EIGENMODES

The wave potentials ϕ that solve the integral equation Eq. (35) are the normal electrostatic modes of the bounded plasma, and any wave satisfying the boundary conditions and the requirement for self-consistency can be described as a superpostion of these modes. Modes which are neither damped nor growing are of particular interest because these are destabilized by any increase in plasma density and limit the densities attainable in confinement experiments.

This condition of marginal stability occurs when the transfer of free energy of the ion distribution into wave energy is balanced by the dissipation of wave energy by phase mixing. Mathematically, marginal stability is determined by the condition that the wave frequency ω be real, and the additional constraint that $k_\perp$ for the wave also be real is imposed to maximize ion-wave coupling.

To calculate the marginally stable eigenmodes either exactly or by the perturbation method first requires evaluation of the response matrices. The electron matrix R^e_{mn} is calculated from Eq. (62), with the μ integration carried out first. Since the orbit integrals S_{mn} and T_{lm} are in general weakly dependent on μ when χ is fixed, they are approximated during numerical integration by cubic spline interpolation between relatively few values. When the confining fields vary nearly quadratically with s, the orbit integrals are replaced by their Bessel function approximations, Eqs. (60) and (61), and R^e_{mn} is calculated from the simpler expression, Eq. (63). In either case, the μ integral is evaluated by a standard variable-step numerical integrator using a path along the real axis. When ω is real, the resonant factor becomes singular at μ_ℓ, defined by

$$\omega = (2\ell+\sigma)\ \omega_b(\chi,\mu_\ell)\ . \tag{99}$$

The imaginary contribution to the integral from the singularity is then calculated analytically by formally deforming the contour below the pole in the complex μ plane. For the principal part of the integral, a nonsingular integrand is produced by adding a term to the integrand that cancels the singular integrand at μ_ℓ and is itself analytically integrable. The exact integral of this added term is then subtracted from the numerically evaluated integral of the new nonsingular integrand. When ω is complex, the pole is in the complex μ plane, and integration of the complex integrand using real μ is straightforward. The resulting μ integral is a slowly varying function of χ, so that a standard trapezoidal rule algorithm is used for the χ integration. Appendix E describes this integration procedure in detail. To evaluate the complex integrals in the R^i_{mn} expression, Eq. (97), the same variable-step numerical integrator used for the μ integrals is employed. For the local approximation integral, Eq. (98), a real s path is used, while to evaluate $I(k_1,k_2,j)$ in the quasi-local integral, Eq. (95), a complex z path discussed in Appendix F is chosen that approaches $z = 0$ along the negative imaginary

axis and avoids the singularities at $z = (ij\Delta\Omega\gamma_m^2/12)^{-1/3}$. For the perpendicular ion distributions considered, Λ_j is evaluated analytically in terms of Bessel functions and is found to depend only on $\zeta = (k_{\perp 0}V_{\perp 0}/\Omega_{i0})$. The delta function, Eq. (21) gives

$$\Lambda_j(\zeta) = \frac{\zeta}{2} J_j(\zeta) \left[J_{j+1}(\zeta) - J_{j-1}(\zeta)\right] , \tag{100}$$

and a spread distribution of the form of Eq. (22) leads to

$$\Lambda_j(\zeta) = \frac{\zeta^2}{4} \exp\left(-\frac{\zeta^2}{4}\right)\left[2I_j\left(\frac{\zeta^2}{4}\right) - I_{j+1}\left(\frac{\zeta^2}{4}\right) - I_{j-1}\left(\frac{\zeta^2}{4}\right)\right] . \tag{101}$$

These functions are shown in Fig. 1 for $j = 1$.

To make the matrix equations for ϕ tractable, the summation over bounce-frequency harmonics in the R^e_{mn} expression, Eq. (62) must be truncated, and R^e_{mn} and R^i_{mn} themselves must be limited to finite dimension. An appropriate number of terms L for the summation is estimated from the approximate $\mathrm{Re}(R^e_{mn})$ expressions, Eqs. (D19) and D27), given in Appendix D. To include the most strongly resonant term, L must be no less than the largest integer ℓ_{res} for which $\omega > (2\ell_{res}+\sigma)\omega_{b0}$, and for adequate convergence, the magnitude of the L+1 term should be small compared with the truncated sum. An upper bound on L then follows from the condition

$$(L+1)^2 - \ell_{res}^2 \gg 1 \tag{102}$$

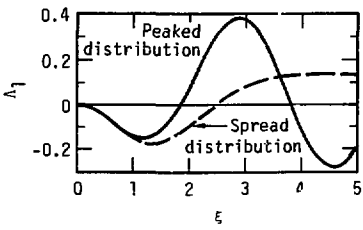

Fig. 1. Λ_1 vs ζ for peaked and spread $v_\perp$ distribution functions.

obtained from the ratio of the L+1 and ℓ_{res} terms. A requirement determining the appropriate matrix dimension M is that the largest elements of R^e_{mn} be retained. From Eqs. (D19) or (D27), this condition is approximately satisfied by the M maximizing

$$\exp\left(-\frac{k_M^2}{2\xi}\right) I_{2\ell_{res}+\sigma}\left(\frac{k_M^2}{2\xi}\right) , \tag{103}$$

where $\xi = (\omega_{b0} s_{max}/V_e)^2$. When $\ell_{res} > 2$, an asymptotic expansion of the Bessel function gives

$$M \sim \frac{(2\xi)^{1/2}}{\pi} (2\ell_{res}+\sigma) \tag{104}$$

as an approximate lower bound on M.

When electron damping due to bounce-frequency spread is sufficiently weak, the real part of the electron response largely determines the character of eigenmodes. This condition occurs in low-density hot-ion mirror plasmas where electrons are confined principally by the ambipolar potential. In this case, a perturbation procedure treating $\mathrm{Im}(R^e_{mn})$ and R^i_{mn} as first order quantities is used to calculate ϕ and the instability threshold densities. Zeroth order eigenfunctions ϕ^0 with Fourier coefficients $\hat{\phi}^0$ satisfying

$$\sum_{m=1}^{\infty} [k_{\perp 0}^2 \lambda_{De0}^2 \, s_{mn} - \mathrm{Re}(R^e_{mn})] \, \hat{\phi}^0_m = 0 \tag{105}$$

for real ω are considered the marginally stable modes for finite $k_\perp$, and because the matrix is real, all positive nondegenerate eigenvalues $\lambda = (k_{\perp 0}\lambda_{De0})^2$ meet the requirement that $k_\perp$ be real. The analytic R^i_{mn} expression, Eq. (D43), in Appendix D indicates that $\mathrm{Re}(R^i_{mn})$ and $\mathrm{Im}(R^i_{mn})$ are of the same order, and at marginal stability the full eigenvalue equation, Eq. (40), gives the first-order condition

$$\sum_{m=1}^{\infty} \sum_{n=1}^{\infty} [\mathrm{Im}(R^e_{mn}) + \mathrm{Im}(R^i_{mn})] \, \hat{\phi}^0_m \, \hat{\phi}^0_n = 0 \, . \tag{106}$$

All terms treated as first order consequently have similar magnitude, and neglecting them in zeroth order is permissible whenever

$$\frac{\left|\sum_{m=1}^{\infty}\sum_{n=1}^{\infty} \mathrm{Im}(R^{e}_{mn})\ \hat{\phi}^{0}_{m}\ \hat{\phi}^{0}_{n}\right|}{\lambda \sum_{m=1}^{\infty} (\hat{\phi}^{0}_{m})^{2}} \ll 1 \ . \tag{107}$$

When Eq. (107) is suitably truncated and solved numerically by a package of matrix solution routines,[44] a set of at most M real eigenvalues λ is returned, each with an M dimensional array of Fourier coefficients $\hat{\phi}^{0}_{m}$ for the corresponding eigenfunctions. Any negative eigenvalues are discarded as spurious, and since the eigenvalue equation determines ϕ^{0} only within a constant factor, the eigenfunctions are normalized to unit maximum amplitude.

The instability threshold density for any of the eigenmodes ϕ^{0} is calculated using the first-order relation, Eq. (106). Since Λ_j appears in the R^{i}_{mn} expression, Eq. (97), as an undetermined factor, Eq. (106) is an algebraic equation for the values of Λ_j at marginal stability. If the electron and ion contributions respectively are written as

$$\Gamma^{e} \equiv \sum_{m=1}^{\infty}\sum_{n=1}^{\infty} \mathrm{Im}(R^{e}_{mn})\ \hat{\phi}^{0}_{m}\ \hat{\phi}^{0}_{n} \tag{108}$$

and

$$\Lambda_j \Gamma^{i} \equiv \sum_{m=1}^{\infty}\sum_{n=1}^{\infty} \mathrm{Im}(R^{i}_{mn})\ \hat{\phi}^{0}_{m}\ \hat{\phi}^{0}_{n} \ , \tag{109}$$

this threshold Λ_j value for the particular mode treated is

$$\Lambda_j = \left|\frac{\Gamma^{e}}{\Gamma^{i}}\right| \ . \tag{110}$$

With either of the analytic expressions, Eqs. (100) or (101) for Λ_j, the corresponding Λ_j argument ζ_{th} is found by a quickly converging secant method. Combining this threshold value of ζ with the eigenvalue λ leads to an expression for the value of density parameter $\varepsilon = (\omega_{pi}/\Omega_{i0})^{2}$ at marginal stability:

$$\varepsilon_{th} = \frac{\zeta^{2}_{th}}{2\lambda}\frac{W_e}{W_i} \ . \tag{111}$$

According to Eq. (10), a necessary condition for instability is that Λ_j be greater than zero, and when more than one solution of Eq. (106) exists, ζ_{th} is taken to be the minimum value because this choice gives the lowest threshold density ϵ_{th}. These constraints restrict ζ_{th} to values between the first zero and first maximum of Λ_j. For $j = 1$, this range is 1.85 to 2.89 for a peaked ion $v_\perp$ distribution and 2.49 to 4.27 for ions with a spread in $v_\perp$. If the Λ_j value given by Eq. (110) is greater than the respective maxima $\Lambda_{max} = 0.385$ and $\Lambda_{max} = 0.133$ for the peaked and spread distributions, then the ion drive is insufficient to cause instability at any density, and the particular mode is said to be unconditionally stable.

When the perturbation validity criterion, Eq. (107), is not satisfied, the full complex matrix equation, Eq. (40), must be solved. Since the eigenvalues are in general complex, an iterative procedure is used to find the value of Λ_j for which $k_\perp$ for a particular eigenmode is real: Λ_j is increased stepwise from zero, and the eigenvalues are recalculated with the new R^i_{mn} until $\mathrm{Im}(k_\perp)$ for the mode changes sign. A secant method is then used to find the desired Λ_j value. The mode is unconditionally stable if the real $k_\perp$ condition cannot be satisfied for $0 < \Lambda_j \leq \Lambda_{max}$. When a marginally stable eigenmode is found, the corresponding ϵ_{th} value is calculated from Λ_j just as in the perturbation treatment.

Since modes with the lowest threshold densities determine plasma stability in mirror experiments, the parameters j and Ω_{i0} in R^i_{mn} are normally chosen to maximize Γ^i. According to the analytic approximation, Eq. (D43), R^i_{mn} increases slowly with j while ζ at the first zero crossing of Λ_j increases directly. Waves that couple to the first gyrofrequency harmonic therefore have the lowest instability threshold densities, and these $j = 1$ modes are the ones examined most thoroughly. The ion centerplane gyrofrequency Ω_{i0} is chosen so that the ion resonance point s_{res} occurs where ion interaction with the wave is strongest. Even eigenfunctions usually have maximum amplitude at $s = 0$. Since density also peaks at the centerplane, the strongest interaction is expected there, and s_{res} is taken to be zero. For odd eigenmodes $s_{res} > 0$, and the imaginary perturbed ion density according to Eq. (83) is approximately proportional to

$$\left| \frac{N(s)\,\phi^2(s)}{\frac{\partial \Omega_i(s)}{\partial s}} \right|_{s=s_{res}} \tag{112}$$

In this case, the electron eigenfunctions ϕ^0 are first found by solving Eq. (105), and then s_{res} is taken to be the position at which $N|\phi^0|^2/s$ is maximum. The resonant gyrofrequency is then $\Omega_{i0} \approx \omega B_0/B(s_{res})$. Also, it is clear from Eq. (111) that modes with the largest λ values become unstable at the lowest densities due to the restrictions on ζ_{th}. For a particular frequency, therefore, ε_{th} is normally calculated only for the modes having the largest real positive eigenvalues.

CALCULATION OF MAXIMUM INSTABILITY GROWTH RATES

At densities above the instability threshold, a wave grows exponentially in time with a growth rate $\gamma \equiv \mathrm{Im}(\omega)$. Although γ is not readily determined experimentally and is modified by nonlinear effects as the wave amplitude becomes measurably large, the observed time for a wave to grow to detectable amplitude should exceed $10\gamma_{max}^{-1}$, where γ_{max} is the maximum growth rate for a particular mode.

Maximum growth rates are calculated in two ways. If the criterion, Eq. (107), for a perturbation treatment of the eigenvalue equation is satisfied, then γ_{max} is estimated by a perturbation method based on the analyticity of $k_{\perp 0}$ as a function of complex ω. The function Λ_j in the R_{mn}^i expression, Eq. (97), is set to Λ_{max} to maximize ion-wave coupling, and the complex eigenvalue equation, Eq. (40), is then solved with real ω, giving in general complex $k_{\perp 0}$ values. In a linear approximation, the imaginary shift in ω required to $\mathrm{Im}(k_{\perp 0})$ for a mode to zero is given by the Taylor expansion

$$0 \approx \mathrm{Im}(k_{\perp 0}) + \left(\frac{\partial[\mathrm{Im}(k_{\perp 0})]}{\partial[\mathrm{Im}(\omega)]}\right)\gamma \ . \tag{113}$$

Using the Cauchy-Riemann equation

$$\frac{\partial[\mathrm{Im}(k_{\perp 0})]}{\partial[\mathrm{Im}(\omega)]} = \frac{\partial[\mathrm{Re}(k_{\perp 0})]}{\partial[\mathrm{Re}(\omega)]} \ ,$$

Eq. (113) is manipulated to give

$$\gamma \approx -\left(\frac{\partial[\mathrm{Re}(k_{\perp 0})]}{\partial[\mathrm{Re}(\omega)]}\right)^{-1} \mathrm{Im}(k_{\perp 0}) \ . \tag{114}$$

Since the derivative in Eq. (114) is constant to first order for a change $i\gamma$ in ω, it is convenient to evaluate it by finite differences at $\mathrm{Im}(k_{\perp 0}) = 0$.

When Eq. (107) is not satisfied, the maximum growth rate is found by a simple search procedure: Using a complex ω in the full matrix equation, Eq. (40), γ is increased stepwise until the $\mathrm{Im}(k_{i0}) = 0$ condition cannot be satisfied by any $\Lambda_j \leq \Lambda_{max}$. A Taylor expansion akin to Eq. (113) is then used to estimate the maximum γ for which the condition can be met with an allowed Λ_j value.

DESCRIPTION OF COMPUTER PROGRAMS

A family of computer codes is used to determine the form and stability of electrostatic bounce modes in the model plasma considered. The programs share the same overall logic, but differ in the approximations employed and in the handling of stored data.

Figure 2 shows the code organization schematically. To allow easy testing and alteration, calculation of each required function is performed in a separate subroutine. These routines are arranged hierarchically: The control program MIRROR reads the plasma and numerical parameters, calculates required dimensionless parameters, and assigns bulk storage space. The response matrices R^e_{mn} and R^i_{mn} are calculated respectively by RESPONSE1 and RESPONSE2. The first of these performs the trapezoidal χ integration of Eq. (62), with the μ integral and orbit integrals S_{mn} and T_{lm} each calculated in separate subroutines. RESPONSE2 calculates the point of strongest ion-wave interaction s_{res} from the appropriate electron eigenfunction, chooses the corresponding $j\Omega_{i0}$, and calls subroutines which carry out the two complex integrations in Eq. (97). The response matrices are then passed to subroutine THRESHOLD, which finds the value of Λ_j for marginal stability and calculates the corresponding threshold density ϵ_{th}. The subprogram makes repeated use of the real and complex matrix eigenvalue equation solution routines EIGEN1 and EIGEN2, and then calls subroutine COLLATE to plot the marginally stable eigenfunctions. The final major routine GROWTHRATE finds γ_{max} either by the perturbation technique of the preceding section or by incrementing γ_{max} and repeating the entire solution procedure until a real k_{i0} mode cannot be calculated. These principal routines use a library of utility subroutines that perform required numerical integrations and evaluate special functions.

All versions of MIRROR use bulk memory and approximations to improve speed. Since the orbit integrals S_{mn} and T_{lm} are independent of ω and the distribution functions, redundant calculation is avoided by evaluating the integrals once at points on a (χ,μ) grid using the algorithm discussed in Appendix F. In subsequent runs with the same unperturbed fields, the values

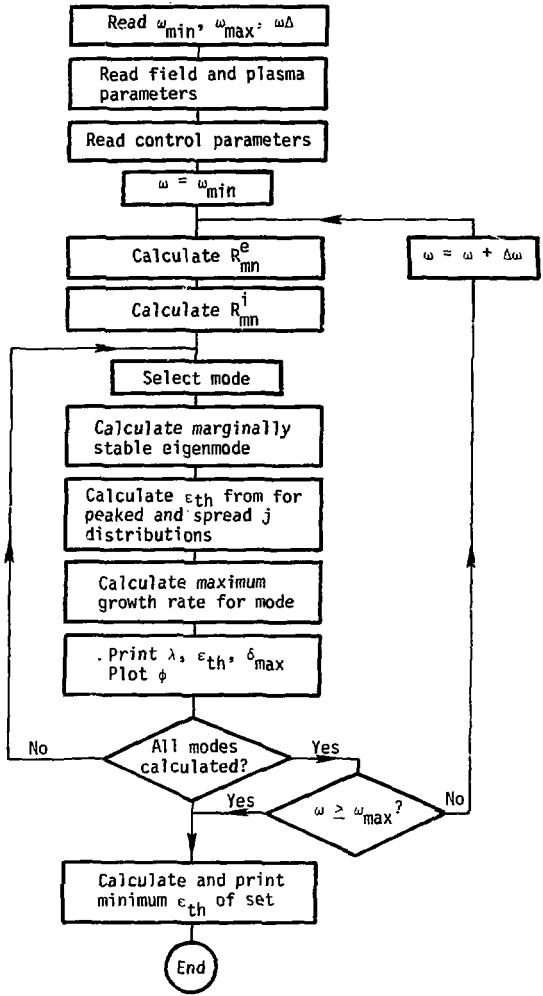

Fig. 2. Organization of the computer code MIRROR.

are recalled as needed, and intermediate values required for numerical integration over μ are approximated by cubic spline interpolation. When the fields are nearly quadratic, further economy is achieved by using the Bessel function approximations, Eqs. (60) and (61), for S_{mn} and T_{lm} because the Bessel functions are generated by an efficient recursion relation procedure and are independent of μ. Other forms of MIRROR either solve only the electron eigenmode problem, Eq. (105), or use the analytic approximations of Appendix D for the response matrices.

Each subroutine used has been extensively checked for accuracy. Where comparison with analytic results is possible, as with the F_e normalization constant and the Bessel function forms of S_{mn} and T_{lm} for quadratic fields, then agreement is exact to within computational error. In limiting cases, the response matrices approach the various analytic approximations in Appendix D, and the values are found to be effectively unchanged by halving integration step sizes. The results are insensitive also to increases in the number of time and space Fourier modes used above the minimum L and M values discussed earlier. The fact that different versions of MIRROR give results that agree within error tolerances for the same problem despite different integration algorithms indicates the absence of significant blunders.

3. Properties of Bounce Modes

EIGENVALUES AND EIGENFUNCTIONS

Important features of bounce-mode behavior are seen in the response of electrons confined only by a quadratic potential

$$\psi(s) = \psi_{max} \frac{s^2}{s_{max}^2} \quad . \tag{115}$$

This idealized plasma shows especially strong bounce resonance effects because all electrons, according to Eq. (D15) of Appendix D, have bounce frequency

$$\omega_{b0} = \left(\frac{2}{m_e} \frac{\psi_{max}}{s_{max}^2} \right)^{1/2} \quad . \tag{116}$$

Even though this case omits the response of ions to the wave and the mirror force on electrons, it illustrates the underlying bounce-mode mechanism, and certain results can be directly compared with earlier work.

Quadratic well eigenmodes with $k_\perp = 0$ are studied by solving Eq. (44) with R^e_{mn} given by Eq. (67) and R^i_{mn} neglected. For each real frequency ω, a finite set of real eigenvalues $\lambda^2_{De0}/s^2_{max}$ is found for odd and even ϕ, and consequently, a plasma with a particular density and length can support parallel bounce modes only at discrete eigenfrequencies. Figure 3 shows the three largest eigenvalues for a quadratic potential with $\psi_{max} = 4.5\ W_e$ over a range of frequencies. The strongly resonant behavior near alternative bounce-frequency harmonics is characteristic of bounce modes and arises because electrons at a particular position always encounter the same wave phase on each transit whenever $\omega = (2\ell+\sigma)\omega_{b0}$. Orbit perturbations on successive passes then add and give a large plasma response for arbitrarily small wave fields. With frequencies above exact resonance, the shift of wave phase that occurs each transit causes some cancellation of earlier perturbations and a consequent weakening of the plasma response. The even and odd modes with the largest respective eigenvalues, referred to hereafter as the principal modes, have obviously different frequency dependence. Since the sum in the electron response matrix expression, Eq. (62), includes a nonresonant $\ell = 0$ term when ϕ is even, the principal eigenvalue remains relatively large at frequencies away from resonance, and the mode persists even at frequencies below the $\omega = 2\omega_{b0}$ resonance. For odd eigenfunctions, only resonant terms appear in the R^e_{mn} summation, so the plasma response drops off rapidly away from the resonances at $\omega = (2\ell+\sigma)\omega_{b0}$. For $\omega > \omega_{b0}$, the odd eigenvalues found by the present treatment closely match the results reported by Harker[29] and by Weibel[28] for Maxwellian electrons in infinite quadratic potential wells. For lower frequencies, Harker claims to find odd eigenmodes on isolated frequency intervals, but since a thorough examination of low-frequency cases with the present method finds no odd solutions, it seems likely that Harker's $\omega < \omega_{b0}$ modes are artifacts resulting from numerical inaccuracies. Weibel treats even modes also, but he finds no mode comparable to the principal mode of Fig. 3(a). This discrepancy results from the choice of boundary conditions. Since Weibel studies an infinite one-dimensional system with no boundary currents, a long wavelength even mode is inadmissible because it would violate charge conservation, whereas the bounded system considered here allows wall currents.

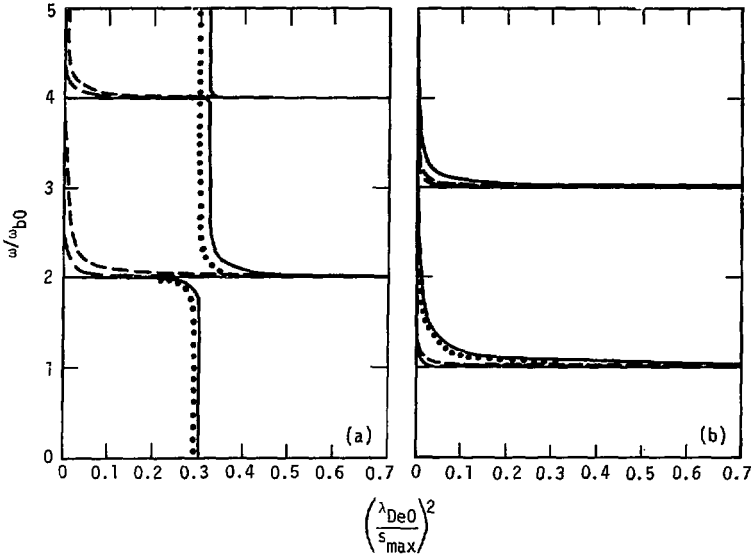

Fig. 3. Eigenvalues for $k_\perp = 0$ electron modes when $B_{max}/B_0 = 1.0$ and $\xi = 4.5$. Dotted lines are analytic approximations: (a) even modes, (b) odd modes.

Finite $k_\perp$ modes are examined by solving the eigenvalue equation, Eq. (105), with the same electron response matrix, Eq. (67), used for the parallel modes. Again, a finite set of eigenvalues $\lambda = k_{\perp 0}^2 \lambda_{De0}^2$ is in general found for each real frequency, but this constraint limits $k_{\perp 0}$ rather than ω to discrete values when density and length are fixed. The three largest eigenvalues for a $\psi_{max} = 4.5\ W_e$ quadratic potential, shown in Fig. 4, have a pattern of resonances similar to the $k_\perp = 0$ modes. The main qualitative differences are expected from the eigenvalue equations treated: Whereas the parallel-mode equation, Eq. (44), is dominated by the m = n = 1 matrix element due to the $\bar{k}_m^{-2} + \bar{k}_n^{-2})$ factor multiplying R^e_{mn}, matrix elements for the higher-mode numbers are larger in Eq. (67) and broaden the $\omega = (2\ell+\sigma)\omega_{b0}$ resonances appreciably.

For electron modes in a finite quadratic potential well, the physical parameter $\xi = \omega_{b0}^2 s_{max}^2 / v_e^2$ reduces to ψ_{max}/W_e and fully characterizes the system. This quantity determines the energy at which the electron distribution is cut

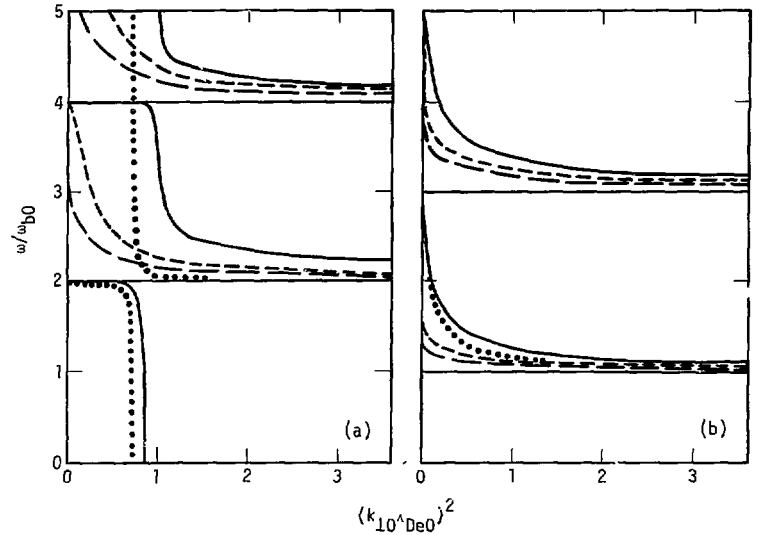

Fig. 4. Eigenvalues for finite $k_\perp$ electron modes when $B_{max}/B_0 = 1.0$ and $\xi = 4.5$. Dotted lines are analytic approximations: (a) even modes, (b) odd modes.

off, and as $\xi \to \infty$ the R^e_{mn} expression approaches the form for Maxwellian electrons in an unbounded potential well. The value $\xi = 4.5$ used for the eigenvalues in Figs. 3 and 4 is a typical value found in Fokker-Planck studies of mirror devices. Figures 5 and 6 show how the principal parallel and finite $k_\perp$ eigenvalues change with ξ. The decreasing sensitivity of eigenvalues to changes in maximum potential for $\xi > 2$ is expected because 78% of the electrons in a Maxwellian distribution have energies below $2W_e$ and are unaffected by variations of ψ_{max}. The increase in minimum eigenvalues found for the principal even modes as ξ is reduced arises mainly from the lowered bounce frequency and consequently greater nonresonant interaction of particles with the wave.

The principal qualitative features of quadratic-well eigenvalues are seen in simple analytic solutions of Eqs. (44) and (105). When $\xi > 2$, the response matrix R^e_{mn} for Maxwellian electrons in a finite quadratic potential is shown in Appendix D to be approximately

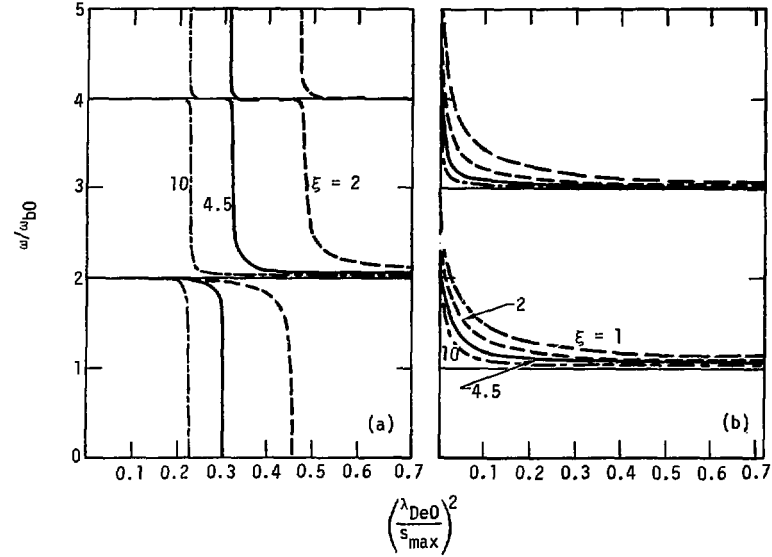

Fig. 5. Variation of principal $k_\perp = 0$ electron mode eigenvalues with ξ when $B_{max}/B_0 = 1.0$: (a) even modes, (b) odd modes.

$$R^e_{mn} \approx -\frac{1}{2}\left(\frac{\pi}{\xi}\right)^{1/2}\left\{\exp\left[-\frac{(\bar{k}_m-\bar{k}_n)^2}{4\xi}\right]+(-1)^\sigma\exp\left[-\frac{(\bar{k}_m+\bar{k}_n)^2}{4\xi}\right]\right.$$

$$\left.-4\exp\left(-\frac{\bar{k}_m^2+\bar{k}_n^2}{4\xi}\right)\sum_{\ell=0}^{\infty}\frac{\omega^2}{\omega^2-(2\ell+\sigma)^2\omega_{b0}^2}\,I_{2\ell+\sigma}\left(\frac{\bar{k}_m\bar{k}_n}{2\xi}\right)\right\}. \qquad (117)$$

For parallel modes, the $m = n = 1$ matrix element in Eq. (44) is dominant, and if only this element is retained, the principal even eigenvalue is estimated by

$$\frac{\lambda_{De0}^2}{s_{max}^2} \approx \frac{2}{\pi^{3/2}\xi^{1/2}}\left\{4\exp\left(-\frac{\pi^2}{8\xi}\right)\left[I_0\left(\frac{\pi^2}{8\xi}\right)+\frac{\omega^2}{\omega^2-(2\ell_{res})^2\omega_{b0}^2}\,I_{2\ell_{res}}\left(\frac{\pi^2}{8\xi}\right)\right]\right.$$

$$\left.-\exp\left(-\frac{\pi^2}{4\xi}\right)-1\right\}. \qquad (118)$$

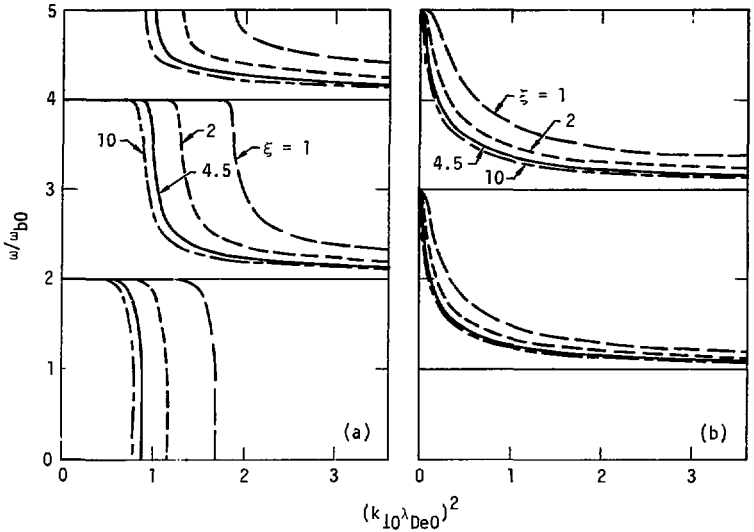

Fig. 6. Variation of principal finite $k_\perp$ electron mode eigenvalues with ξ when $B_{max}/B_0 = 1.0$: (a) even modes, (b) odd modes.

Here, ℓ_{res} is the largest integer giving a frequency shift from resonance $\delta_{res} \equiv [\omega - (2\ell_{res}+\sigma)\omega_{b0}]/\omega_{b0}$ greater than zero and identifies the most strongly resonant contribution to the sum in Eq. (117). It is clear from Eq. (118) that the $\ell = 0$ term of the sum leads to a positive nonresonant contribution to the principal even eigenvalue that should persist for $\omega < 2\omega_{b0}$ and scale roughly like $\xi^{-1/2}$. The $k_\perp = 0$ eigenvalue for odd is similarly approximated by

$$\frac{\lambda_{De0}^2}{s_{max}^2} \approx \frac{1}{2\pi^{3/2}\xi^{1/2}} \left[\frac{4\omega^2}{\omega^2 - (2\ell_{res}+1)^2\omega_{b0}^2} \exp\left(-\frac{\pi^2}{2\xi}\right) I_{2\ell_{res}+1}\left(\frac{\pi^2}{2\xi}\right) + \exp\left(-\frac{\pi^2}{\xi}\right) - 1 \right]. \tag{119}$$

Since the nonresonant contribution to this expression is negative, the eigenvalue should decrease toward zero as δ_{res} increases and should become negative and therefore spurious for $\omega < \omega_{b0}$. In both approximate eigenvalue expressions, the $I_{2\ell_{res}+\sigma}$ factor in the resonant term becomes small for $\ell_{res} > 1$, so that resonances at higher are much less pronounced. The analytic approximations

given by Eqs. (118) and (119) are plotted on Fig. 3 as dotted lines. For finite $k_\perp$ modes, the analytic approximations of λ obtained from the $m = n = 1$ term of Eq. (117) are

$$\lambda \approx \frac{1}{2}\left(\frac{\pi}{\xi}\right)^{1/2}\left\{4\exp\left(-\frac{\pi^2}{8\xi}\right)\left[I_0\left(\frac{\pi^2}{8\xi}\right) + \frac{\omega^2}{\omega^2 - (2\ell_{res})^2\omega_{b0}^2} I_{2\ell_{res}}\left(\frac{\pi^2}{8\xi}\right)\right] - \exp\left(-\frac{\pi^2}{4\xi}\right) - 1\right\} \tag{120}$$

for even ϕ and

$$\lambda \approx \frac{1}{2}\left(\frac{\pi}{\xi}\right)^{1/2}\left[\frac{4\omega^2}{\omega^2 - (2\ell_{res}+1)^2\omega_{b0}^2}\exp\left(-\frac{\pi^2}{2\xi}\right) I_{2\ell_{res}+1}\left(\frac{\pi^2}{2\xi}\right) + \exp\left(-\frac{\pi^2}{\xi}\right) - 1\right] \tag{121}$$

for odd ϕ. These functions, shown as dotted lines on Fig. 2, are poorer estimates of the principal eigenvalues than the parallel mode results because the eigenvalue equation, Eq. (105), is not in general dominated by the lowest Fourier modes. It is apparent from the R^e_{mn} expression, Eq. (117), that the largest contribution is from diagonal elements maximizing the $I_{2\ell_{res}+\sigma}$ term. Since the maximum of $\exp(-x)I_p(x)$ is of the order of p^2, the dominant matrix elements should satisfy the relation

$$m = n \sim \frac{(2\xi)^{1/2}}{\pi}(2\ell_{res}+\sigma) + \frac{1-\sigma}{2}\,. \tag{122}$$

The approximations given by Eqs. (120) and (121) therefore omit significant higher mode contributions when $\ell_{res} > 1$ or $\xi > 2$.

Typical eigenfunctions associated with the largest eigenvalues for $k_\perp = 0$ and finite $k_\perp$ modes are presented respectively in Figs. 7 and 8 for $\delta_{res} = 1$. In each instance, eigenfunctions for the principal even and odd modes have the longest parallel wavelengths and are well represented by the first few terms of appropriate Fourier series. Eigenfunctions made up mainly of higher Fourier components have progressively smaller eigenvalues, indicating a weaker electron response to the wave. This decrease of eigenvalues reflects the fact that electron orbit perturbations due to higher Fourier components of a wave oscillate more rapidly and tend to cancel. This effect is evident mathematically in the decrease in orbit integrals S_{mn} and T_{lm} for larger indices.

For parallel modes, the dominance of the m = n = 1 matrix element results in principal odd and even eigenfunctions that are well represented by the lowest Fourier component alone and therefore are effectively independent of δ_{res}. In contrast, finite $k_\perp$ modes have significant contributions from higher Fourier components when δ_{res} is small, and since these result from the resonant term in R^e_{mn}, they become less pronounced as δ_{res} increases. Figure 9 illustrates this shift. At a constant value of δ_{res}, the prominence of higher Fourier components in finite $k_\perp$ eigenfunctions increases with ℓ_{res} and with ξ, as Figs. 10 and 11 show. The dependence on the harmonic number is expected because indices of the dominant matrix elements, determined approximately by Eq. (122), increase linearly with ℓ_{res}. The shift to higher Fourier components with ξ is likewise evident in the linear $\xi^{1/2}$ dependence of Eq. (122) and occurs because as ψ_{max} increases the wave is largely confined to a region in which F_e is appreciable, given approximately by $|s|^2 < 2W_e s^2_{max}/\psi_{max}$.

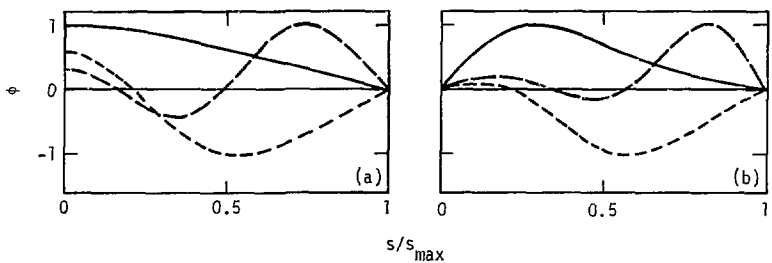

Fig. 7. Eigenfunctions for $k_\perp = 0$ electron modes when $B_{max}/B_0 = 1.0$, $\xi = 4.5$, and $\delta_{res} = 1.0$: (a) even modes, (b) odd modes.

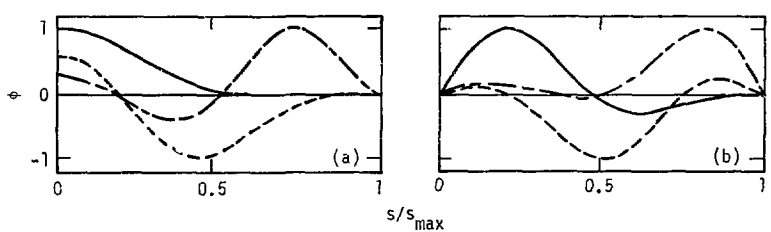

Fig. 8. Eigenfunctions for finite $k_\perp$ electron modes when $B_{max}/B_0 = 1.0$, $\xi = 4.5$, and $\delta_{res} = 1.0$: (a) even modes, (b) odd modes.

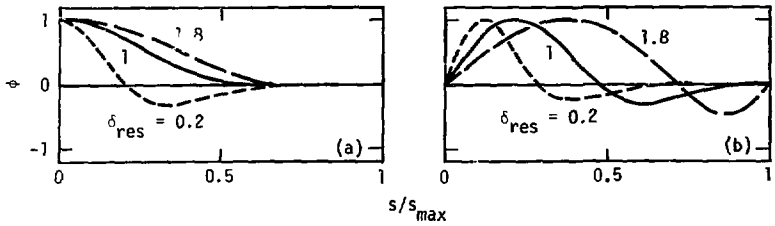

Fig. 9. Variation of principal finite $k_\perp$ electron mode eigenfunctions with δ_{res} when $B_{max}/B_0 = 1.0$ and $\xi = 4.5$: (a) even modes, (b) odd modes.

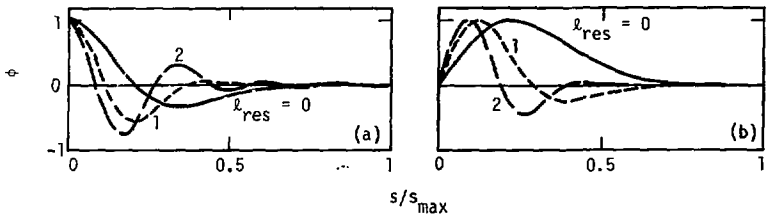

Fig. 10. Variation of principal finite $k_\perp$ electron mode eigenfunctions with ℓ_{res} when $B_{max}/B_0 = 1.0$, $\xi = 4.5$, and $\delta_{res} = 0.2$: (a) even modes, (b) odd modes.

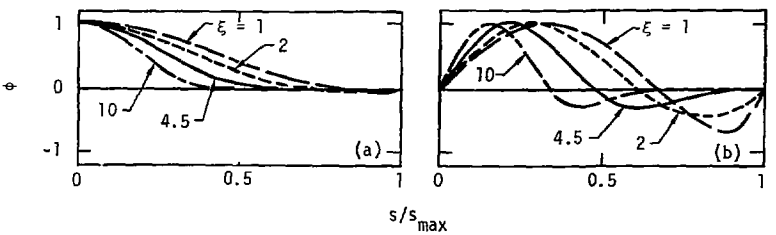

Fig. 11. Variation of principal finite $k_\perp$ electron mode eigenfunctions with ξ when $B_{max}/B_0 = 1.0$ and $\delta_{res} = 1.0$: (a) even modes, (b) odd modes.

For the collisionless plasma considered, both the mirror force $-\mu\nabla_{\parallel}B$ and any anharmonic spatial dependence of ψ spread electron-bounce frequencies. If the potential is a quartic function of s,

$$\psi(s) = A_1 s^2 + A_2 s^4 \ , \tag{123}$$

and B is quadratic,

$$B(s) = B_0 + B_1 s^2 \ , \tag{124}$$

then for $A_1 >> A_2\, s_{max}^2$ the bounce frequency is shown in Appendix D to be approximately

$$\omega_b(\chi,\mu) \approx \left[\frac{2}{m_e}\left(A_1 + \mu B_1 + \frac{3}{2} A_2 \chi^2 s_{max}^2\right)\right]^{1/2} \ . \tag{125}$$

This expression shows how the two spreading mechanisms differ: Whereas B_1 is positive for monotonic mirror fields and always increases ω_b, the χ term can have either sign. The frequency is increased by positive A_2 since the potential well is sharpened, while a negative A_2 reduces ω_b by flattening the central field. Also, the magnitude of the μ term in Eq. (125) is unbounded, but the shift in ω_b^2 from the χ term is no greater than $3A_2 s_{max}^2/m_e$ for cutoff electron distributions. The zero-energy bounce frequency

$$\omega_{b0} \equiv \lim_{\substack{\chi\to 0 \\ \mu\to 0}} \omega_b(\chi,\mu) = \left(\frac{2A_1}{m_e}\right)^{1/2} \tag{126}$$

is the same here as for the pure electrostatic field, Eq. (115), because ω_{b0} is determined by the quadratic potential variation alone. The spread in ω_b has two principal effects on eigenmodes. Since electrons resonate at different frequencies, the strong resonances at harmonics of ω_{b0} found for quadratic ψ are shifted in frequency and broadened. In addition, the electron damping introduced by phase mixing tends to stabilize waves. All $k_\perp = 0$ modes are damped because they do not couple with the ions, and modes with finite $k_\perp$ are normally stabilized at frequencies where damping is strongest. Since these phenomena are independent, it is convenient to separate them by first considering the effect of bounce-frequency spread on undamped electron modes.

Eigenvalues of the electron equation, Eq. (105), for $B_{max}/B_0 = 1.5$, presented in Fig. 12, illustrate the effect of a quadratic mirror field. Since $\omega_b > \omega_{b0}$ for all electrons, the maxima of λ occur at frequencies shifted approximately $\delta_{res} = (2\ell_{res}+\sigma)^2 \langle\mu\rangle B_1/m_e\omega_{b0}$ from the $B_{max}/B_0 = 1$ resonances, and the maxima becomes less pronounced as ℓ_{res} increases because the $(2\ell_{res}+\sigma)^2$ harmonic factor spreads resonances over a wider frequency range. Since $B_1 = (B_{max}-B_0)/s_{max}^2$ for a quadratic B field, increasing B_{max}/B_0 results in greater frequency spread and a weakening of the electron response. The eigenvalue curves in Fig. 13 for several values of B_{max}/B_0 show this behavior. Scaling of these mirror force effects may be estimated from the approximate $\mathrm{Re}(R^e_{mn})$ expression derived in Appendix D:

$$R^e_{mn} \simeq -\frac{1}{2}\left(\frac{\pi}{\xi}\right)^{1/2}\left\{\exp\left[-\frac{(\bar{k}_m-\bar{k}_n)^2}{4\xi}\right]+(-1)^\sigma\exp\left[-\frac{(\bar{k}_m+\bar{k}_n)^2}{4\xi}\right]-4\exp\left(-\frac{\bar{k}_m^2+\bar{k}_n^2}{4\xi}\right)\right.$$
$$\left.\left[(1-\sigma)I_0\left(\frac{\bar{k}_m\bar{k}_n}{2\xi}\right)+\sum_{\ell=1-\sigma}^{\infty}\frac{B_0}{B_{max}-B_0}\,\xi\,\frac{\omega^2}{\omega_{b0}^2}\,\frac{\exp(-\nu_\ell)E_i(\nu_\ell)I_{2\ell+\sigma}\left(\frac{\bar{k}_m\bar{k}_n}{2\xi}\right)}{(2\ell+\sigma)^2}\right]\right\}, \quad (127)$$

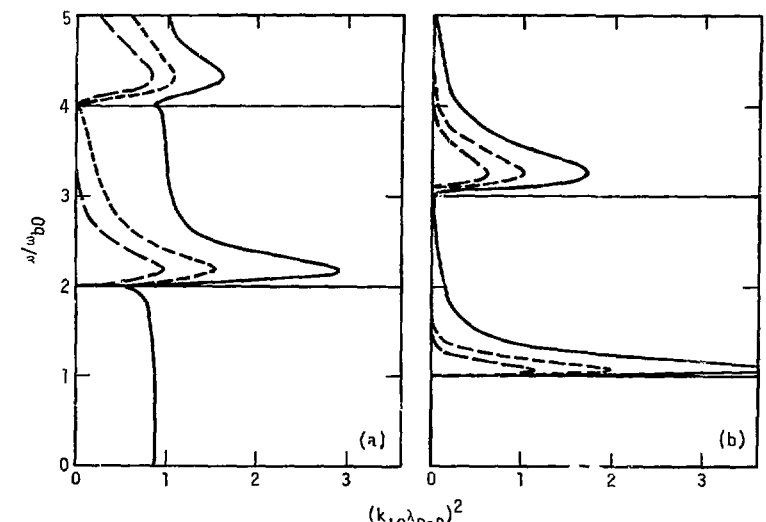

Fig. 12. Eigenvalues for undamped electron modes when $B_{max}/B_0 = 1.5$ and $\xi = 4.5$: (a) even modes, (b) odd modes.

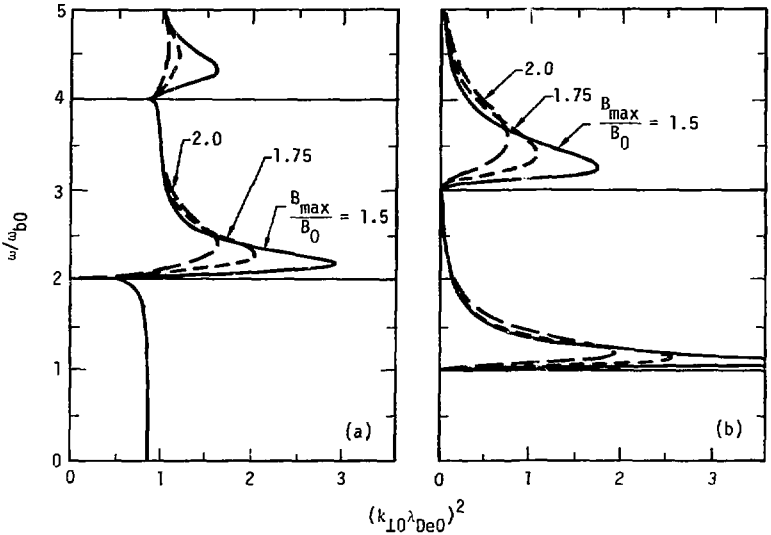

Fig. 13. Variation of principal undamped electron mode eigenvalues with B_{max}/B_0 when $\xi = 4.5$: (a) even modes, (b) odd modes.

where

$$\nu_\ell \equiv \frac{B_0\xi}{B_{max}-B_0} \frac{\omega^2 - (2\ell+\sigma)^2\omega_{b0}^2}{(2\ell+\sigma)^2\omega_{b0}^2} ,$$

and E_i is the real exponential integral defined in Appendix E by Eq. (E4). The principal difference betweeen Eq. (127) and the $B_{max}/B_0 = 1$ result is that the resonant factor $\omega^2/[\omega^2-(2\ell+\sigma)^2\omega_{b0}^2]$ in Eq. (117) is replaced by a factor proportional to $\exp(-\nu_\ell)E_i(\nu_\ell)$. Since the function is peaked at $\nu_\ell = 1.4$, the maximum eigenvalues should occur for frequencies

$$\omega = (2\ell+\sigma)\left(1.4\,\frac{B_{max}-B_0}{B_0\xi} + 1\right)^{1/2}\omega_{b0} . \qquad (128)$$

Figure 14 compares the resonant factors for $B_{max}/B_0 = 1$ and $B_{max}/B_0 = 2$. The $I_{2\ell+\sigma}$ factor in the Eq. (127) resonant term accounts for the weakening of principal mode resonances as ℓ_{res} increases, and this weakening together with the greater spread of resonances at higher ℓ_{res} causes bounce-resonance effects to become inconsequential for

$$\frac{1}{2}\,(2\ell_{res}+\sigma)\,\frac{B_{max}-B_0}{\xi B_0} >> 1\ . \tag{129}$$

Since nonresonant terms in R^e_{mn} are unaffected by ω_b, λ for the principal even mode shows that same limiting value and ξ dependence for $\delta_{res} \approx 2$ as the $B_{max}/B_0 = 1$ case. The principal change in the eigenfunctions introduced by a mirror force is a somewhat greater localization near the centerplane. This is caused physically by the enhanced electron confinement and is seen by comparing the $B_{max}/B_0 = 1.5$ eigenfunctions of Fig. 15 with those in Fig. 8 for $B_{max}/B_0 = 1$.

If a nonquadratic potential

$$\psi(s) = \psi_{max}\left[(1-\alpha)\,\frac{s^2}{s_{max}^2} + \alpha\,\frac{s^4}{s_{max}^4}\right] \tag{130}$$

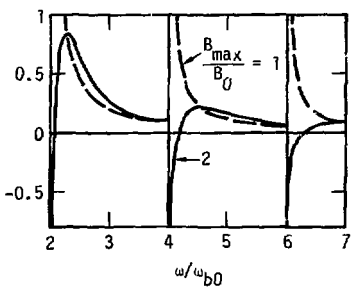

Fig. 14. Approximate even-mode resonant factors for $B_{max}/B_0 = 1.0$ and 2.0 when $\xi = 4.5$ and $\ell = \ell_{res}$.

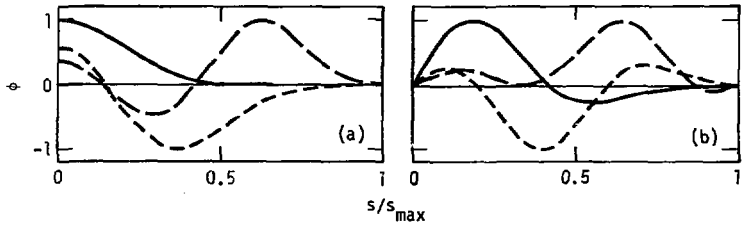

Fig. 15. Eigenfunctions for undamped electron modes when $B_{max}/B_0 = 1.5$, $\xi = 4.5$, and $\delta_{res} = 1.0$: (a) even modes, (b) odd modes.

is combined with the quadratic B field, Eq. (124), the anharmonic potential term has two main effects on bounce modes. The $(1-\alpha)$ factor introduced in the quadratic term of ψ to keep ψ_{max} constant changes ξ by a $(1-\alpha)^{-1}$ factor by altering ω_{b0}. Since the R^e_{mn} expression, Eq. (128), remains an acceptable approximation when $\alpha/(1-\alpha)$ is small, this ξ change affects the relative magnitude of the resonant term and, through ν_ℓ, the frequencies at which the principal eigenvalues are greatest. In addition, the quartic term in Eq. (130) causes a shift of $3\alpha\psi_{max} \langle\chi^2\rangle / (m_e s^4_{max})$ in the mean squared bounce frequency, which further shifts the λ maxima. These changes are apparent when the eigenvalues in Fig. 16 for $\alpha = 0.5$ and $B_{max}/B_0 = 1.5$ are compared with the $\alpha = 0$ results in Fig. 12. From Fig. 17 it is evident that a positive α broadens the resonance, while negative α tends to cancel the mirror force spread in ω_b and to sharpen resonances. According to Eq. (122), changes in ξ caused by nonzero α also shift the mode numbers that are dominant in the response matrix. The small differences seen in the principal even-mode eigenfunctions of Fig. 18 illustrate this effect.

When terms for electron damping and the ion response are included in the eigenvalue equation for ϕ, they affect bounce modes principally by stabilizing the waves at frequencies near the $\omega = (2\ell+\sigma)\omega_{b0}$ resonances where damping is strongest. Even though eigenvalues are in general altered by the added terms, $\mathrm{Im}(R^e_{mn})$ is normally small enough for parameters of interest that the validity condition, Eq. (107), for a perturbation treatment of ϕ is approximately satisfied whenever marginally stable modes exist. Consequently, $\mathrm{Re}(R^e_{mn})$ is still the dominant matrix term in these cases, and the eigenvalues calculated from the undamped electron equation, Eq. (105), are close approximations to correct values. Figure 19 compares even-mode eigenvalues of the full matrix

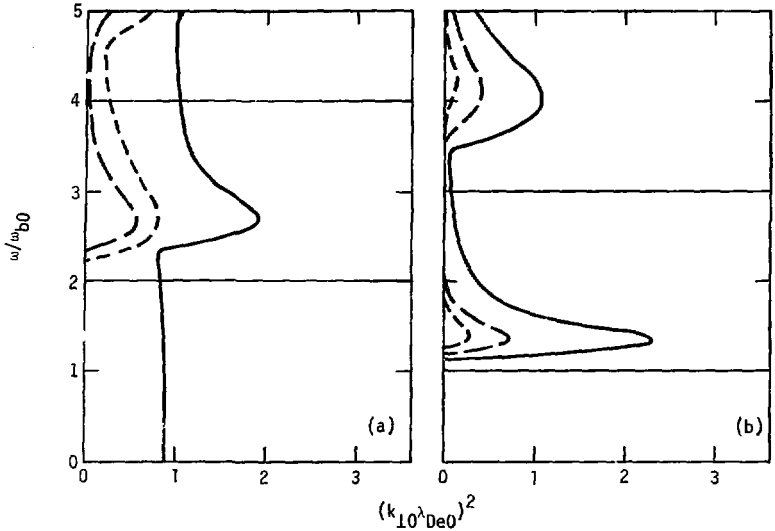

Fig. 16. Eigenvalues for undamped electron modes in a quartic potential with $\psi_{max}/W_e = 4.5$ and $\alpha = 0.5$ when $B_{max}/B_0 = 1.5$: (a) even modes, (b) odd modes.

equation with results of Eq. (105) for the same parameters. The small eigenvalue discrepancies arise principally from including the real ion term in the matrix equation for φ, and since the ion response tends to cancel electron charge density perturbations, λ for the principal modes is reduced when the ion term is added. The corresponding eigenfunctions obtained by the two methods are found to differ by less than 0.5% at each point in this example.

Although the results presented are calculated for the gradually cutoff Maxwellian electron distribution, Eq. (18), the corresponding λ values for an abruptly cutoff Maxwellian distribution differ by no more than 1.5% when $\xi = 4.5$, and choosing a Maxwellian without loss regions for F_e reduces λ typically by 4%. This insensitivity results mainly from the fact that the cutoff factor in Eq. (18) becomes appreciable only near $E = \mu B_{max} + \psi_{max}$, where the exponential factor in F_e is small.

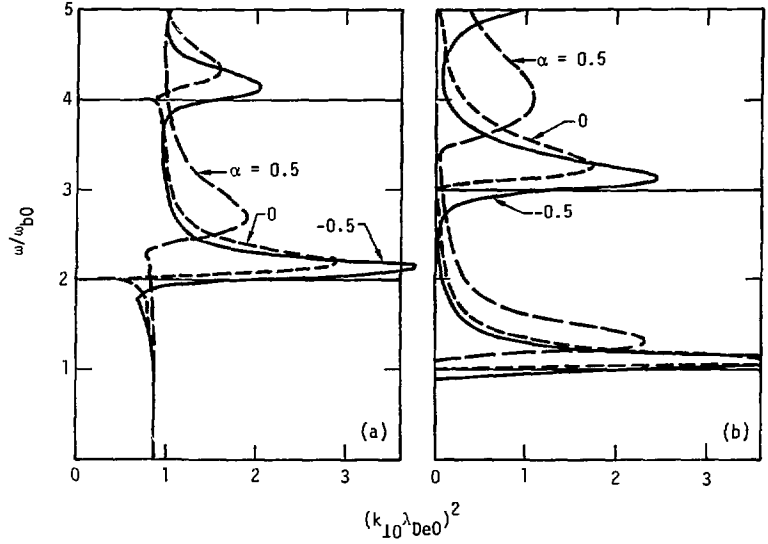

Fig. 17. Variation of principal undamped electron-mode eigenvalues with α in a quartic potential when $B_{max}/B_0 = 1.5$ and ψ_{max}/W_e: (a) even modes, (b) odd modes.

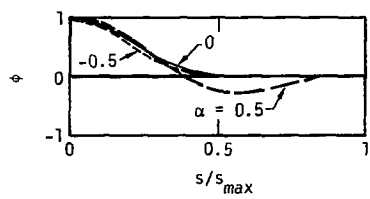

Fig. 18. Variation of principal even undamped electron-mode eigenfunctions with α in a quartic potential when $B_{max}/B_0 = 1.5$, $\psi_{max}/W_e = 4.5$, and $\delta_{res} = 1.0$.

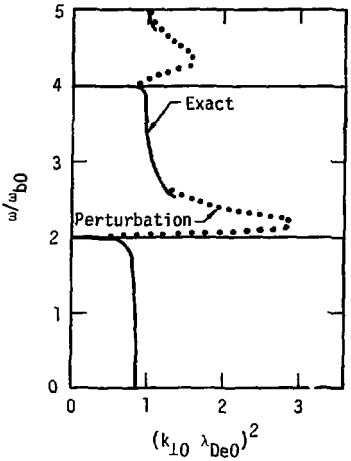

Fig. 19. Comparison of principal even mode eigenvalues with undamped electron mode eigenvalues when $B_{max}/B_0 = 1.5$, $\xi = 4.5$, and $W_e/W_i = 4.5 \times 10^{-3}$.

INSTABILITY THRESHOLD DENSITIES

The stability of bounce modes is governed by the relative magnitudes of the electron damping and ion drive terms of R^e_{mn} and R^i_{mn}. For the quadratic B field given by Eq. (124), and a quartic potential, Eq. (123), with small $A_2 s^2_{max}/A_1$ and $A_2 s^2_{max}/\langle\mu\rangle B_1$, the imaginary part of R^e_{mn} is shown in Appendix D to be approximately

$$\mathrm{Im}(R^e_{mn}) \approx -2\pi^{3/2} \frac{B_0 \xi}{B_{max}-B_0} \sum_{\ell=1-\sigma}^{\ell_{res}} \frac{\exp(-\nu_\ell)\ \exp\left(-\frac{\bar{k}_m^2+\bar{k}_n^2}{4\xi_\ell}\right) I_{2\ell+\sigma}\left(\frac{\bar{k}_m \bar{k}_n}{\xi_\ell}\right)}{\xi_\ell^{1/2}} . \quad (131)$$

where

$$\nu_\ell = \frac{B_0 \xi}{B_{max}-B_0} \frac{\omega^2 - (2\ell+\sigma)^2 \omega_{b0}^2}{(2\ell+\sigma)^2 \omega_{b0}^2} ,$$

and

$$\xi_\ell = \left[\frac{\omega^2}{(2\ell+\sigma)^2 \omega_{b0}^2} - \frac{3A_2}{m_e} \frac{B_0}{B_{max}-B_0} \frac{s^2_{max}}{\omega_{b0}^2} \right] \xi .$$

Here, ℓ_{res} is the largest integer solution of

$$\omega^2 - (2\ell_{res}+\sigma)^2 \left[\omega_{b0}^2 + \frac{3\ \max(0,A_2)\ s_{max}^2}{m_e}\right] > 0 \ . \tag{132}$$

For even modes with $\omega < 2\omega_{b0}$, the harmonic factor $2\ell_{res}+\sigma$ is zero and the mode is undamped. The damping represented by $\mathrm{Im}(R_{mn}^e)$ results from the mixing of bounce-orbit phases that occurs when the mirror force or any nonquadratic field variation spreads ω_b. The bounce-frequency spread has three effects on the matrix elements: The relative spread due to the mirror force, given approximately by

$$\frac{\Delta\omega_b}{\omega_{b0}} \approx \frac{B_{max}-B_0}{2B_0\xi} \ , \tag{133}$$

controls the exponential decrease of $\mathrm{Im}(R_{mn}^e)$ with $\delta_{res} \equiv [\omega - (2\ell_{res}+\sigma)\omega_{b0}]/\omega_{b0}$ in the small A_2 limit considered here. In addition, the strength of damping at resonance is altered by the $B_0\xi/[\xi_\ell^{1/2}(B_{max}-B_0)]$ factor, which tends to sharpen resonances as $\Delta\omega/\omega_{b0}$ decreases and the appearance of ξ_ℓ^{-1} in the Bessel function argument affects which of the matrix elements are dominant according to Eq. (122). The $(2\ell+\sigma)^{-2}$ factor in ν_ℓ causes a weaker exponential frequency dependence in Eq. (131) as ℓ_{res} increases because particle resonances are spread over a greater frequency range. An upper bound on the magnitude of the ion drive term is given by Eq. (D44) in Appendix D:

$$\mathrm{Im}(R_{mn}^i) \approx 1.9\ \Lambda_j \frac{W_e}{W_i}\left(\frac{B_0}{B_{max}-B_0}\right)^{2/3}\left(\xi\frac{\omega^2}{\omega_{b0}^2}\frac{v_e^2}{v_\parallel^2}\right)^{1/6} \ . \tag{134}$$

The weak frequency dependence of Eq. (134) results from the assumption of ion resonance $\omega \sim j\Omega_i$, and the expression is independent of indices m and n because spatial variation of ϕ is neglected.

A marginal stability condition obtained from Eqs. (131) and (134) shows the important qualitative features of threshold density behavior. Provided that the validity criterion, Eq. (107), for a perturbation treatment of ϕ is satisfied, the ratio of imaginary electron and ion contributions, Eq. (110), gives the value of Λ_j at threshold. When

$$(2\ell_{res}+\sigma)\frac{\Delta\omega_b}{\omega_{b0}} \approx (2\ell_{res}+\sigma)\frac{B_{max}-B_0}{2B_0\xi} \lesssim 1 \ , \tag{135}$$

the sum in Eq. (131) is dominated by the ℓ_{res} term, and an estimate of the electron contribution, obtained from the dominant $\mathrm{Im}(R^e_{mn})$ matrix element, is

$$\Gamma^e \approx -2^{1/2}\pi\,\frac{\omega_{b0}}{2\Delta\omega_b}\,\frac{1}{\xi_{\ell_{res}}^{1/2}}\,\frac{\exp\left[-\dfrac{\omega_{b0}\delta_{res}}{(2\ell_{res}+\sigma)\Delta\omega_b}\right]}{2\ell_{res}+\sigma} \ , \tag{136}$$

where the approximations $\nu_{\ell_{res}} \approx \omega_{b0}\delta_{res}/(2\ell_{res}+\sigma)\Delta\omega_b$ and

$$max\left[\exp\left(-\frac{\bar{k}_m\bar{k}_n}{2\xi_\ell}\right) I_{2\ell+\sigma}\left(\frac{\bar{k}_m\bar{k}_n}{2\xi_\ell}\right)\right] \sim \frac{1}{(2\pi)^{1/2}(2\ell+\sigma)} \tag{137}$$

have been used to simplify Eq. (131). If $\Lambda_j\Gamma^i$ is approximated by the $\mathrm{Im}(R^i_{mn})$ expression, Eq. (134), then the threshold Λ_j value for the principal modes is

$$\Lambda_j = \left|\frac{\Gamma^e}{\Gamma^i}\right| \approx 5\,\frac{W_i}{W_e}\left(\frac{\xi}{\xi_{\ell_{res}}}\right)^{1/2}\left(\frac{\omega_{b0}}{2\Delta\omega_b}\right)^{1/3}\left(\frac{1}{\xi}\frac{v_n^2}{v_e^2}\frac{\omega_{b0}^2}{\omega^2}\right)^{1/6}\frac{\exp\left[-\dfrac{\omega_{b0}\,\delta_{res}}{(2\ell_{res}+\sigma)\Delta\omega_b}\right]}{2\ell_{res}+\sigma} \ , \tag{138}$$

which vanishes for $2\ell_{res}+\sigma = 0$. Since this value must be less than $\Lambda_{max} \lesssim 0.385$ for instability to occur, electron modes should be stable at the lowest bounce resonances whenever $W_i \geq W_e$. In this case, Eq. (138) predicts three regimes of qualitatively different threshold density variation. For frequencies with

$$\delta_{res} \lesssim (2\ell_{res}+\sigma)\frac{\Delta\omega_b}{\omega_{b0}}\ln\left(\frac{\Lambda_{res}}{\Lambda_{max}}\right) \ , \tag{139}$$

where Λ_{res} is the Λ_j value at $\omega = (2\ell_{res}+\sigma)\omega_{b0}$, $\Lambda_j/\Lambda_{max} > 1$, and the mode is stable. In the transition region where $\Lambda_j/\Lambda_{max} \lesssim 1$, the argument ζ_{th} of Λ_j drops as ω increases from the value at the first Λ_j maximum toward the value at the first zero crossing. The corresponding threshold density ε_{th}, given by Eq. (111), likewise decreases due to its ζ^2 dependence. When $\Lambda_j/\Lambda_{max} \ll 1$,

ζ_{th} remains at approximately the value at the first zero of Λ_j independent of ω, and the principal ε_{th} frequency dependence then comes from the λ^{-1} factor in Eq. (111).

Calculated threshold densities for the three longest-wavelength modes, plotted in Fig. 20, show the expected frequency dependences. Values are calculated from the full complex eigenvalue equation, Eq. (40), using a sharply peaked $v_\perp$ distribution and quadratic B and ψ fields with $B_{max}/B_0 = 1.5$ and $\psi_{max}/W_e = 4.5$ nominally. The energy ratio $W_e/W_i = 4.5 \times 10^{-3}$ is low enough that all modes are unconditionally stable just above resonances, and at frequencies where electron damping is exponentially small, thresholds for all except the principal even mode increase rapidly with frequency due to decreasing λ. For the principal even mode, ε_{th} varies gradually with ω in the $\Lambda_j/\Lambda_{max} \ll 1$ region because λ approaches a constant nonzero value. The nonresonant even mode below $\omega = 2\omega_{b0}$ is unstable independent of density since it is undamped when the fields vary quadratically. Threshold densities for ions with a spread in $v_\perp$ differ from the peaked distribution results of Fig. 20 in two respects: Since the first zero of Λ_j for the broad $v_\perp$ distribution, Eq. (22) is higher than the peaked distribution value by a factor 1.3, the ε_{th} curves are greater by a factor of 1.7 at frequencies where Λ_j/Λ_{max} is small. Also, the smaller Λ_{max} value for a spread distribution, according to Eq. (139), results in a larger interval above resonances in which modes are stable. The pattern of strong bounce resonances in Fig. 20 is expected to vanish when ℓ_{res} is large enough that the coherence condition, Eq. (135) is violated since particle resonances from different bounce harmonics then begin to overlap. Figure 21 shows that with the same plasma parameters as Fig. 20, the resonance structure is substantially lost for $\omega/\omega_{b0} \gtrsim 9$.

A higher energy ratio W_e/W_i both broadens the $\Lambda_j/\Lambda_{max} > 1$ frequency interval by increasing Λ_{res} in Eq. (139) and affects the minimum threshold values due to the linear W_e/W_i dependence of the ε_{th} expression, Eq. (111). These effects are seen in the threshold curves of Fig. 22. Changes in bounce-frequency spread, in contrast, leave ε_{th} effectively unaltered in regions where $\Lambda_j/\Lambda_{max} \ll 1$, but can shift and broaden the $\Lambda_j/\Lambda_{max} > 1$ and transitional $\Lambda_j/\Lambda_{max} \lesssim 1$ intervals. Threshold curves in Fig. 23 show the effect of changing the spread due to the mirror force. The $\Lambda_j/\Lambda_{max} > 1$ region is broadened with increasing B_{max}/B_0 as expected from Eq. (139), and the transition region becomes more prominent. Figure 24 illustrates two effects of changes in ψ_{max}: Increasing the potential strengthens the exponential dependence of

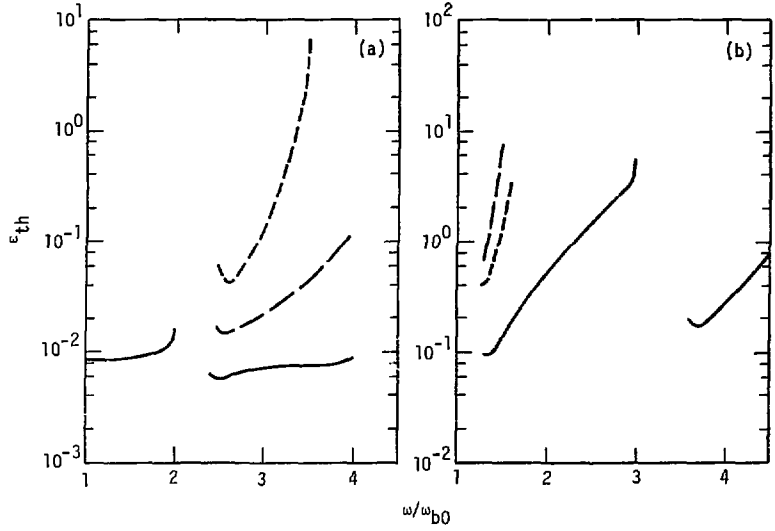

Fig. 20. Threshold densities for the longest-wavelength modes when $W_e/W_i = 4.5 \times 10^{-3}$, $B_{max}/B_0 = 1.5$, and $\xi = 4.5$: (a) even modes, (b) odd modes.

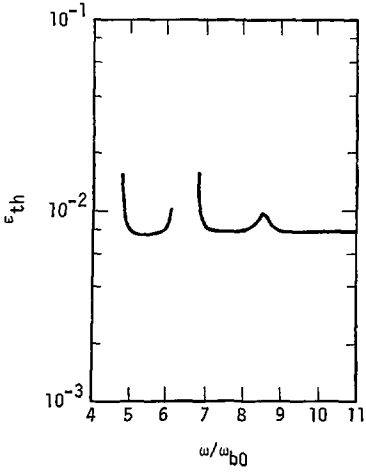

Fig. 21. Principal even-mode threshold density for higher ω/ω_{bo} when $W_e/W_i = 4.5 \times 10^{-3}$, $B_{max}/B_0 = 1.5$, and $\xi = 4.5$.

electron damping by raising the zero-energy bounce frequency ω_{b0}, substantially reducing the frequency range where waves are stable. Also, the values of ε_{th} in the $\Lambda_j/\Lambda_{max} \ll 1$ regime are altered because of the shift in λ discussed in the preceding section. Introducing a nonquadratic potential with the form of Eq. (130) likewise increases the size of the $\Lambda_j/\Lambda_{max} > 1$ frequency interval by changing ω_{b0}, but in addition shifts the regions of greatest damping, as Fig. 25 shows. The shift of $\Lambda_j/\Lambda_{max} > 1$ intervals results from the change in ℓ_{res} due to the A_2 term in Eq. (132), and comparing the threshold curves in Fig. 26 with Fig. 25(a) indicates that this shift is independent of W_e/W_i.

The calculated instability threshold densities for the principal even modes are insensitive to details of the physical model. According to Eq. (111), any change in ε_{th} when W_e/W_i is fixed requires variation in either λ or ξ_{th}. The eigenvalue studies in the preceding section indicate that λ for the principal even mode is approximately constant over the frequency range where

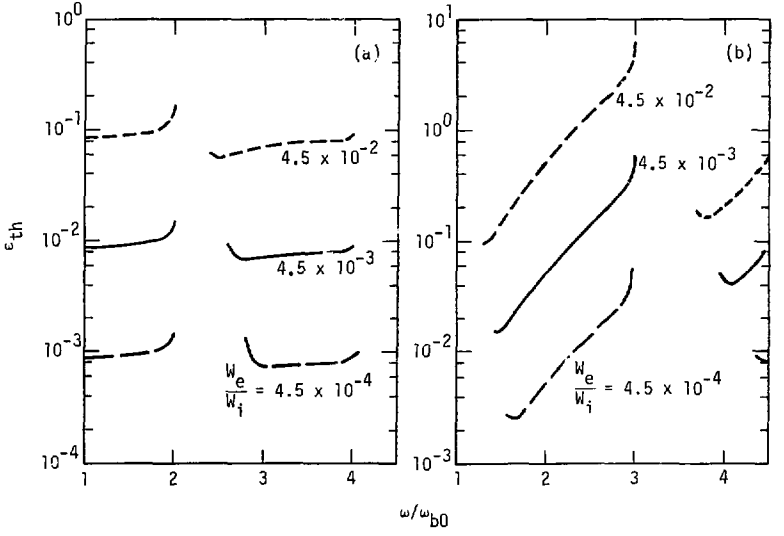

Fig. 22. Variation of principal mode threshold densities with W_e/W_i when $B_{max}/B_0 = 1.5$ and $\xi = 4.5$: (a) even modes, (b) odd modes.

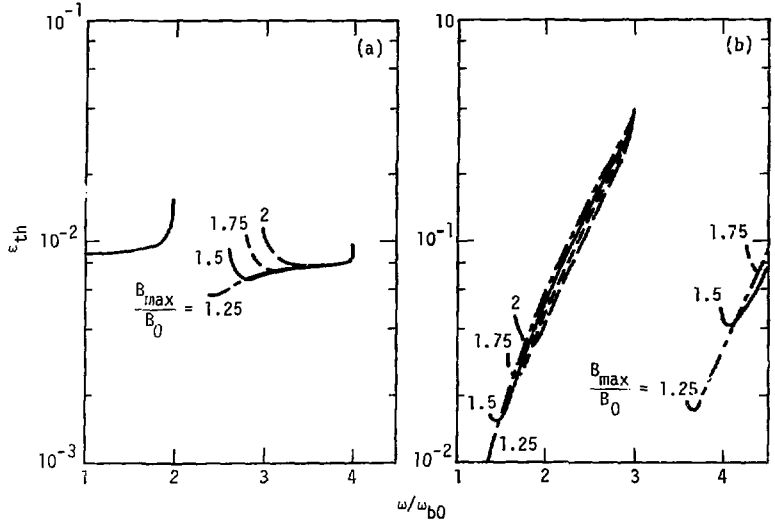

Fig. 23. Variation of principal mode threshold densities with B_{max}/B_0 when $W_e/W_i = 4.5 \times 10^{-3}$ and $\xi = 4.5$: (a) even modes, (b) odd modes.

electron damping is weak enough to allow instability, and the minimum value is principally affected by ψ_{max}/W_e rather than by the plasma distribution functions or spatial dependences of the fields. Similarly, ζ_{th} is effectively constant over most of the frequency range of possible instability so long as the condition in Eq. (135) is met, since Λ_j/Λ_{max} is exponentially small. Changing $F_\perp$ does alter this ζ_{th} value by shifting the first zero of Λ_j, but for plausible distributions such as multiply peaked functions or superpositions of peaked and spread functions, the first zero is bracketed by values for the forms of Eqs. (21) and (22). Using different $F_\parallel$ or $V_\parallel/V_\perp$ expressions normally alters Γ^i in Eq. (110) by a factor of the order of unity. Since this change principally affects the size of the Λ_j/Λ_{max} interval through the logarithmic Λ_{max} dependence of Eq. (139), the choice of the distributions has negligible effect on the minimum ε_{th} in typical devices. Only when the principal even mode is actually suppressed, either by stronger damping or by weakened ion drive, is a substantial change in the minimum ε_{th} expected.

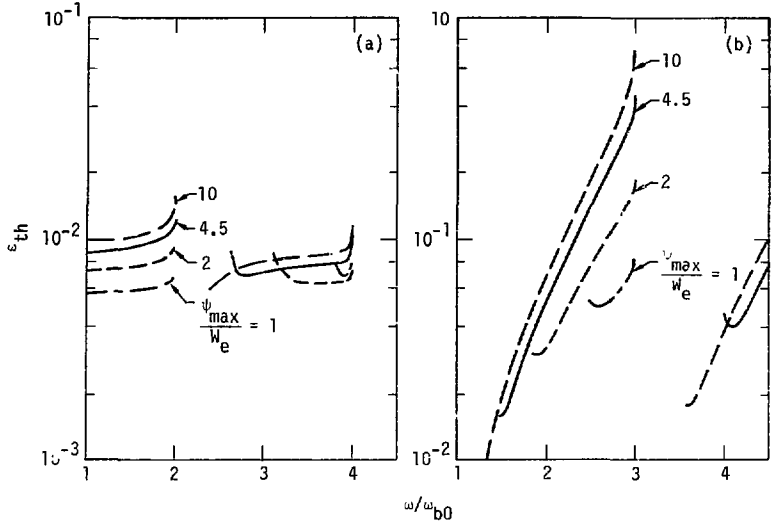

Fig. 24. Variation of principal mode threshold densities with ψ_{max}/W_e when $W_e/W_i = 4.5 \times 10^{-3}$ and $B_{max}/B_0 = 1.5$: (a) even modes, (b) odd modes.

MAXIMUM INSTABILITY GROWTH RATES

For electrostatic bounce modes with real $k_\perp$, the greatest growth rate for any real frequency $\omega_r \equiv \mathrm{Re}(\omega)$ occurs for the density at which either maximum ion-wave coupling is achieved or ions begin to weaken the electron response by cancelling electron density perturbations. The first mechanism is important when elements of $\mathrm{Re}(R^i_{mn})$ evaluated using the maximum value of Λ_1 are small compared with the dominant elements of $\mathrm{Re}(R^e_{mn})$, and the maximum $\gamma \equiv \mathrm{Im}(\omega)$ is then calculated by the perturbation method of Chapter 2. In most cases, the ion response with $\Lambda_1 = \Lambda_{max}$ is strong enough to reduce λ appreciably when it is included in the matrix equation for ϕ. Direct calculation of the real $k_\perp$ eigenfunctions for increasing γ values is then carried out to find the maximum.

When $\gamma << \omega_r$, a Taylor expansion of the imaginary part of Eq. (40) leads to an analytic estimate of γ_{max}. To first order in γ,

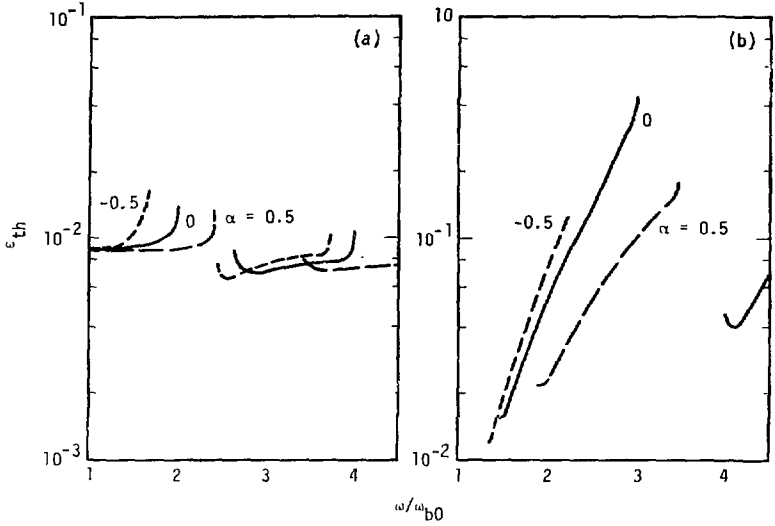

Fig. 25. Variation of principal mode threshold densities with α in a quartic potential when $W_e/W_i = 4.5 \times 10^{-4}$, $B_{max}/B_0 = 1.5$, and $\psi_{max}/W_e = 4.5$: (a) even modes, (b) odd modes.

$$\sum_{m=1}^{\infty}\sum_{n=1}^{\infty}\left\{\mathrm{Im}(R^{e}_{mn}) + \mathrm{Im}(R^{i}_{mn}) + \mathrm{Im}\left[i\gamma\,\frac{\partial}{\partial\omega}\left(R^{e}_{mn} + R^{i}_{mn}\right)_{\omega=\omega_r}\right]\right\}\phi^{0}_{m}\,\phi^{0}_{n} \quad 0\ , \tag{140}$$

where ϕ^{0}_{m} are the Fourier coefficients for an undamped electron mode. Since R^{i}_{mn} according to the analytic approximation given by Eq. (D44) varies like $\omega^{1/3}$, the R^{i}_{mn} derivative in Eq. (140) is discarded. Using Λ_{max} in R^{i}_{mn} then gives

$$\gamma_{max} \approx \frac{\sum_{m=1}^{\infty}\sum_{n=1}^{\infty}\left[\mathrm{Im}(R^{e}_{mn}) + \mathrm{Im}(R^{i}_{mn})\right]\phi^{0}_{m}\,\phi^{0}_{m}}{\sum_{m=1}^{\infty}\sum_{n=1}^{\infty}\left[\frac{\partial}{\partial\omega_r}\,R_e(R^{e}_{mn})\right]\phi^{0}_{m}\,\phi^{0}_{n}} = \frac{I^{e} + \Lambda_{max}\,I^{i}}{\frac{\partial\Lambda}{\partial\omega_r}\sum_{m=1}^{\infty}\sum_{n=1}^{\infty}\phi^{e}_{m}\,\phi^{0}_{n}}\ , \tag{141}$$

where Eqs. (108) and (109) respectively define I^{e} and I^{i}, and the Cauchy-Riemann equation result

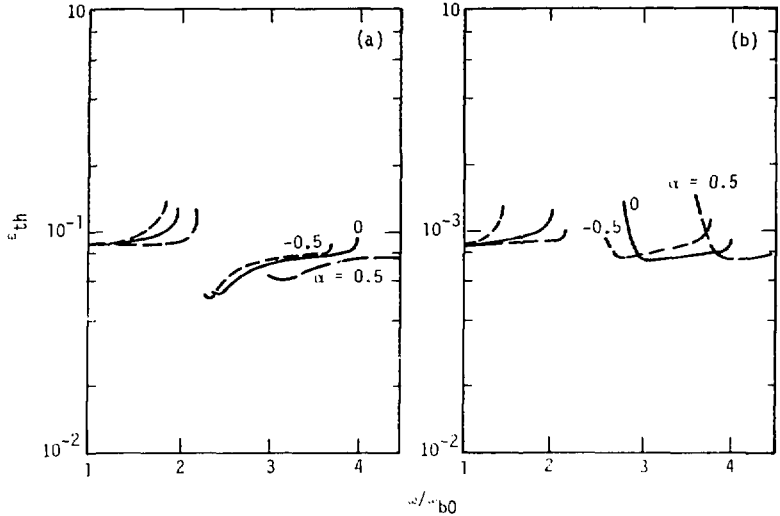

Fig. 26. Variation of principal even-mode threshold densities with α in a quartic potential when $B_{max}/B_0 = 1.5$ and $\omega_{max}/\omega_c = 4.5$: (a) $W_e/W_i = 4.5 \times 10^{-2}$, (b) $W_e/W_i = 4.5 \times 10^{-4}$.

$$\mathrm{Im}\left(\varepsilon_{th}\frac{\omega}{\omega_{b0}}R^e_{nn}\right) = \frac{\omega}{\omega_r}\,\mathrm{Re}(E^e_{nn}) \tag{142}$$

has been used. If the dominant mode approximation, Eq. (130), is used for I^e and Eq. (134) is substituted for Λ_{ij}^{ef}, then Eq. (141) becomes

$$\nu_{max} \approx \frac{1}{3\sqrt{3}\omega_r}\left\{1.9\Lambda_{max}\frac{W_e}{W_i}\left(\frac{B_0}{B_{max}-B_0}\right)^{2/3}\left(\frac{\omega_c^2}{\omega_{b0}^2}\frac{V_e^2}{V_n^2}\right)^{1/6}\right.$$
$$\left. - 4.4\,\frac{B_0^2}{B_{max}-B_0}\,\frac{\exp\left[-\frac{2(B_{max}-B_0)^2}{(2\sigma_{res}^2+\nu)B_0^2}\right]}{(2\sigma_{res}^2+\nu)^{1/2}\sigma_{res}^2}\right\}. \tag{143}$$

With the calculated electron eigenfunctions from Fig. 12, qualitative features of the γ_{max} frequency dependence are apparent from Eq. (143). According to Eq. (110), a mode is stable when $\Gamma^e + \Lambda_j \Gamma^i \leq 0$ and γ_{max} is zero. At higher frequencies, γ_{max} should increase from zero to a peak value proportional to Γ^i, and as $\delta_{res} \to 2$, γ_{max} is expected to drop rapidly back to zero due to the increase in $|\partial\lambda/\partial\omega_r|$. Since the λ derivative for the principal even mode is generally smaller than odd-mode values where marginally stable modes exist, Eq. (143) predicts higher γ_{max} values for even modes. From Eq. (D27), $\partial\lambda/\partial\omega_r \sim \partial \mathrm{Re}(R^e_{mn})/\partial\omega_r$ has approximately linear dependences on $(2\ell_{res}+\sigma)^{-1}$ and $\xi^{-1/2}$ for $\delta_{res} \gtrsim 2$, independent of B_{max}/B_0. The peak γ_{max} should therefore scale roughly as $B_0\xi(2\ell_{res}+\sigma)/(B_{max}-B_0)$.

Calculated growth rates for sufficiently small W_e/W_i show the predicted qualitative behavior. In Fig. 27, γ_{max} for the principal even and odd modes for $W_e/W_i = 4.5 \times 10^{-3}$ is plotted over a range of frequencies. Again, the values $B_{max}/B_0 = 1.5$ and $\psi_{max}/W_e = 4.5$ are used, and quadratic spatial dependence of the fields is assumed. The maxima for successive ℓ_{res} values have nearly the expected $2\ell_{res}+\sigma$ proportionality, and a rapid dropoff near $\delta_{res} = 2$ occurs. Figure 28 and Fig. 29 show how the growth rate curve for the principal even mode varies respectively with B_{max}/B_0 and ξ. Since the perturbation approximation is acceptable for the W_e/W_i value used, growth rate dependences are in good agreement with the predictions, and γ_{max} values calculated both by the perturbation and direct methods of Chapter 2 differ by no more than 3%. For $W_e/W_i = 4.5 \times 10^{-2}$, the ion term is large enough to affect the eigenvalues and require direct calculation of γ_{max}. Growth rate curves in Fig. 30 for this higher energy ratio show reduced dependence of γ_{max} on ℓ_{res} because the important limit on γ is the relative magnitudes of the real ion and electron terms of the matrix equation. Scaling of growth rates with B_{max}/B_0 is not significantly affected by W_e/W_i since these dependences enter through multiplicative factors.

APPLICATION TO MIRROR EXPERIMENTS

The numerical model is used to test whether electrostatic bounce modes were an important instability mechanism in the Baseball I (BBI) and Baseball II (BBII) experiments. Since most idealizations in the model are appropriate for low-density mirror devices, the calculated instability threshold densities and growth rates should be close to experimental values if destabilized bounce modes were the dominant cause of instability in the two machines. The general

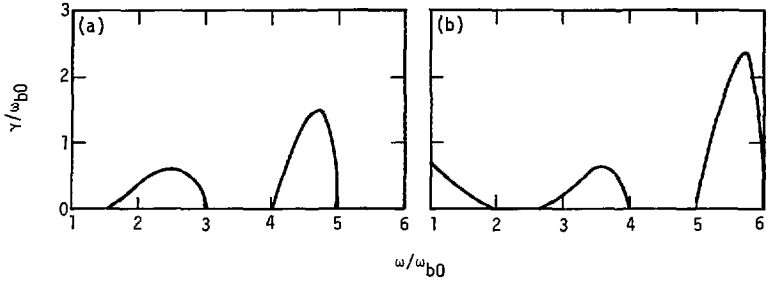

Fig. 27. Maximum instability growth rates when $W_e/W_i = 4.5 \times 10^{-3}$, $B_{max}/B_0 = 1.5$, and $\xi = 4.5$: (a) even modes, (b) odd modes.

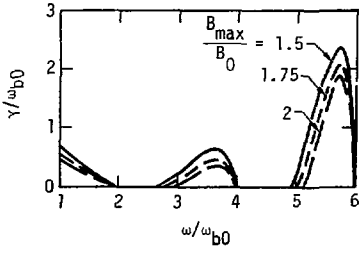

Fig. 28. Variation of maximum even-mode instability growth rates with B_{max}/B_0 when $W_e/W_i = 4.5 \times 10^{-3}$ and $\xi = 4.5$.

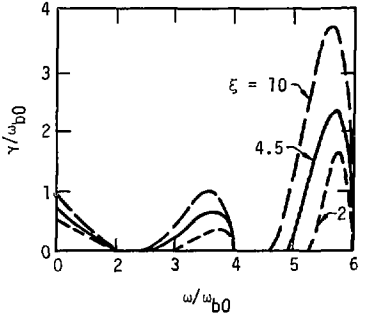

Fig. 29. Variation of maximum even-mode instability growth rates with ξ when $W_e/W_i = 4.5 \times 10^{-3}$ and $B_{max}/B_0 \cong 1.5$.

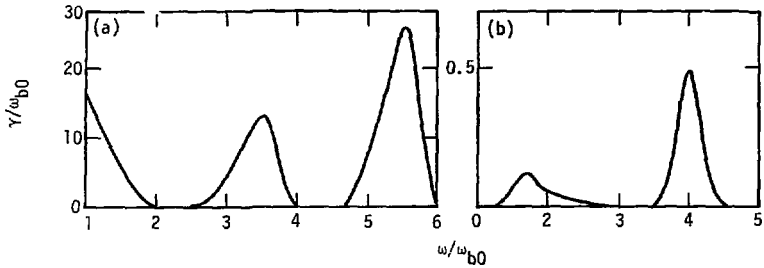

Fig. 30. Maximum instability growth rates when $W_e/W_i = 4.5 \times 10^{-2}$, B_{max}/B_0 1.5, and ξ=4.5: (a) even modes, (b) odd modes.

approach is to choose parameters in the model to simulate the BBI and BBII plasmas, and then to compare predicted threshold values and parametric dependences with the findings of a large number of experimental runs.

General features of bounce modes are consistent with the observations of instabilities in low-density mirror experiments. Electrostatic probe measurements indicate rapidly growing disturbances with typical wavelengths along field lines comparable with the plasma length,[2,45] and the instability threshold densities are affected by changes in plasma length and the distribution functions near the mirror centerplane, as expected of nonlocal modes. Instability was detected by ejected electrons in BBI and by the onset of radiofrequency (rf) activity in BBII. As density was increased above the threshold, rf signals appeared first at the ion gyrofrequency and then at successively higher harmonics. This finding agrees with the theoretical result that thresholds for frequencies $\omega \simeq j\Omega_{i0}$ increase with j. The rf activity also was found to cease when the neutral beam used to generate energetic ions was turned off. This effect and the prominence of gyrofrequency harmonics in the rf spectrum together indicate that the instability was driven by coupling to an anisotropic ion distribution.

Comparison of experimental threshold densities in BBI and BBII with theoretical values is the principal quantitative test of the bounce-mode mechanism. Since the onset of instability during plasma buildup is an important and accessible experimental diagnostic, threshold densities were routinely measured in both experiments over a wide range of field and plasma parameters. In contrast, growth-rate information is limited to the observation

that instabilities grew to full amplitude in about 10 gyroperiods. This figure provides no more than a lower bound on γ since the plasma density during buildup could not have been at the value required for maximum growth, and interpretation is further complicated by the fact that the linear perturbation theory used to analyze bounce modes is invalid for waves of the strength observed. Likewise, other predictions of the theory, such as bounce-mode dispersion characteristics and spatial wave forms, are not directly comparable with experimental data.

Since a quantitative comparison of predicted bounce-mode threshold densities with experimental values is intended, the experimental parameters must be carefully related to quantities in the theoretical model. The experimental threshold values of ε for BBI and BBII buildup tests were calculated from the maximum plasma number density N_0 measured at the onset of rf activity and the minimum magnetic field strength B_0 found at the centerplane. Corresponding values of W_e/W_i were calculated from the maximum plasma potential ψ_{max} and measurements of W_i. The maximum N_0 values were estimated in most cases by applying a conversion factor to average density measurements from a microwave interferometer. The potential ψ_{max} was equated to the minimum energy of escaping ions, determined by a gridded detector, and the mean ion energy was estimated either from the energy spectrum of charge-exchange neutrals or from the energy of the injected neutral particles. In BBII tests and in some BBI tests using low-energy ions, the neutral beam used for plasma buildup produced substantial fractions of H atoms with half and a third of the rated energy. The W_i value used in these cases to calculate the energy ratio was an appropriately weighted average of the beam components. Other BBI tests used a nearly monoenergetic H beam. In both devices, the vacuum magnetic field close to the mirror axis had a nearly quadratic spatial dependence both along flux lines and across the centerplane, and the mirror ratios on axis were about 2.1 for BBI and 1.9 for BBII. The respective mirror points were 30 cm and 45 cm from the centerplane.[46,47]

Since the numerical model describes electrostatic modes along a field line, the parameters B_{max} and ψ_{max}, and all s = 0 quantities in R^e_{mn} and R^i_{mn} are values appropriate for a particular flux surface. Accounting for the variation of B_0 on different flux surfaces is especially important because the range of field strengths found at the centerplane determines the frequency interval over which the ion resonance condition $\omega = \Omega_{i0}$ can be satisfied in a finite plasma. For BBI and BBII, the plasma radius was about 10 cm, and Ω_{i0}

on the outer flux surface was approximately 15% above the mirror axis value. This limited range is allowed for numerically by searching for minimum threshold densities only at frequencies matching gyrofrequencies found within the plasma. The calculated threshold densities ε_{th} must also be corrected to mirror axis values for comparison with experiment. If ε_{th}, N_0 and B_0 are all considered functions of the flux surface radius r, then the correction factor for ε_{th} is

$$\varepsilon_{th}(0) = \varepsilon_{th}(r) \frac{N_0(0)}{N_0(r)} \frac{B_0(r)}{B_0(0)} . \qquad (144)$$

For this correction, N_0 is assumed to have the form $N_0(r) = N_0(0)\exp(-r/r_{max})$. Because the parameter studies presented earlier indicate that threshold densities are not strongly affected by changes in ψ_{max} or B_{max}/B_0, the experimental values on axis are used in calculations. No more than 5% error is expected from this approximation. No experimental information was obtained about the ratio ψ_{max}/W_e, the spatial dependence of ψ, or details of the electron and ion equilibrium distribution functions, so plausible approximations like those in the parameter studies are used. Again, $\psi_{max}/W_e = 4.5$ is chosen, and since Post[48] and BenDaniel[49] find ψ/B to vary slowly with position, ψ is taken to be a quadratic function of s. For the unperturbed distribution functions, the forms of Eqs. (18) and (20) are used, with either a delta function, Eq. (21), or a spread distribution, Eq. (22), chosen for $F_\perp$. The ratio of mean squared ion velocities, Eq. (24), for magnetically confined ions is used throughout, even though the ion distribution function assumed for the derivation is inappropriate for BBI and BBII. Since $V_\parallel$ enters the approximate imaginary ion response matrix, Eq. (134), as $V_\parallel^{-1/3}$, the calculated threshold densities are insensitive to the choice. In specifying the mean ion velocities, W_i is treated as the ion thermal energy, so that $W_i = \frac{1}{2} m_i(V_\perp^2 + V_\parallel^2)$. This is not strictly correct for the multiple-peaked distributions expected from the BBII neutral beam injection, but test calculations indicate that using the average beam energy introduces only a 1% error in threshold compared with values for a doubly-peaked distribution.

A typical sample of theoretical and experimental threshold densities for BBI and BBII is shown in Fig. 31. The calculated values of ε_{th} are minima found for frequencies within the range of centerplane ion gyrofrequencies after being corrected to mirror axis values according to Eq. (144). Thresholds

found for the sharply peaked and spread distributions are taken to define limits within which the actual ion distribution is likely to be found. Accordingly, the range of ε between these two cases is plotted as a vertical bar in Fig. 31 for each value of W_e/W_i. In each case, the theoretical threshold densities are calculated from the full complex matrix eigenvalue equation, and except for a few low values of W_e/W_i, all the theoretical ε_{th} correspond to the principal even mode. No resonances with harmonics of the ion gyrofrequency above the fundamental are considered because in experimental tests instabilities with $\omega \approx \Omega_{i0}$ were detected at the lowest densities. The corresponding experimental ε_{th} values are presented as data points in Fig. 31, with results from BBI and BBII denoted respectively by circles and squares. Although no error limits are shown, the experimental threshold densities are certain only with ±50%, and the W_e/W_i value for each case has about a ±25% uncertainty.[3] A series of BBII tests was carried out to determine the effect of reducing the plasma length.[3] A conical metal limiter was placed on the mirror axis, and the threshold density was found to vary sharply with the limiter position. The experimental instability thresholds are plotted in Fig. 32 along with lines bracketing the range of threshold values expected from theory. A similar strong variation of the experimental threshold density was observed when other conditions such as background gas density and the injected neutral beam cross section were changed, but predicted thresholds are not presented for these cases since the numerical model does not incorporate the investigated conditions.

The BBII threshold densities show close agreement with theoretical predictions. In Fig. 31, about 70% of the experimental values fall between the thresholds calculated for the spread and peaked perpendicular ion distributions, and none of the other data points is farther away from the theoretical range than experimental uncertainties could explain. Many of the BBII thresholds found in the axial limiter tests likewise fall within the range of predicted values, as Fig. 32 shows. The experimental densities are closer to thresholds expected for a peaked distribution for smaller W_e/W_i, while for larger energy ratios the experimental values are near to predictions for ions with a spread in $v_\perp$. This behavior is consistent with the expectation that at higher threshold densities electron drag spread the initially peaked ion distribution. Since the electron drag time defined by Spitzer[50] is around 30 s for the BBII cases with the lowest ε_{th} and varies inversely with N_0, the effect should become important above $\varepsilon_{th} \approx 0.1$. In the collisional regime, a

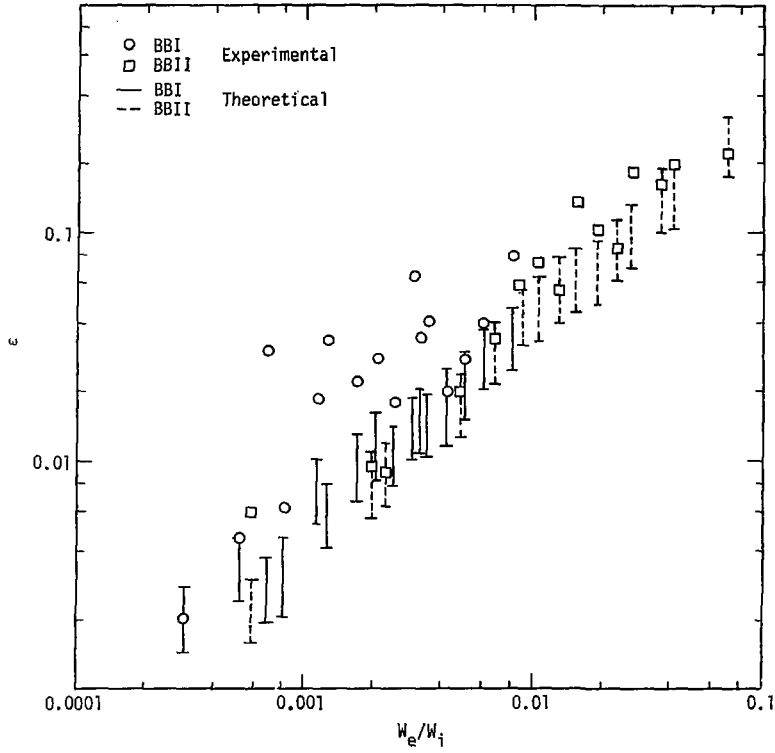

Fig. 31. Theoretical and experimental threshold densities for BBI and BBII when $\xi = 4.5$.

further adjustment of the theoretical ε_{th} is needed to account for the decrease of W_i of about 15% due to electron drag for tests of the duration reported. The corresponding 15% increase in the calculated thresholds improves the agreement with experimental threshold.

The BBI threshold densities presented in Fig. 31 are systematically higher than the theoretical values. Even though experimental values show the approximately linear dependence on W_e/W_i expected from Eq. (111), typical threshold densities are greater than the theoretical predictions for ions with

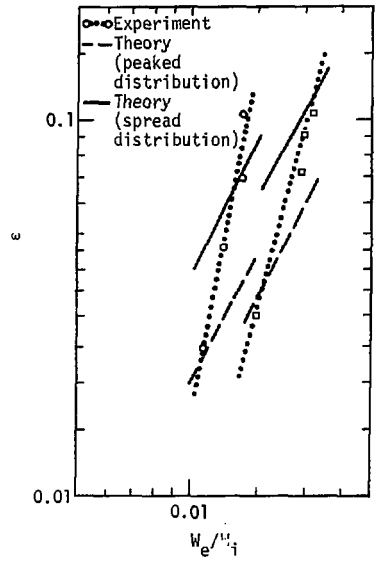

Fig. 32. Theoretical and experimental threshold densities for BBII when axial length is varied and $\xi = 4.5$.

a spread in $v_\perp$ by a factor of 2 to 3, and since plasma densities remain relatively low, no correction of W_i for electron drag is justified. Also, the scatter of experimental thresholds from a linear W_e/W_i dependence is markedly greater than that of calculated values. These discrepancies between theory and experiment are greater than experimental uncertainties and cannot be eliminated by reasonable changes in the plasma potential profile or the ion velocity distribution functions.

Several differences between the BBI and BBII experiments have been examined to account for the systematic deviation of BBI thresholds from predicted values:

- The plasma buildup procedure in BBI resulted in an ion distribution quite different from that of BBII. Although both devices produced plasma by neutral beam injection, the beam in BBI was angled 61° to the mirror axis, whereas the BBII beam was perpendicular. Because of finite beam diameter and the angle of off-axis field lines, the Gaussian form, Eq. (23), chosen for $F_\parallel$ is appropriate for BBII, but the BBI parallel ion velocity distribution would have been peaked around $V_\parallel \approx 0.6\ V_\perp$ near

the axis, with few particles near $v_\parallel = 0$ at the centerplane. The qualitative effect of this double-humped $v_\parallel$ distribution can be determined using the distribution function

$$F_\parallel(v_\parallel) = C_\parallel \left[\exp\left(- \frac{1-\nu^3}{1-\nu} \frac{v_\parallel^2}{V_\parallel^2} \right) - \exp\left(- \frac{1}{\nu^2} \frac{1-\nu^3}{1-\nu} \frac{v_\parallel^2}{V_\parallel^2} \right) \right], \tag{145}$$

with

$$C_\parallel = \frac{(1-\nu^3)^{1/2}}{(1-\nu)^{3/2}} \frac{1}{\pi^{1/2} V_\parallel} ,$$

and $1-\nu$ chosen to be a small positive number. This distribution has maxima near $v_\parallel = \pm V_\parallel$ a ` has the same mean parallel velocity as Eq. (23). Recalculating sample BBI instability thresholds using Eq. (145) gives values greater than using a Gaussian for $F_\parallel$ by only 2%. Dominant elements of the ion response matrix are reduced by nearly 30% when the double-humped distribution is used due to the poorer coupling to the wave, but the imaginary electron term in the matrix equation, Eq. (40), is small enough in this regime that $\Lambda_j \sim 10^{-2}$ at marginal stability, making the calculated ε_{th} values insensitive to changes in the parallel ion response.

- The beam injection angles also make appropriate choices of the rms parallel velocity $V_\parallel$ different for the two machines. The velocity ratio, Eq. (24), used for the thresholds shown in Fig. 31 is obtained by assuming the phase space volume within the loss surfaces to be filled with F_j peaked near $v_\parallel = 0$. While this assumption is acceptable for BBII, $V_\parallel/V_\perp$ for BBI should be about 0.6 on flux surfaces near the axis. Even though this value is about 20% above that calculated using Eq. (145) and increases ion response matrix elements by nearly 6% due to the approximate $V_\parallel^{-1/3}$ dependence of R^i_{mn}, the theoretical threshold densities show less than 0.5% change.
- The neutral beam injection angles used in BBI and BBII resulted in dissimilar number density profiles along field lines. Whereas N was sharply peaked near the centerplane in BBII due to the narrow spread, the BBI number density had a maximum about 7 cm from the center. This peak occurred because particles trapped on a flux surface had nearly the

same parallel velocity and therefore similar turning points. The principal effect on bounce modes of these differing profiles results from changes of the self-consistent electrostatic potential along field lines and the corresponding modification of electron-bounce frequencies. For each machine, a quartic potential with the form of Eq. (130) can be specified with α chosen to give the resulting number density the same half width as densities calculated in numerical buildup simulations. The half-width for BBII was 6.5 cm,[51] and this value is reproduced by a quartic potential with $\alpha \simeq -1.0$. The flatter BBI density profile had a calculate alf-width of 12 cm,[52] and the best quartic aproximation has $\alpha \simeq 0.4$. When theoretical threshold densities for BBI and BBII are recalculated using these quartic potentials, the BBI predictions are still systematically below observed values, while BBII results give a slightly improved fit of the data. Even though the positive α used for BBI calculations increases the spread in ω_b, electron damping is in fact weakened in the frequency range $\omega \sim \Omega_{i0}$ because the imaginary part of R^e_{mn} from Eq. (D31) of Appendix D has both an $\xi^{1/2}$ factor which is proportional to ω_{b0} and a Bessel series that decreases as ℓ_{res} becomes larger.

- Because BBI had a weaker mirror field and normally a higher mean ion energy than BBII, typical ion gyroradii at the centerplane were greater in the earlier experiment. While BBII had gyroradii around 0.5 cm, BBI values were as large as 3.5 cm. The requirement that the azimuthal wavelength of a mode $2\pi/k_\theta$ fit an integral number of times around a flux surface restricts $k_\perp$ to discrete values $k_\perp^2 = k_r^2 + k_\theta^2$ where the radial wavenumber k_r is assumed fixed and greater than π/r_{max}. In BBI, typical ion gyroradii are large enough that some practical limitation on allowed ε_{tn} results. To assess the importance of this effect, the radial wavenumber is neglected compared with $k_\perp$, and flux surfaces are assumed to be circular. Then $k_\perp = n/r$ on a flux surface of radius r and n a positive integer. Since the marginal stability condition, Eq. (138), gives an approximate relation $k_{i0}a_{i0} \simeq 1.85$ for the sharply peaked $v_\perp$ distribution expected in BBI, the threshold condition can be satisfied only on flux surfaces with radii

$$r_n \simeq \frac{n a_{i0}}{1.85} . \tag{146}$$

For approximate treatment, the radial dependence of a_{i0} is ignored. If ω does not nearly equal the ion gyrofrequency on one of the flux surfaces determined by Eq. (146), the coupling of ions to the wave is weakened. Recalculating thresholds for a typical BBI plasma, allowing only values of Ω_{i0} on those critical flux surfaces, gives ε_{th} for the principal even mode the frequency dependence shown in Fig. 33. The minima occur at the exact resonances and equal the previously calculated values, while the threshold density is increased off resonance. Since several flux surfaces satisfying Eq. (146) are found within BBI plasmas even in the extreme case with $k_r = 0$, the periodicity constraint on $k_\perp$ results in only slight changes in calculated minimum thresholds.

Even through these refinements of the model distribution functions and fields have little effect on theoretical threshold densities for the principal even mode, the experimental data suggest that the mode was stabilized in BBI. Stabilization of the mode would allow density to increase during buildup to the thresholds for odd modes or shorter-wavelength even modes. Since these densities are higher by factors of 2 to 5 than ε_{th} for the principal even mode, they are near observed values, and because small changes in parameters can destabilize the plasma, more scatter of threshold values would be expected. Two requirements for stabilization of bounce modes are that $|\Gamma^e/\Gamma^i|$ in Eq. (138) be greater than Λ_{max} in the region of strongest Landau damping and that the spread of bounce frequencies, given approximately by Eq. (135), be great enough that Γ^e does not become exponentially small in the frequency range of interest. Each modification of the model considered alters Γ^e or Γ^i in the direction of stability: Nonquadratic ψ reduces the dropoff of Γ^e at frequencies away from resonance, while the changes in $V_\parallel$ and $F_\parallel$ weaken the ion drive. If damping in BBI were higher than calculated by a factor of the order

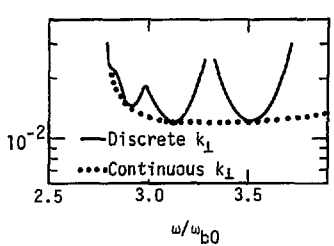

Fig. 33. Comparison of theoretical even-mode threshold densities in BBI for discrete and continuous $k_\perp$ when $W_e/W_i = 6.0 \times 10^{-3}$, $B_{max}/B_0 = 1.9$, and $\xi = 4.5$.

of 10 due to such conditions as field line fanning or asymmetry, a strongly anharmonic potential profile, or nonlinear effects, or if radial localization of the wave correspondingly reduced ion coupling, the principal even mode would have been stable according to theory. To verify this conjecture about stabilization of the principal even mode would require both a considerably more detailed plasma model than the present one and information about the plasma that is not available from experimental data.

4. Conclusion

Electrostatic bounce modes can be an important instability mechanism in certain mirror plasmas. If most ions have a gyrofrequency near low harmonics of typical electron-bounce frequencies, then within a range of densities a long parallel wavelength electron mode with $k_{\perp 0}a_{i0} \sim 2$ and $\omega \sim \Omega_{i0}$ can be destabilized by ions with a peaked perpendicular velocity distribution. These conditions were satisfied in the BBII experiment, and threshold density calculations indicate that the rapidly growing instabilities observed in the device resulted from the bounce-mode mechanism. In BBI, the longest-wavelength even mode appears from experimental data to be stable. The greater bounce-frequency spread and poorer ion coupling to the wave in the BBI regime as well as such complications as field line fanning and radial wave structure are likely causes of this stability. For high W_e/W_i values, the higher marginal stability densities make wave currents more important. The resulting electromagnetic effects give a parallel electric field[53]

$$E_{\parallel}(s) = \frac{k_{\perp}^2(s)c^2}{k^2(s)c^2 + \omega_{pe}^2(s)} \frac{d\phi(s)}{ds} \quad , \tag{147}$$

so that plasma response to electrostatic waves is substantially weakened. Consequently, electromagnetic instabilities like the drift-cyclotron loss-cone mode[36] are dominant instability mechanisms in high-density mirror machines like 2XIIB[54] and the proposed MFTF device.[55]

The present numerical model of bounce modes improves on infinite-medium analyses principally in using complete electron histories in calculating the perturbed number density. Retaining the periodicity of orbits allows mathematically for the regeneration of density perturbations that causes bounce modes. In addition, solving the matrix eigenvalue equation for the plasma

normal modes avoids the short wavelength restriction of WKB formalism. The model is more complete than previous work on mirror plasma electrostatic modes since the ion response and damping terms are retained in the eigenmode calculations and a wide range of equilibrium fields and plasma distribution functions may be used. The principal simplications are the neglect of perpendicular wave structure and use of qualitatively plausible idealizations, such as a quartic plasma potential and truncation of the plasma at s_{max}, where little experimental data is available. With BBII, ion drive is sufficiently strong to make predicted instability threshold densities insensitive to the choice of distributions and fields, and in these cases close agreement is found between theoretical thresholds and experimental values. For BBI parameters where the system is more sensitive to changes in electron damping and ion response, the idealizations result in predicted thresholds consistently below those observed.

Several refinements and extensions of the bounce mode model are possible:

- Specifying an asymmetrical magnetic field like those in minimum-B mirror devices would test whether the assumption of exact symmetry significantly reduces wave damping. Also, replacing the approximation $k_\perp^2(s)/k_{\perp 0}^2 = B(s)/B_0$ with a $k_\perp(s)$ that accounts accurately for the change in flux surface perimeter with s would incorporate effects of flux line fanning into the one-dimensional formalism. Work by Baldwin[38] suggests that fanning helps stabilize long-wavelength modes.

- A more accurate expression for the perturbed ion density could be obtained by Fourier analyzing ion orbits in time as in the electron treatment. This approach would allow use of more general distribution functions and would take into account the bounce motion of ions confined near the centerplane.
- Since $k_\perp >> k_\parallel$ for unstable bounce modes in typical mirror experiments, Poisson's equation nearly separates into parallel and perpendicular parts. Baldwin[56] has suggested that approximate solutions for the wave potential in realistic geometries could be obtained by treating the radial dependence of ϕ as a perturbation of the one-dimensional model used in the present work. In principal, the effect of field line fanning can likewise be treated as a perturbation provided that $k_\perp(s)$ varies slowly enough. An approximate solution of this sort for three-

dimensional eigenmodes is probably necessary for an adequate treatment of small W_e/W_i plasmas like that in BBI.

- Electromagnetic bounce modes could be analyzed by using accurate electron trajectories as in Chapter 2 to calculate the perturbed distribution function and then obtaining an integral equation for the wave electric field from the linearized Ampere equation. This analysis would be appropriate for proposed high-density mirror experiments such as MFTF.

Even though electrostatic bounce modes are not a significant instability mechanism in the plasma regimes currently under study, the underlying phenomenon of periodic trapped particle motion supporting plasma modes is found whenever coherent disturbances can persist longer than a typical bounce period. Trapped particle modes in tokamak devices[57] are an example. The integral equation method used here for electrostatic modes is generally useful in other geometries so long as particle motion remains periodic over time scales of interest.

Appendix A. Notation

The following symbols are consistently used throughout the text:

a_α	gyroradius of species α
$\underline{B}$	magnetostatic field
B	magnetic field strength
C_α	normalization constant for distribution function of species α
c	speed of light
E	total particle energy
e	electron charge
F_α	particle distribution function of species α
f_α	perturbation of F_α due to wave
$\underline{k}$	wave propagation vector
k_m	wave number for mth Fourier mode
m_α	particle mass of species α
N_α	number density of species α
n_α	perturbation of N_α due to wave
q_α	particle charge of species α
$\hat{k}_{mn}$	response matrix for species α
r	flux surface radius
S_{mn}	mth Fourier coefficient of $sc(k_n s)$
s	distance coordinate along a flux line
sc	sine or cosine respectively for odd or even Fourier series
T_{lm}	mth Fourier coefficient of $sc[(2\ell+\sigma)\omega t]$
t	time
V_α	thermal speed of species
$V_\parallel$	rms ion velocity along a flux line
$V_\perp$	rms ion velocity perpendicular to a flux line
$\underline{v}$	particle velocity

v	particle velocity magnitude
W_α	thermal energy of species α
$\underset{\sim}{x}$	particle position
Γ^α	imaginary response of species α
γ	wave growth rate
δ_{res}	relative frequency shift from resonance
ϵ	dimensionless centerplane density parameter $(\omega_{pi0}/\Omega_{i0})^2$
ζ	dimensionless parameter $k_{\perp 0} v_{\perp 0}/\Omega_{i0}$
θ	particle gyrophase
Λ_j	ion coupling coefficient for jth ion gyrofrequency harmonic
λ	dimensionless parameter $(k_{\perp 0}\lambda_{De0})^2$
λ_{De0}	electron centerplane Debye length
μ	particle magnetic moment
ξ	dimensionless parameter $(\omega_{b0} s_{max}/v_e)^2$
σ	parity parameter
Φ	plasma electrostatic potential
ϕ	perturbation of Φ due to wave
$\hat{\phi}_m$	mth Fourier coefficient of ϕ
χ	dimensionless distance coordinate along a flux line s/s_{max}
ψ	electron electrostatic potential energy $-e\Phi$
Ω_α	gyrofrequency of species α
ω	wave frequency
ω_b	electron bounce frequency
$\omega_{p\alpha}$	plasma frequency of species α
ω_r	real part of wave frequency

In addition, several modifying subscripts are used consistently. For a vector or scalar quantity A, the following meanings are associated with subscripted A:

$A_\parallel$	vector component of $\underset{\sim}{A}$ along a flux line
$A_\perp$	vector component of $\underset{\sim}{A}$ perpendicular to a flux line

A_e	value of A for electrons
A_i	value of A for ions
A_0	value of A at the mirror field centerplane s = 0
A_{max}	maximum occurring value of A
A_{res}	value of A associated with resonance
A_{th}	value of A associated with the onset of instability

Mathematical operations and constants are denoted conventionally, and the notation of Abramowitz and Stegun[58] is adopted for special functions:

B(w,z)	beta function $B(w,z) = \int_0^1 dy\ y^{w-1}(1-y)^{z-1}$
$E_1(z)$	complex exponential integral $E_1(z) = \int_z^\infty dy\ y^{-1}\exp(-y)$
$E_i(z)$	real exponential integral $E_i(z) = -\int_{-z}^\infty dy\ y^{-1}\exp(-y)$
erf(z)	error function $\mathrm{erf}(z) = \int_0^z dy\ \exp(-y^2)$
exp(z)	exponential function
$I_\ell(z)$	modified Bessel function of the first kind
Im(z)	imaginary part of z
i	$(-1)^{1/2}$
$J_\ell(z)$	Bessel function of the first kind
$K(\alpha)$	complete elliptic integral of the first kind $K(\alpha) = \int_0^{\pi/2} dy\ (1 - \alpha \sin^2 y)^{-1/2}$
$\max(\alpha,\beta,\ldots)$	maximum of set $\alpha,\beta,\ldots$
$\min(\alpha,\beta,\ldots)$	minimum of set $\alpha,\beta,\ldots$
$O(\alpha)$	of the order of α
Re(z)	real part of z
$\Gamma(\alpha)$	gamma function $\Gamma(\alpha) = \int_0^\infty dy\ y^{\alpha-1}\exp(-y)$

$\Gamma(\alpha,z)$ incomplete gamma function $\Gamma(\alpha,z) = \int_z^\infty dy\ y^{\alpha-1}\exp(-y)$

$\gamma(\alpha,z)$ incomplete gamma function $\gamma(\alpha,z) = \int_0^z dy\ y^{\alpha-1}\exp(-y)$

π 3.14159265358979

$|\alpha|$ absolute magnitude of vector or scalar α

Where dimensioned quantities are used, cgs-Gaussian units are understood. Jackson[59] discusses this choice of units and gives conversions to other systems. In these units,

$$e = 4.8 \times 10^{-10}\text{esu}$$

$$\omega_{pe} = \left(\frac{4\pi\ e^2\ N_e}{m_e}\right)^{1/2} = 5.64 \times 10^4\left[N_e(\text{cm}^{-3})\right]^{1/2}\ \text{s}^{-1}$$

$$\omega_{pi} = \left(\frac{4\pi\ e^2\ N_i}{m_i}\right)^{1/2} = 1.32 \times 10^3\left[N_i(\text{cm}^{-3})\right]^{1/2}\ \text{s}^{-1}\ \text{for } H^+ \text{ ions}$$

$$\Omega_e = \frac{eB}{m_e c} = 1.76 \times 10^7\ B(G)\ \text{s}^{-1}$$

$$\Omega_i = \frac{eB}{m_i c} = 9.59 \times 10^3\ B(G)\ \text{s}^{-1}\ \text{for } H^+ \text{ ions}$$

$$\lambda_{De} = \left(\frac{W_e}{4\pi\ e^2\ N_e}\right)^{1/2} = 7.44 \times 10^2\left[\frac{W_e(\text{eV})}{N_e(\text{cm}^{-3})}\right]\ \text{cm}$$

Appendix B. Normalization of Distribution Functions

The electron distribution function $F_e^{\pm}(E,\mu)$ is normalized so that

$$N(s) = 2\pi \frac{N_0\, B(s)}{m_e^2} \int_0^{\infty} d\mu \int_{\mu B(s)+\psi(s)}^{\mu B_{max}+\psi_{max}} \frac{dE\; F_e^{+}(E,\mu) + F_e^{-}(E,\mu)}{\left[\frac{2}{m_e}\left(E-\mu B(s) - \psi(s)\right)\right]^{1/2}}, \quad \text{(B1)}$$

where all symbols are defined in Appendix A.

For a Maxwellian distribution,

$$F_e(E,\mu) = C_e \exp\left(-\frac{E}{W_e}\right), \quad \text{(B2)}$$

the E integration in Eq. (B1) is conveniently written in terms of variables $x = \mu B/W_e$ and $y = (E - \mu B - \psi)/W_e$:

$$\frac{N}{N_0} = \pi C_e V_e^3 \exp\left(-\frac{\psi}{W_e}\right) \int_0^{\infty} dx \exp(-x) \int_0^{\Delta\psi + \frac{\Delta B}{B}x} dy \frac{\exp(-y)}{y^{1/2}}, \quad \text{(B3)}$$

where $\Delta B = B_{max} - B$ and $\Delta\psi = (\psi_{max} - \psi)/W_e$, and the s dependence of N, B, and ψ has been suppressed. The integral may be formally evaluated as follows:

$$\int_0^{\infty} dx \exp(-x) \int_0^{\alpha+\beta x} dy \frac{\exp(-y)}{y^{1/2}} = \left[-\exp(-x)\gamma\left(\frac{1}{2},\ \alpha + \beta x\right)\right]_0^{\infty}$$

$$+ \beta \int_0^{\infty} dx \frac{\exp[-\alpha - (1+\beta)x]}{(\alpha+\beta x)^{1/2}}$$

$$= \gamma\left(\frac{1}{2},\alpha\right) + \left(\frac{\beta}{1+\beta}\right)^{1/2} \exp\left(\frac{\alpha}{\beta}\right)\Gamma\left(\frac{1}{2},\ \alpha\frac{1+\beta}{\beta}\right), \quad \text{(B4)}$$

where the incomplete gamma functions γ and Γ are defined[60]

$$\gamma(\alpha,x) \equiv \int_0^x dy\, y^{a-1}\exp(-y),$$

$$\Gamma(a,x) \equiv \int_x^\infty dy\ y^{a-1}\exp(-y) = \Gamma(a) - \gamma(a,x). \tag{B5}$$

If the identifications $\alpha = \Delta\psi$ and $\beta = \Delta B/B$ are made in Eq. (B3) and the relation $\gamma\left(\frac{1}{2},x\right) = \pi^{1/2}\ \mathrm{erf}(x^{1/2})$ is used, then Eq. (B3) reduces to

$$\frac{N}{N_0} = \pi^{3/2}\ C_e V_e^{\ 3}\left\{\exp\left(\frac{-\psi}{W_e}\right)\mathrm{erf}\left[(\Delta\psi)^{1/2}\right] + \left(\frac{\Delta B}{B_{max}}\right)^{1/2}\exp\left(\frac{B\psi_{max} - B_{max}\psi}{W_e\ \Delta B}\right)\left(1-\mathrm{erf}\left[\left(\frac{B_{max}}{\Delta B}\ \Delta\psi\right)^{1/2}\right]\right)\right\}. \tag{B6}$$

Since $\psi = 0$ at the centerplane, Eq. (B6) yields

$$C_e^{-1} = \pi^{3/2}\ V_e^{\ 3}\left\{\mathrm{erf}\left[\left(\frac{\psi_{max}}{W_e}\right)^{1/2}\right] + \left(\frac{B_{max}-B_0}{B_{max}}\right)^{1/2}\exp\left(\frac{B_0}{B_{max}-B_0}\ \frac{\psi_{max}}{W_e}\right)\left(1-\mathrm{erf}\left[\left(\frac{B_{max}}{B_{max}-B_0}\ \frac{\psi_{max}}{W_e}\right)^{1/2}\right]\right)\right\}. \tag{B7}$$

As $B_{max} \to B_0$, the asymptotic expansion

$$\mathrm{erf}(z) \sim 1 - \frac{1}{\pi^{1/2}\ z}\exp(-z^2) \tag{B8}$$

may be used to find C_e in this limit:

$$C_e^{-1} \approx \pi^{3/2} V_e^3\ \mathrm{erf}\left[\left(\frac{\psi_{max}}{W_e}\right)^{1/2}\right]. \tag{B9}$$

This form approaches the normalization constant

$$C_e^{-1} \approx \pi^{3/2} V_e^3 \tag{B10}$$

of an unconfined Maxwellian distribution as ψ_{max}/W_e becomes large.

For a cutoff Maxwellian distribution,

$$F_e(E,\mu) = C_e(\mu B_{max} + \psi_{max} - E)\exp\left(-\frac{E}{W_e}\right), \tag{B11}$$

The number density integral, Eq. (B1), is rewritten in terms of x and y as

$$\frac{N}{N_0} = \pi C_e V_e^3 W_e \exp\left(-\frac{\psi}{W_e}\right)\int_0^\infty dx \exp(-x, \int_0^{\Delta\psi + \frac{\Delta B}{B}x} dy$$

$$\left(\Delta\psi + \frac{\Delta B}{B}x - y\right)\frac{\exp(-y)}{y^{1/2}} \quad . \tag{B12}$$

The first integral required has the same form as Eq. (B4). The remaining two are evaluated as follows:

$$\int_0^\infty dx\ x \exp(-x)\int_0^{\alpha+\beta x} dy\ \frac{\exp(-y)}{y^{1/2}}$$

$$= \left[-(1+x)\exp(-x)\gamma\left(\frac{1}{2},\ \alpha+\beta x\right)\right]_0^\infty + \beta\int_0^\infty dx\ (1+x)\ \frac{\exp[-a\ -\ (1+\beta)x]}{(\alpha+\beta x)^{1/2}}$$

$$= \gamma\left(\frac{1}{2},\alpha + \frac{\beta}{1+\beta}\right)^{1/2}\left[\left(\frac{\beta-\alpha}{\beta}\right)\Gamma\left(\frac{1}{2},\ \frac{1+\beta}{\beta}\ \alpha\right) + \frac{1}{1+\beta}\ \Gamma\left(\frac{3}{2},\ \frac{1+\beta}{\beta}\ \alpha\right)\right]\exp\left(\frac{\alpha}{\beta}\right) \tag{B13}$$

and

$$\int_0^\infty dx \exp(-x)\int_0^{\alpha+\beta x} dy\ y^{1/2}\exp(-y)$$

$$= \left[-\exp(-x)\gamma\left(\frac{3}{2},\ \alpha+\beta x\right)\right]_0^\infty + \beta\int_0^\infty dx\ (\alpha+\beta x)^{1/2}\exp\left[-\alpha-(1+\beta)x\right]$$

$$= \gamma\left(\frac{3}{2},\alpha\right)+\left(\frac{\beta}{1+\beta}\right)^{3/2}\exp\left(\frac{\alpha}{\beta}\right)\Gamma\left(\frac{3}{2},\ \frac{1+\beta}{\beta}\ \alpha\right). \tag{B14}$$

Substituting Eqs. (B4), (B13), and (B14) into Eq. (B12) and again taking $\alpha = \Delta\psi$ and $\beta = \Delta B/B$ gives

$$\frac{N}{N_0} = \pi C_e V_e^3 W_e \left\{\pi^{1/2}\exp\left(-\frac{\psi}{W_e}\right)\left(\Delta\psi + \frac{\Delta B}{B} - \frac{1}{2}\right)\mathrm{erf}\left[(\Delta\psi)^{1/2}\right]\right.$$

$$\left. + \left(\frac{\pi\ \Delta B^3}{B^2 B_{max}}\right)^{1/2}\exp\left(\frac{B\psi_{max} - B_{max}\psi}{W_e\ \Delta B}\right)\left(1-\mathrm{erf}\left[\left(\frac{B_{max}}{\Delta B}\ \Delta\psi\right)^{1/2}\right]\right) + (\Delta\psi)^{1/2}\ \exp\left(-\frac{\psi_{max}}{W_e}\right)\right\}. \tag{B15}$$

Evaluating Eq. (B15) at the centerplane then leads to

$$C_e^{-1} = \pi V_e^3 W_e \left\{ \pi^{1/2} \left(\frac{\psi_{max}}{W_e} + \frac{B_{max}}{B_0} - \frac{3}{2} \right) \text{erf} \left[\left(\frac{\psi_{max}}{W_e} \right)^{1/2} \right] \right.$$

$$+ \left[\frac{\pi (B_{max} - B_0)^3}{B_0^2 B_{max}} \right]^{1/2} \exp \left(\frac{B_0}{B_{max} - B_0} \frac{\psi_{max}}{W_e} \right) \left(1 - \text{erf} \left[\left(\frac{B_{max}}{B_{max} - B_0} \frac{\psi_{max}}{W_e} \right)^{1/2} \right] \right)$$

$$\left. + \left(\frac{\psi_{max}}{W_e} \right)^{1/2} \exp \left(- \frac{\psi_{max}}{W_e} \right) \right\} . \qquad \text{(B16)}$$

In the limit $B_{max} \to B_0$, Eq. (B16) reduces to

$$C_e^{-1} = \pi V_e^3 W_e \left\{ \pi^{1/2} \left(\frac{\psi_{max}}{W_e} - \frac{1}{2} \right) \text{erf} \left[\left(\frac{\psi_{max}}{W_e} \right)^{1/2} \right] + \left(\frac{\psi_{max}}{W_e} \right)^{1/2} \exp \left(- \frac{\psi_{max}}{W_e} \right) \right\} . \qquad \text{(B17)}$$

For large ψ_{max}/W_e, the first ψ_{max} term is dominant, and Eq. (B17) again reduces to the normalization constant for an unbounded Maxwellian distribution, Eq. (B10), multiplied by ψ_{max}.

For the ion distribution treated,

$$F_i(s, v_{\parallel}, v_{\perp}) = \frac{N(s)}{N_0} F_{\parallel}(v_{\parallel}) F_{\perp}(v_{\perp}^2), \qquad \text{(B18)}$$

the functions $F_{\parallel}$ and $F_{\perp}$ are unit normalized separately. The parallel distribution must satisfy

$$\int_{-\infty}^{\infty} dv_{\parallel} F_{\parallel}(v_{\parallel}) = 1, \qquad \text{(B19)}$$

and for a Gaussian form,

$$F_{\parallel}(v_{\parallel}) = C_{\parallel} \exp(-\alpha v_{\parallel}^2), \qquad \text{(B20)}$$

Eq. (B19) gives

$$C_{\parallel} = \left(\frac{\alpha}{\pi}\right)^{1/2}. \tag{B21}$$

The average of $v_{\parallel}^2$,

$$\langle v_{\parallel}^2 \rangle = C_{\parallel} \int_{-\infty}^{\infty} dv_{\parallel}\, v_{\parallel}^2\, F_{\parallel}(v_{\parallel}) = \frac{C_{\parallel}}{2} \frac{\pi^{1/2}}{\alpha^{3/2}}, \tag{B22}$$

leads to the relation

$$\alpha = \frac{1}{2\langle v_{\parallel}^2 \rangle} \equiv \frac{1}{V_{\parallel}^2}. \tag{B23}$$

The perpendicular distribution is normalized so that

$$\pi \int_0^{\infty} dv_{\perp}^2\, F_{\perp}(v_{\perp}^2) = 1. \tag{B24}$$

For a sharply peaked distribution,

$$F_{\perp}(v_{\perp}^2) = C_{\perp}\, \delta(v_{\perp}^2 - \alpha), \tag{B25}$$

Eq. (B24) gives immediately

$$C_{\perp} = \frac{1}{\pi}, \tag{B26}$$

and the integral of v^2 yields

$$\langle v_{\perp}^2 \rangle = \pi \int_0^{\infty} dv_{\perp}^2\, v_{\perp}^2\, F_{\perp}(v_{\perp}^2) = \alpha. \tag{B27}$$

For the family of spread distribution functions

$$F_{\perp}^{(j)}(v_{\perp}^2) = C_{\perp}^{(j)} v_{\perp}^{2j} \exp\left[-(j+1)\alpha v_{\perp}^2\right], \tag{B28}$$

Eq. (B24) leads to

$$C_{\perp}^{(j)} = \frac{[(j+1)\alpha]^{j+1}}{\pi j!}, \tag{B29}$$

and calculating $\langle v_\perp^2 \rangle$ gives the result $\alpha = V_\perp^{-2}$. In particular, for j = 1

$$C_\perp = \frac{4}{\pi V_\perp^4} \quad . \tag{B30}$$

Since the parallel and perpendicular ion distributions are treated as independent, there is formally no relation between $V_\parallel$ and $V_\perp$. An expression relating the two root mean squared velocities appropriate for magnetically confined ions may nonetheless be derived by taking

$$F_i\ (E,\mu) = C_i\ (\mu B_{max} - E)\ \exp -\left(\frac{E}{W_i}\right) . \tag{B31}$$

The electrostatic potential has been neglected here because $W_i \gg W_e \sim \psi_{max}$ is normally valid in mirror devices. If the velocity components are written as $v_\parallel^2 = 2(E - \mu B)/m_i$ and $v_\perp^2 = 2\mu B/m_i$, the parallel average is

$$V_\parallel^2 = 2\langle v_\parallel^2 \rangle = \frac{8\pi B}{m_i^2} C_i \int_0^\infty d\mu \int_{\mu B}^{\mu B_{max}} dE \left[\frac{2}{m_i}(E-\mu B)\right]^{1/2} (\mu B_{max} - E)\ \exp\left(-\frac{E}{W_i}\right), \tag{B32}$$

where the s dependence of B is again suppressed. In terms of variables $x = \mu B/W_i$ and $y = (E-\mu B)/W_i$, Eq. (B32) is written

$$V_\parallel^2 = 2\pi\ C_i V_i^5 W_i \int_0^\infty dx\ \exp(-x) \int_0^{\beta x} dy\ y^{1/2}\ (\beta x - y)\ \exp(-y), \tag{B33}$$

where $\beta = (B_{max} - B)/B$. Since

$$\int_0^\infty ix\ x\ \exp(-x) \int_0^{\beta x} dy\ y^{1/2}\ \exp(-y) = \beta^{3/2} \int_0^\infty dx\ x^{1/2}\ (1-x)\ \exp\left[-(1+\beta)x\right]$$

$$= \left(\frac{\beta}{1+\beta}\right)^{3/2} \left[\Gamma\left(\frac{3}{2}\right) + \frac{\Gamma\left(\frac{5}{2}\right)}{1+\beta}\right], \tag{B34}$$

and

$$\int_0^\infty dx\, \exp(-x) \int_0^{\beta x} dy\, y^{3/2} \exp(-y) = \beta^{5/2} \int_0^\infty dx\, x^{3/2} \exp[-(1+\beta)x]$$

$$= \left(\frac{\beta}{1+\beta}\right)^{5/2} \Gamma\left(\frac{5}{2}\right), \tag{B35}$$

the $V_\parallel^2$ expression, Eq. (B33) reduces to

$$V_\parallel^2 = 2\pi C_i V_i^5 W_i \frac{\beta^{5/2}\, \Gamma\left(\frac{3}{2}\right)}{(1+\beta)^{3/2}}. \tag{B36}$$

The $V_\perp^2$ integral,

$$V_\perp^2 \equiv \langle v_\perp^2 \rangle = \frac{4\pi B}{m_i^2} C_i \int_0^\infty d\mu \int_{\mu B}^{\mu B_{max}} dE\, \frac{2\mu B}{m_i} \left[\frac{2}{m_i}(E-\mu B)\right]^{1/2} \exp\left(-\frac{E}{W_i}\right), \tag{B37}$$

is similarly rewritten in terms of x,y, and β:

$$V_\perp^2 = \pi C_i V_i^5 W_i \int_0^\infty dx\, x \exp(-x) \int_0^{\beta x} dy\, \frac{\beta x - y}{y^{1/2}} \exp(-y). \tag{B38}$$

The required integrals are Eq. (B34) and

$$\int_0^\infty dx\, x^2 \exp(-x) \int_0^{\beta x} dy\, \frac{\exp(-y)}{y} = \beta^{1/2} \int_0^\infty dx\, \frac{x^2 - 2x + 2}{x^{1/2}} \exp[-(1+\beta)x]$$

$$= \left(\frac{\beta}{1+\beta}\right)^{1/2} \left[\frac{\Gamma\left(\frac{5}{2}\right)}{(1+\beta)^2} + \frac{2\Gamma\left(\frac{3}{2}\right)}{1+\beta} + 2\Gamma\left(\frac{1}{2}\right)\right]. \tag{B39}$$

Substituting Eqs. (B34) and (B39) into Eq. (B38) gives

$$V_\perp^2 = \pi C_i V_i^5 W_i \left(\frac{\beta}{1+\beta}\right)^{3/2} \left[\Gamma\left(\frac{3}{2}\right) + 2\Gamma\left(\frac{1}{2}\right)(1+\beta)\right]. \tag{B40}$$

The velocity ratio is then

$$\frac{V_{\parallel}^2}{V_{\perp}^2} = \frac{2\beta}{1 + 2(1+\beta)\,\Gamma(1/2)/\Gamma(3/2)} = \frac{2(B_{max} - B)}{4\,B_{max} + B} \,. \tag{B41}$$

Even though the loss-cone distribution, Eq. (B31), is inconsistent with Eq. (B18), the velocity ratio, Eq. (B41), may be evaluated at the ion resonance point s_{res} defined by $\omega = j\Omega_i(s_{res})$ and then used to relate the mean squared velocity components appearing in $F_{\parallel}$ and $F_{\perp}$. This is a useful approximation because it is accurate where ion-wave interaction is strongest.

Appendix C. Symmetry of Eigenfunctions

The integral equation for the wave potential ϕ is given by the perturbed Poisson equation, Eq. (27), with the density perturbation, Eq. (36):

$$-K_{\perp 0}^2\,\phi(s) = 2\pi B_0 \sum_{\alpha} \frac{\omega_{p\alpha 0}^2}{m_\alpha} \int_0^\infty d\mu \int_{\mu B(s)+\psi(s)}^{\mu B_{max}+\psi_{max}} \frac{dE}{|v_\parallel(s)|} \left\{ 2\,\frac{\partial F_\alpha}{\partial E}\,\phi(s) \right.$$

$$-i \sum_{j=-\infty}^{\infty} \left[\omega\,\frac{\partial F_\alpha}{\partial E} + \frac{j\Omega}{B}\,\frac{\partial F_\alpha}{\partial \mu} \right] J_j^2\left(\frac{K_\perp v_\perp}{\Omega}\right) \sum_{\pm} \int_{-\infty}^{t} dt'\, \phi\left[s_\alpha^{\pm}(t')\right]$$

$$\left. \exp\left[-i \int_{t'}^{t} dt'' \left(\omega - j\Omega_\alpha\left[s_\alpha^{\pm}(t'')\right] \right) \right] \right\} . \qquad \text{(C1)}$$

As in Chapter 2, $s_\alpha^{\pm}(t')$ denote positive and negative going particle trajectories intersecting s at time t, and the E and μ dependences of integrand quantities have been suppressed. To display the symmetries of Eq. (C1), it is convenient to rewrite the equation as follows:

$$0 = \sum_{\pm} \sum_{\alpha} \int_{-\infty}^{t} dt' \int_0^\infty d\mu \int_{\mu B(s)+\psi(s)}^{\mu B_{max}+\psi_{max}} \frac{dE}{|v_\parallel(s)|} \left\{ C_\alpha\,\delta(t-t') \right.$$

$$\left. - \sum_{j=-\infty}^{\infty} C_{\alpha j} \exp\left[-i \int_{t'}^{t} dt'' \left(\omega - j\Omega_\alpha\left[s_\alpha^{\pm}(t'')\right] \right) \right] \right\} \phi\left[s_\alpha^{\pm}(t')\right] \qquad \text{(C2)}$$

where

$$C_\alpha \equiv \frac{\omega_{p\alpha 0}^2}{m_\alpha} \left(\frac{\partial F_\alpha}{\partial E} + \frac{K_{\perp 0}^2\, F_\alpha}{8\pi\, B_0} \right),$$

and

$$C_{\alpha j} \equiv \frac{i\,\omega_{p\alpha 0}^2}{m_\alpha} \left(\omega\,\frac{\partial F_\alpha}{\partial E} + \frac{j\Omega}{B}\,\frac{\partial F_\alpha}{\partial \mu} \right) J_j^2 \left[\frac{K_\perp}{\Omega} \left(\frac{2B\mu}{m_\alpha} \right)^{1/2} \right] .$$

When a trajectory $s_\alpha(t')$ defined as in Chapter 2 crosses the centerplane with positive velocity at time $t' = 0$, the relations, Eq. (49), allow the sum over positive and negative going orbits Eq. (C2) to be performed:

$$0 = \sum_\alpha \int_{-\infty}^{t} dt' \int_0^\infty d\mu \int_{\mu B(s)+\psi(s)}^{\mu B_{max}+\psi} dE \frac{1}{|v_\parallel(s)|}$$

$$\times \left\{ \left[C_\alpha \, \delta(t-t') - \sum_{j=-\infty}^{\infty} C_{\alpha j} \exp\left[-i \int_{t'}^{t} dt'' \left(\omega - j\Omega_\alpha \left| s_\alpha(t'-t_0) \right| \right) \right] \right] \phi \left| s_\alpha(t'-t_0) \right| \right.$$

$$\left. + \left[C_\alpha \delta(t-t') - \sum_{j=-\infty}^{\infty} C_{\alpha j} \exp\left[-i \int_{t'}^{t} dt'' \left(\omega - j\Omega_\alpha \left| s_\alpha(2t-t'-t_0) \right| \right) \right] \right] \phi \left| s_\alpha(2t-t'-t_0) \right| \right\}$$

$$= \sum_\alpha \int_{-\infty}^{\infty} d\tau' \int_0^\infty d\mu \int_{\mu B(s)+\psi(s)}^{\mu B_{max}+\psi_{max}} dE \frac{1}{|v_\parallel(s)|} \tag{C3}$$

$$\times \left\{ C_\alpha \, \delta(\tau' - t + t_0) - \sum_{j=-\infty}^{\infty} C_{\alpha j} \exp\left[-i \int_{\tau'}^{t-t_0} |d\tau''| \left(\omega - j\Omega_\alpha \left| s_\alpha(\tau'') \right| \right) \right] \right\} \phi \left| s_\alpha(\tau') \right| \, .$$

From the definition of t_0, Eq. (50), the quantity

$$\tau \equiv t - t_0(s) = \int_0^s \frac{ds'}{|v_\parallel(s')|} \tag{C4}$$

is a single-valued function of s, and the inverse function is

$$s = s_\alpha(\tau) \, . \tag{C5}$$

The integral equation, Eq. (C3), may then be written

$$0 = \sum_\alpha \int_{-\infty}^{\infty} d\tau' \, K_\alpha(\tau,\tau') \, \phi \left| s_\alpha(\tau') \right| \, , \tag{C6}$$

where

$$K_\alpha(\tau,\tau') \equiv \int_0^\infty d\mu \int_{\mu B[s_\alpha(\tau)]}^{\mu B_{max}+\psi_{max}} dE \frac{1}{|v_\parallel[s_\alpha(\tau)]|} \left\{ C_\alpha \, \delta(\tau-\tau') - \sum_{j=-\infty}^{\infty} C_{\alpha j} \right.$$

$$\left. \exp\left[-i \int_{\tau'}^{\tau} d\tau'' \left(\omega - j\Omega_\alpha \left| s_\alpha(\tau'') \right| \right) \right] \right\} .$$

When B and ψ are even functions of s, the trajectories s_α are odd functions of time. In this case, K_a has the symmetry

$$K_\alpha(\tau,\tau') = K_\alpha(-\tau,-\tau'), \tag{C7}$$

and since a solution ϕ must be valid for any τ, it follows that

$$0 = \sum_\alpha \int_{-\infty}^{\infty} d\tau'\ K_\alpha(-\tau,\tau')\ \phi\left|s_\alpha(\tau')\right| = \sum_\alpha \int_{-\infty}^{\infty} d\tau'\ K_\alpha(-\tau,-\tau')\ \phi\left|s_\alpha(-\tau)\right|$$

$$= \sum_\alpha \int_{-\infty}^{\infty} d\tau'\ K_\alpha\ (\tau,\tau')\ \phi\left|-s_\alpha(\tau')\right| . \tag{C8}$$

The function $\phi(-s)$ is therefore also a solution of the integral equation. Because Eq. (C6) determines ϕ within a constant factor, Eq. (C8) gives

$$\phi(s) = C\phi(-s). \tag{C9}$$

Repeated substitution of Eqs. (C7) and (C9) in the integral equation then yields

$$\sum_\alpha \int_{-\infty}^{\infty} d\tau'\ K_\alpha(\tau,\tau')\ \phi\left|s_\alpha(\tau')\right| = C \sum_\alpha \int_{-\infty}^{\infty} d\tau'\ K_\alpha(\tau,-\tau')\ \phi\left|s_\alpha(\tau')\right|$$

$$= C^2 \sum_\alpha \int_{-\infty}^{\infty} d\tau'\ K_\alpha(\tau,\tau')\ \phi\left|s_\alpha(\tau')\right|. \tag{C10}$$

Since $C^2 = 1$ according to Eq. (C10), $C = \pm 1$, and ϕ is either an even or odd function of s.

Appendix D. Analytic Approximations of R^e_{mn} and R^i_{mn}

Analytic approximations of the electron and ion response matrices R^e_{mn} and R^i_{mn} are useful both to check the numerical evaluation procedures and to show the explicit dependences of the matrices on plasma and field parameters.

A simplified expression for R^e_{mn} is obtained from Eq. (56) by assuming Maxwellian electrons and by treating electron orbits as simple harmonic motion. A Maxwellian electron distribution is written in terms of χ and μ as

$$F_e = C_e \exp\left[-\frac{\mu B(\chi s_{max}) + \psi(\chi s_{max})}{W_e}\right], \tag{D1}$$

where Eq. (B7) gives the normalization constant. This form is used both because electrostatically trapped electrons are expected to be near thermal equilibrium and because the resulting R^e_{mn} expressions are significantly simpler than those derived for a cutoff Maxwellian distribution. The assumption of sinusoidal electron orbits is made to permit exact evaluation of the integrals S_{mn} and T_{lm} in terms of Bessel functions. Since an electron turns at $s_t = \chi s_{max}$, the appropriate sinusoidal trajectory for a bounce frequency ω_b is

$$s(t;E,\mu) = \chi s_{max} \sin\left|\omega_b(\chi,\mu)t\right|. \tag{D2}$$

This expression is exact for quadratic ψ and B fields. In this case, S_{mn} from Eq. (57) takes the form

$$S_{mn}(\chi,\mu) = \frac{4}{\pi}\int_0^{\pi/2} d\bar{t}\ sc\left|\bar{k}_m \chi \sin(\bar{t})\right| sc\left|\bar{k}_n \chi \sin(\bar{t})\right|, \tag{D3}$$

where $\bar{t} = \omega_b(\chi,\mu)t$ and $\bar{k}_m = k_m s_{max}$. With the identity

$$sc(x)sc(y) = \frac{1}{2}\,\mathrm{Re}\left\{\exp[i(x-y)] + (-1)^{\sigma}\exp[i(x+y)]\right\} \tag{D4}$$

and the integral representation of Bessel functions of the first kind

$$J_n(x) = \frac{1}{2\pi}\int_{-\pi}^{\pi} dy\ \exp[-iny + i\,x\sin(y)], \tag{D5}$$

Eq. (D3) is rewritten

$$S_{mn}(\chi,\mu) = \frac{1}{\pi}\int_{-\pi/2}^{\pi/2} d\bar{t}\,\left\{\exp\left[i(\bar{k}_m-\bar{k}_n)\chi\,\sin(\bar{t})\right]+(-1)^{\sigma}\exp\left[i(\bar{k}_m+\bar{k}_n)\,\sin(\bar{t})\right]\right\}$$

$$= J_0\left[(\bar{k}_m-\bar{k}_n)\chi\right] + (-1)^{\sigma} J_0\left[(\bar{k}_m+\bar{k}_n)\chi\right] . \qquad (D6)$$

The integral T_{1m} from Eq. (52) is similarly reformulated as

$$T_{1m}(\chi,\mu) = \frac{4}{\pi}\int_0^{\pi/2} d\bar{t}\,\mathrm{sc}\left[(2\ell+\sigma)\bar{t}\right]\mathrm{sc}\left[\bar{k}_m\chi\,\sin(\bar{t})\right]$$

$$= \frac{1}{2\pi}\int_{-\pi}^{\pi} d\bar{t}\,\left\{\exp\left[i(2\ell+\sigma)\bar{t} - ik_m\,\sin(\bar{t})\right]+(-1)^{\sigma}\exp\left[i(2\ell+\sigma)\bar{t} + ik_m\chi\,\sin(\bar{t})\right]\right\}$$

$$= J_{-(2\ell+\sigma)}(-\bar{k}_m\chi) + (-1)^{\sigma}J_{-(2\ell+\sigma)}(\bar{k}_m\chi)$$

$$= 2J_{2\ell+\sigma}(\bar{k}_m\chi). \qquad (D7)$$

Here, the Bessel function symmetry relations apparent in Eq. (D5)

$$J_n(-x) = J_{-n}(x) = (-1)^n J_n(x)$$

have been used. These orbit integral expressions are exact when the unperturbed fields are quadratic functions of s, and they are close approximations except for strongly nonquadratic fields. When Eqs. (D6) and (D7) are substituted for S_{mn} and T_{1m}, the R^e_{mn} expression reduces to Eq. (63).

The bounce frequency ω_b required to evaluate the μ integrals I_1 and I_2 in Eq. (63) is found as an explicit function of χ and μ by approximately evaluating Eq. (45) for general symmetric equilibrium fields. If terms of higher order than s^4 are negligible in the power series

$$\psi(s) = A_1 s^2 + A_2 s^4 + \ldots$$

and

$$B(s) = B_0 + B_1 s^2 + B_2 s^4 + \ldots \tag{D8}$$

representing ψ and B, then Eq. (45) becomes

$$\frac{\pi}{2\omega_b(\chi,\mu)} \approx \int_0^{\chi} dx \, \frac{1}{\left(\frac{2}{m_e}\right)^{1/2} \left|\beta_1(\chi^2 - x^2) + \beta_2'^{\,4} - x^4)\right|^{1/2}} , \tag{D9}$$

where $x = s/s_{max}$ is used as the integration variable, and $\beta_j \equiv (A_j + \mu B_j) s_{max}^{2j-2}$ are understood to be functions of μ. When $\beta_2 \geq 0$, the change of variables $\cos y = x/\chi$ reduces Eq. (D9) to

$$\frac{\pi}{2\omega_b(\chi,\mu)} \approx \left(\frac{m_e}{2}\right)^{1/2} \int_0^{\pi/2} dy \, \frac{1}{\left|\beta_1 + \beta_2\chi^2(1 + \cos^2 y)\right|^{1/2}}$$

$$\approx \left(\frac{m_e}{2} \frac{1}{\beta_1 + 2\beta_2\chi^2}\right)^{1/2} K\left(\frac{\beta_2\chi^2}{\beta_1 + 2\beta_2\chi^2}\right) , \tag{D10}$$

where K denotes a complete elliptic integral of the first kind

$$K(\alpha) \equiv \int_0^{\pi/2} dy \, \frac{1}{(1 - \alpha \sin^2 y)^{1/2}} \quad \text{for } \alpha \geq 0. \tag{D11}$$

Similarly, the substitution $\sin y = x/\chi$ gives

$$\frac{\pi}{2\omega_b(\chi,\mu)} \approx \left(\frac{m_e}{2} \frac{1}{\beta_1 - |\beta_2|\chi^2}\right)^{1/2} K\left(\frac{|\beta_2|\chi^2}{\beta_1 - |\beta_2|\chi^2}\right) \tag{D12}$$

for $\beta_2 \leq 0$. Since B and Φ are required to be monotonic, the denominator $\beta_1 - |\beta_2|\chi^2$ in Eq. (D12) is always positive. The bounce frequency for quartic fields is then

$$\omega_b(\chi,\mu) = \frac{\pi}{2}\left(\frac{2}{m_e}\right)^{1/2} \frac{\left[\dfrac{A_1+\mu B_1 + 2(A_2+\mu B_2)\chi^2 s^2_{max}}{(A_2+\mu B_2)\chi^2 s^2_{max}}\right]^{1/2}}{k\left[\dfrac{(A_2+\mu B_2)\chi^2 s^2_{max}}{A_1+\mu B_1 + 2(A_2+\mu B_2)\chi^2 s^2_{max}}\right]} \quad \text{for } A_2+\mu B_2 \geq 0 \tag{D13}$$

$$= \frac{\pi}{2}\left(\frac{2}{m_e}\right)^{1/2} \frac{\left[\dfrac{A_1+\mu B_1 - |A_2+\mu B_2|\chi^2 s^2_{max}}{|A_2+\mu B_2|\chi^2 s^2_{max}}\right]^{1/2}}{k\left[\dfrac{|A_2+\mu B_2|\chi^2 s^2_{max}}{A_1+\mu B_1 - |A_2+\mu B_2|\chi^2 s^2_{max}}\right]} \quad \text{for } A_2+\mu B_2 \leq 0;$$

and since $K(0) = \frac{\pi}{2}$, the zero-energy bounce frequency is

$$\omega_{b0} \equiv \lim_{\substack{\chi\to 0 \\ \mu\to 0}} \omega_b(\chi,\mu) = \left(\frac{2A_1}{m_e}\right)^{1/2} . \tag{D14}$$

The simplest case that shows bounce resonance effects is that of electrons confined by a quadratically varying electrostatic potential

$$\psi(s) = A_1 s^2. \tag{D15}$$

In this case, the bounce frequency expression, Eq. (D13) reduces to

$$\omega_b = \omega_{b0} = \left(\frac{2}{m_e} A_1\right)^{1/2} \tag{D16}$$

for all electrons. The simpler equation for R^e_{mn}, Eq. (67), is then valid, and for the Maxwellian electron distribution, Eq. (D1),

$$\frac{\partial F_e(\chi)}{\partial \chi} = -\frac{2C_e\,\xi\chi}{s_{max}} \exp(-\xi\chi^2) , \tag{D17}$$

where the parameter $\xi \equiv \omega^2_{b0} s^2_{max}/v^2_e$ is given by ψ_{max}/W_e for the quadratic field, Eq. (D15). The integrals then appearing in Eq. (67) are approximated by noting that the maximum potential ψ_{max} in typical mirror devices is greater than W_e by a factor 2 or more. For the nominal value $\psi_{max}/W_e = 4.5$, the exponential factor in Eq. (D17) is less than 0.01, and negligible error is introduced by extending the integration to $\chi = \infty$. The resulting integrals are[62]

$$\int_0^\infty d\chi\ \chi\ \exp(-\xi\chi^2) J_0(\bar{k}\chi) = \frac{1}{2\xi} \exp\left(-\frac{\bar{k}^2}{4\xi}\right), \tag{D18}$$

and

$$\int_0^\infty d\chi\ \chi\ \exp(-\xi\chi^2) J_{2\ell+\sigma}(\bar{k}_m\chi) J_{2\ell+\sigma}(\bar{k}_n\chi) = \frac{1}{2\xi} \exp\left(-\frac{k_m^2+k_n^2}{4\xi}\right) I_{2\ell+\sigma}\left(\frac{\bar{k}_m \bar{k}_n}{2\xi}\right), \tag{D19}$$

where $I_{2\ell+\sigma}$ is a modified Bessel function of the first kind. With Eqs. (D18) and (D19), the R^e_{mn} expression, Eq. (67) yields

$$R^e_{mn} \approx -\frac{1}{2}\left(\frac{\pi}{\xi}\right)^{1/2} \left\{ \exp\left[-\frac{(\bar{k}_m - \bar{k}_n)^2}{4\xi}\right] + (-1)^\sigma \exp\left[-\frac{(\bar{k}_m + \bar{k}_n)^2}{4\xi}\right] - 4 \exp\left(-\frac{\bar{k}_m^2 + \bar{k}_n^2}{4\xi}\right) \sum_{\ell=0}^{\infty} \frac{\omega^2}{\omega^2 - (2\ell+\sigma)^2\, \omega_{b0}^2} I_{2\ell+\sigma}\left(\frac{\bar{k}_m \bar{k}_n}{2\xi}\right) \right\}. \tag{D20}$$

Here, the approximate form $C_e \simeq \left(\pi^{3/2} v_e^3\right)^{-1}$ from Eq. (B10) has been used. In this case, R^e_{mn} is real valued because there is no spread in bounce frequency to attenuate the wave.

When electrons are confined by both the quadratic potential, Eq. (D15), and a quadratically varying B field

$$B(s) = B_0 + B_1 s^2, \tag{D21}$$

the bounce frequency from Eq. (45) becomes

$$\omega_b(\mu) = \left[\frac{2}{m_e}(A_1 + \mu B_1)\right]^{1/2}, \tag{D22}$$

and for the Maxwellian distribution, Eq. (D1),

$$\frac{\partial F_e(\chi,\mu)}{\partial \chi} = -\frac{2C_e (A_1+\mu B_1) s_{max}^2}{W_e} \chi \exp\left[-\frac{\mu B_0 + (A_1+\mu B_1)\chi^2 s_{max}^2}{W_e}\right]$$

$$= - 2C_e \xi\chi \frac{\omega_{b0}^2(\mu)}{\omega_{b0}^2} \exp\left[-\xi\chi^2 - \frac{\mu\left(B_0 + B_1\chi^2 s_{max}^2\right)}{W_e}\right] . \quad (D23)$$

To estimate the real part of R_{mn}^e, the condition

$$\frac{B_1 s_{max}^2}{B_0 \zeta} = \frac{B_{max} - B_0}{B_0} \frac{W_e}{\psi_{max}} << 1 \quad (D24)$$

is imposed. The μ dependence of ω_b then affects R_{mn}^e principally by spreading the bounce-frequency resonances. In the R_{mn}^e expression, Eq. (63), the μ integrals I_1 and I_2 may then be approximated by replacing the nonresonant ω_b factors by ω_{b0}:

$$I_1(\chi) \approx - \frac{2C_e \xi\chi}{\omega_{b0}} \exp(-\xi\chi^2) \int_0^\infty d\mu \exp\left[-\frac{\mu\left(B_0 + B_1\chi^1 s_{max}\right)}{W_e}\right]$$

$$\approx - \frac{C_e m_e \xi\chi}{\omega_{b0}} \frac{v_e^2}{B_0 + B_1\chi^2 s_{max}^2} \exp(-\xi\chi^2), \quad (D25)$$

and

$$I_2(\chi,\ell) \approx - \frac{2C_e \xi\chi}{\omega_{b0}} \exp(-\xi\chi^2) \int_0^\infty d\mu \frac{\exp\left[\frac{-\mu\left(B_0 + B_1\chi^2 s_{max}^2\right)}{W_e}\right]}{1 - \frac{2}{m_e}\left(\frac{2\ell+\upsilon}{\omega}\right)^2 (A_1 + \mu B_1)}$$

$$\approx \frac{C_e m_e \omega^2 \xi\chi}{\omega_{b0}} \frac{\exp(-\xi\chi^2) \exp\left[-\nu_e(0)\right] E_1\left[-\nu_e(0)\right]}{(2\ell+\sigma) B_1} \quad \text{for } 2\ell+\sigma > 1 \quad (D26)$$

$$= I_1(\chi), \quad \text{for } 2\ell+\sigma = 0$$

where

$$\nu_e(\chi) = \frac{B_0 + B_1\chi^2 s_{max}^2}{(2\ell+\sigma)^2 B_1 v_e^2} \left[\omega^2 - (2\ell+\sigma)^2 \omega_{b0}^2\right] ,$$

and E_1 is the complex exponential integral (63)

$$E_1(z) \equiv \int_x^\infty dy \, \frac{\exp(-y)}{y} \quad . \tag{D27}$$

When the inequality in Eq. (D24) is satisfied, the spatial variation of B may be neglected in the integrations of Eq. (66), and the upper integration limits may again be extended to infinity. The integrals then have the same form as Eqs. (D18) and (D19). In this approximation, the real part of R^e_{mn} is

$$R_e\left(R^e_{mn}\right) \approx -\frac{1}{2}\left(\frac{\pi}{\xi}\right)^{1/2}\left\{\exp\left[-\frac{\left(\bar{k}_m-\bar{k}_n\right)^2}{4\xi}\right]+(-1)^\sigma \exp\left[-\frac{\left(\bar{k}_m+k_n\right)^2}{4\xi}\right]\right.$$

$$-4\exp\left(-\frac{\bar{k}_m^2+\bar{k}_n^2}{4\xi}\right)\left[(1-\sigma)I_0\left(\frac{\bar{k}_m\bar{k}_n}{2\xi}\right)+\frac{B_0\zeta}{B_{1_{max}}-B_0}\frac{\omega}{\omega_{b0}^2}\sum_{\ell=1-\sigma}^{\infty}\right.$$

$$\left.\left.\frac{\exp\left[-\nu_e(0)\right]E_i\left[\nu_e(0)\right]I_{2\ell+\sigma}\left(\frac{\bar{k}_m\bar{k}_n}{2\xi}\right)}{(2\ell+\sigma)^2}\right]\right\}, \tag{D28}$$

where $E_i(x) = -\mathrm{Re}\left[E_1(-x)\right]$ is the real exponential integral defined by Eq. (E4). The imaginary part of R^e_{mn} comes only from the singularity in I_2 and may be evaluated without the restriction of Eq. (D24). Whenever the I_2 singularity

$$\mu_\ell = \frac{m_e}{2B_1}\frac{\omega^2-(2\ell+\sigma)^2\omega_{b0}^2}{(2\ell+\sigma)^2} \tag{D29}$$

occurs on the positive μ axis, ω is assumed to have an infinitesimal positive imaginary part to satisfy causality. Since the real axis integration path in I_2 then passes beneath the singularity, the imaginary contribution is

$$\mathrm{Im}\left[I_2(\chi,\ell)\right] = -\frac{\pi C_e m_e}{B_1}\frac{\xi\chi}{2\ell+\sigma}\frac{\omega}{2\ell+\sigma}\exp(-\xi\chi^2)\exp\left[-\frac{\mu_\ell\left(B_0+B_1\chi^2 s^2_{max}\right)}{W_e}\frac{1}{B_1}\right]. \tag{D30}$$

Extending the χ integration limit in Eq. (63) to infinity again gives as integral with the form of Eq. (D19) and leads to

$$\mathrm{Im}\left(R^{e}_{mn}\right) \approx -\, 2\pi^{3/2}\, \frac{B_0\, \xi}{B_{max}-B_0} \sum_{\ell=1-\sigma}^{\ell_{res}} \exp\left(\frac{\bar{k}_m^2+\bar{k}_n^2}{\xi_\ell}\right) \frac{\exp\left[-\nu_\ell(0)\right]\; I_{2\ell+\sigma}\left(\frac{\bar{k}_m \bar{k}_n}{2\xi_\ell}\right)}{\xi_\ell^{1/2}}\,, \qquad \text{(D31)}$$

where

$$\xi_\ell \equiv \frac{\omega^2}{(2\ell+\sigma)^2 \omega_{b0}^2}\, \xi\,,$$

and ℓ_{res} is the largest integer giving a positive μ_ℓ.

The effect on R^{e}_{mn} of a slightly nonquadratic potential is seen when B is given by Eq. (D21), and the potential is taken to have a quartic form

$$\psi(s) = A_1 s^2 + A_2 s^4\,. \qquad \text{(D32)}$$

If the further condition

$$A_1 \gg 2A_2\, s_{max}^2$$

is imposed, then the elliptic integral series expansion

$$k^{-2}(x) = \left[\frac{\pi}{2}\left(1 + \frac{x}{4} + \frac{9}{64}\, x^2 + \ldots\right)\right]^{-2} \approx \frac{4}{\pi^2}\left(1 - \frac{x}{2} - \frac{3}{32}\, x^2 + \ldots\right)$$

(D33)

may be used in the bounce frequency expression, Eq. (D13), and leads to the result

$$\omega_b^2(\chi,\mu) = \frac{2}{m_e}\left(A_1 + \mu B_1 + \frac{3}{2} A_2 \chi^2 s_{max}^2\right) + O(\chi^4)\,. \qquad \text{(D34)}$$

The quartic potential term acts principally to further alter bounce-frequency resonances. In evaluating the real part of R^{e}_{mn}, the approximate forms of the μ integrals I_1 and I_2 given by Eqs. (D25) and (D26) remain valid provided ν_ℓ is redefined

$$\nu_\ell(\chi) = \frac{B_0 + B_1\chi^2 s_{max}^2}{(2\ell+\sigma)^2 B_1 S_{max}^2}\left[\omega^2 - (2\ell+\sigma)^2\left(\omega_{b0}^2 + \frac{3A_2\chi^2 s_{max}^2}{m_e}\right)\right]. \quad \text{(D35)}$$

This alteration makes the singularity at $\nu_\ell = 0$ in Eq. (D26) integrable and shifts the peak of the resonant factor $\exp(-\nu_\ell)E_1(\nu_\ell)$ in frequency by about $\frac{3}{2}\left(A_2 s_{max}^2/m_e\,\omega_{b0}^2\right)\langle\chi^2\rangle$. If the condition in Eq. (D24) is again assumed satisfied, then the $\mathrm{Re}(R_{mn}^e)$ approximation for the nonquadratic potential becomes identical to Eq. (D28) in lowest order. The imaginary part of R_{mn}^e for the slightly nonquadratic potential is obtained in the same way as the $A_2=B_2=0$ case. The singularity in I_2 then occurs at

$$\mu_\ell(\chi) = \frac{m_e}{2B_1}\,\frac{\omega^2 - (2\ell+\sigma)^2\left(\omega_{b0}^2 + \frac{3A_2\chi^2 s_{max}^2}{m_e}\right)}{(2\ell+\sigma)^2}. \quad \text{(D36)}$$

If μ_ℓ is positive for all $\chi^2 \le 1$, then when χ^4 terms are neglected, the $\mathrm{Im}(R_{mn}^e)$ expression becomes formally identical to Eq. (D31) with ζ_ℓ redefined

$$\xi_\ell = \left(\frac{\omega^2}{(2\ell+\sigma)^2\omega_{b0}^2} - \frac{B_0}{B_{max}-B_0}\,\frac{3A_2 s_{max}^2}{m_e\,\omega_{b0}^2}\right)\zeta. \quad \text{(D37)}$$

In this approximation, the quartic potential term affects electron damping both by changing the magnitude of R_{mn}^e through the $\xi_\ell^{-1/2}$ factor in Eq. (D31) and by determining through the Bessel function argument which matrix element is dominant. When μ_ℓ from Eq. (D37) is negative for some ℓ values less than unity, the χ integration in Eq. (66) must be limited to the range giving $\mu_\ell > 0$, and the resulting $\mathrm{Im}(R_{mn}^e)$ expression is more complicated than Eq. (D31).

An analytic estimate of ion response matrix elements R_{mn}^i is obtained by evaluating $I(k_1,k_2,j)$ defined by Eq. (97). The strongest ion interaction for even modes is expected when $\omega=j\Omega_{i0}$ in the integral and the oscillatory exponential factors involving k_1 and k_2 are unity. In this approximation, the remaining integral is

$$I(k_1,k_2,j) \sim \int_0^\infty dz \frac{1}{(ij\Delta\Omega z)^{1/2}\left(1 + \frac{ij\Delta\Omega}{12} v_n^2 z^3\right)^{1/2}}$$

$$\sim \frac{1}{i\ (j\Delta\Omega)^{1/2}\left(\frac{j\Delta\Omega v_n}{12}\right)^{1/6}} \int_0^\infty dy \frac{1}{y^{1/2}(1 - y^3)^{1/2}} . \quad \text{(D38)}$$

If a path along the real axis is chosen, the integral in Eq. (D34) splits immediately into real and imaginary parts.

$$\int_0^\infty dy \frac{1}{y^{1/2}(1 - y^3)^{1/2}} = \int_0^1 dy \frac{1}{y^{1/2}(1 - y^3)^{1/2}} - i \int_1^\infty dy \frac{1}{y^{1/2}(y^3 - 1)^{1/2}}$$

(D39)

By using the beta-function relation[64]

$$B(\alpha,\beta) \equiv \int_0^1 dy\ y^{\alpha-1}\ (1-y)^{\beta-1} = \frac{\Gamma(\alpha)\Gamma(\beta)}{\Gamma(\alpha+\beta)} ,$$

the integrals in Eq. (D39) are immediately evaluated:

$$\int_0^1 dy \frac{1}{y^{1/2}(1-y^3)^{1/2}} = \frac{1}{3} \int_0^1 dw\ w^{-5/6}(1-w)^{-1/2} = \frac{1}{3} B\left(\frac{1}{6},\frac{1}{2}\right) , \quad \text{(D40)}$$

$$= 2.43$$

and

$$\int_1^\infty dy \frac{1}{y^{1/2}(y^3-1)^{1/2}} = \frac{1}{3} \int_0^1 dw\ w^{-2/3}(1-w)^{-1/2} = \frac{1}{3} B\left(\frac{1}{3},\frac{1}{2}\right)$$

$$= 1.40, \quad \text{(D41)}$$

For a quadratically varying B field

$$\Delta\Omega \equiv \frac{1}{2}\left(\frac{\partial^2\Omega_1}{\partial s^2}\right)_{s=0} = \frac{\Omega_{i0}}{s_{max}^2} \frac{B_{max} - B_0}{B_0} . \quad \text{(D42)}$$

Eq. (D38) may then be written

$$I(k_1,k_2,j) \sim \left(\frac{B_0}{B_{max}-B_0}\ \frac{s_{max}^2}{j\Omega_{i0}}\right)^{2/3}\left(\frac{12}{V_n^2}\right)^{1/6}(1.40 - 2.43\ i), \qquad \text{(D43)}$$

and from Eq. (94) the corresponding response matrix elements are

$$R_{mn}^{i} \sim -\frac{\pi^{1/2}}{2}\ \Lambda_j\ \frac{W_e}{W_i}\left(\frac{12j^2\Omega_{i0}^2 s_{max}^2}{V_n^2}\right)^{1/6}\left(\frac{B_0}{B_{max}-B_0}\right)^{2/3}(2.43 - 1.40\ i), \qquad \text{(D44)}$$

Since the integrand of Eq. (D38) neglects oscillatory factors, the magnitude of Eq. (D44) is an upper bound on $|R_{mn}^{i}|$ calculated from the complete quasi-local expression, Eq. (94).

Appendix E. Evaluation of R^i_{mn} and R^e_{mn}

The integrals in the response matrix expressions, Eqs. (65) and (97), have singular integrands that require careful treatment in numerical evaluation.

The integral in R^e_{mn} is calculated along the real μ axis, and when frequency ω is real, the resonant factor is singular at positive values μ_ℓ satisfying

$$\omega = (2\ell+\sigma)\omega_b(\chi,\mu_\ell). \tag{E1}$$

In this case, the singularity is removed by adding an integrable term that cancels the singularity at $\mu=\mu_\ell$ and subtracting the analytic integral of that new term. Near μ_ℓ, a Taylor expansion of ω_b^2 gives

$$\omega_b^2(\chi,\mu) \approx \frac{\omega^2}{(2\ell+\sigma)^2} + \left(\frac{\partial\omega_b^2}{\partial\mu}\right)_{\mu=\mu_\ell}\left[\mu-\mu_\ell(\chi)\right] . \tag{E2}$$

The singular term of the μ integral is then formally rewritten

$$\int_0^\infty d\mu\, G_{\ell mn}(\chi,\mu)\,\frac{\omega^2}{\omega^2-(2\ell+\sigma)^2\omega_b^2(\chi,\mu)}$$

$$\approx \int_0^\infty d\mu\, \exp[-\nu(\chi,\mu)]\left\{ G_{\ell mn}(\chi,\mu)\,\frac{\omega^2}{\omega^2-(2\ell+\sigma)^2\omega_b^2(\chi,\mu)} + \frac{G_{\ell mn}\left[\chi,\mu_\ell(\chi)\right]}{(2\ell+\sigma)^2\left(\frac{\partial\omega_b^2}{\partial\mu}\right)_{\mu=\mu_\ell}\left|\mu-\mu_\ell(\chi)\right|}\right\}$$

$$- \frac{B(\chi s_{max})}{W_e}\frac{G_{\ell mn}\left[\chi,\mu_\ell(\chi)\right]}{(2\ell+\sigma)^2\left(\frac{\partial\omega_b^2}{\partial\mu}\right)_{\mu=\mu_\ell}} \exp\left[-\nu_\ell(\chi)\right]\left\{E_1\left[\nu_\ell(\chi)\right] - i\,\pi\right\}, \tag{E3}$$

where

$$G_{\ell mn}(\chi,\mu) \equiv \frac{1}{\omega_b(\chi,\mu)}\,\frac{\partial F_e(\chi,\mu)}{\partial\chi}\,T_{\ell m}(\chi,\mu)\,T_{\ell n}(\chi,\mu)\,\exp[\nu(\chi,\mu)] ,$$

$$\nu(\chi,\mu) = \frac{\mu B}{W_e}(\chi s_{max}) ,$$

and

$$\nu_\ell(\chi) = \nu\left[\chi, \mu_\ell(\chi)\right] .$$

The final term in Eq. (E3) is the integral of the added μ integrand term, the principal value being the real exponential integral[63]

$$E_1(x) = -\int_{-x}^{\infty} dy \, \frac{\exp(-y)}{y} \quad , \tag{E4}$$

and the $i\pi$ term being the residue contribution at μ_ℓ. In performing the integration along the real μ axis, the contour has been deformed so that μ is always below μ_ℓ, and therefore $\mathrm{Im}(\omega)>0$ as required by causality. Near μ_ℓ the integrand in Eq. (E3) goes to a constant value

$$\frac{-\exp\left[-\nu_\ell(\chi)\right]}{(2\ell+\sigma)^2} \left[\frac{\partial G_{\ell mn}(\chi,\mu)}{\partial\mu}\right]_{\mu=\mu_\ell} \left[\frac{\partial \omega_b^2(\chi,\mu)}{\partial\mu}\right]^{-1}_{\mu,\mu_\ell} ,$$

so the integral may be evaluated by standard numerical techniques. The function S_{mn} has no singularities and may likewise be integrated conventionally over μ.

The exponential integral in Eq. (E3) introduces a logarithmic singularity at values of χ where μ_ℓ vanishes. To integrate the term over χ, the integral is written as a sum of subintegrals, each of which is approximated analytically. If the quantity

$$\mu_{\ell mn}(\chi) \equiv \frac{B(\chi s_{max})}{W_e} \frac{G_{\ell mn}\left[\chi, \mu_\ell(\chi)\right]}{(2\ell+\sigma)^2 \left(\frac{\partial \omega_b}{\partial \mu}\right)_{\mu=\mu_\ell}} \tag{E5}$$

is treated as a slowly varying function of χ, the required integral is written

$$I_{\ell mn} = \int_0^1 d\chi \, H_{\ell mn}(\chi) \exp\left[-\nu_\ell(\chi)\right] \left\{E_i\left[\nu_\ell(\chi)\right] - i\pi\right\}$$

$$= \sum_{j=1}^{J} H_{\ell mn}(\chi_j) \int_{\chi_j^-}^{\chi_j^+} d\chi \exp\left[-\nu_\ell(\chi)\right] \int_{-\nu_\ell(\chi)}^{\infty} dy \, \frac{\exp(-y)}{y} , \tag{E6}$$

where χ_j are midpoints of the intervals $\Delta^j\chi$ bounded by points $\chi_j^{\pm} = \chi_j \pm \frac{\Delta^j\chi}{2}$, and the exponential integral factor has been replaced by a complex integral. Using ν_ℓ as an integration variable and integrating Eq. (E6) by parts then gives

$$I_{\ell mn} \simeq - \sum_{j=1}^{J} \frac{H_{\ell mn}(\chi_j)}{\left(\frac{\partial \nu_\ell}{\partial \chi}\right)_{\chi=\chi_j}} \left\{ \exp(-y)\left[E_i(y) - i\pi\right] - \frac{\ln(y)}{y} \right\}_{\nu_\ell\left(\chi_j^-\right)}^{\nu_\ell\left(\chi_j^+\right)} . \qquad \text{(E7)}$$

Here the ν_ℓ derivative has been assumed to be slowly varying over $\Delta^j\chi$. The μ integrals of S_{mn} and the first term of Eq. (E3) are both smooth functions of χ and may be approximated by trapezoidal rule integration. If the intervals $\Delta^j\chi$ are taken equal to the step size $\Delta\chi$ used for numerical integration, then R^e_{mn} from Eq. (65) may be written

$$R^e_{mn} \simeq \frac{\pi^2 v_e^2 B_o}{m_e s_{max}} \sum_{j=1}^{J} \left\{ \sum_{\ell=1}^{\infty} \left[I_{\ell mn}(\chi_j) + w_j II_{\ell mn}\left(\chi_j^+\right) \right] + w_j III_{mn}\left(\chi_j^+\right) \right\} , \qquad \text{(E8)}$$

where

$$I_{\ell mn}(\chi) \equiv \frac{B(\chi s_{max})}{W_e} \frac{G_{\ell mn}\left[\chi, \mu_\ell(\chi)\right]}{(2\ell+\sigma)^2 \left(\frac{\partial \omega_b}{\partial \mu}\right)_{\mu=\mu_\ell} \left(\frac{\partial \nu_\ell}{\partial \chi}\right)_{\chi=\chi_j}}$$

$$\left\{ \frac{\ln(y)}{y} - \exp(-y)\left[E_i(y) - i\pi\right] \right\}_{\nu_\ell\left(\chi - \frac{\Delta\chi}{2}\right)}^{\nu_\ell\left(\chi + \frac{\Delta\chi}{2}\right)} ,$$

$$II_{\ell mn}(\chi) \equiv \int_0^{\infty} d\mu \, \exp\left[-\nu(\chi,\mu)\right] \left\{ \frac{\omega^2 G_{\ell mn}(\chi,\mu)}{\omega^2 - (2\ell+\sigma)^2 \omega_b^2(\chi,\mu)} + \frac{G_{\ell mn}\left[\chi, \mu_\ell(\chi)\right]}{(2\ell+\sigma)^2 \left(\frac{\partial \omega_b^2}{\partial \mu}\right)_{\mu=\mu_\ell} \left[\mu - \mu_\ell(\chi)\right]} \right\} ,$$

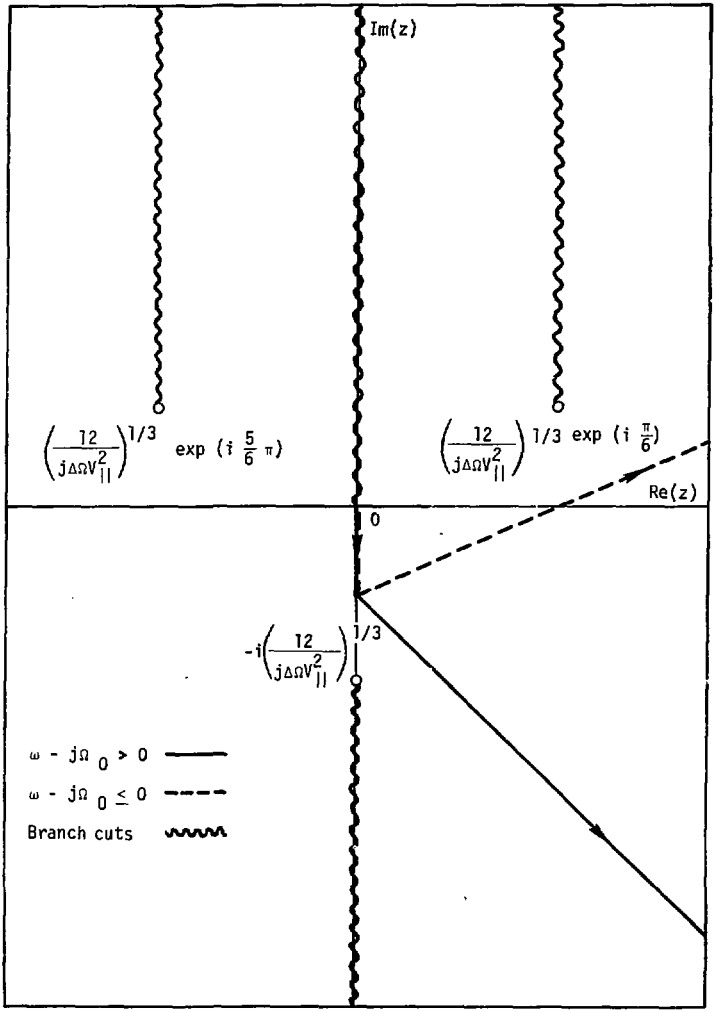

Fig. E-1. Integration path for $I(k_1,k_2,j)$.

$$III_{mn}(\chi) = \int_0^\infty d\mu \frac{1}{\omega_b(\chi,\mu)} \frac{\partial F_e(\chi,\mu)}{\partial \chi} S_{mn}(\chi,\mu) ,$$

and

$$w_j = \Delta\chi \qquad j < J$$
$$= \frac{1}{2}\Delta\chi \qquad j = J .$$

Here the weight factors w_j are correct for trapezoidal rule integration with $II_{lmn} = III_{lmn} = 0$ at $\chi = 0$. In practice, the leading factor in I_{lmn} is approximated at χ_j by linear interpolation between values at χ_j^+ and χ_j^-.

The ion response matrix R^i_{mn} requires evaluation of complex integrals $I(k_1,k_2,j)$ and $II(k_m,k_n,j)$ given respectively by Eqs. (95) and (98). For $I(k_1,k_2,j)$, an integration path in the complex z plane is chosen that avoids all integrand singularities. From Eq. (95) there are several considerations governing choice of a contour:

- For large $|z|$, Im(z) should have the same sign as $\omega - j\Omega_{i0}$.
- As $|z| \to 0$, z should approach the negative real axis so that the exponential in Eq. (95) is strongly damped and nonoscillatory.
- The three singularities at $z = (-ij\Delta\Omega v_n^2/12)^{-1/3}$ should be avoided.

Appropriate paths for $\omega - j\Omega_{i0}$ greater and less than zero are shown in Fig. E-1. The angle either path makes with the positive real z-axis is selected to give the integrand a large negative real exponential factor for large $|z|$. $I(k_1,k_2,j)$ is then evaluated by numerical integration of the real and imaginary parts of the integrand along the complex z path, and integration is terminated when the integrand has become sufficiently small. The approximate criterion for convergence of the integral is

$$\min\left[\frac{Im(z)}{\omega - j\Omega_{i0}} , \frac{1}{2}\left(\frac{j\Delta\Omega v_n^2}{12}\right)^{1/3} z\right] > 10. \qquad (E9)$$

Because the plasma dispersion function is analytic, the integral $II(k_m,k_n,j)$ is evaluated by numerical integration of the real and imaginary parts along the positive s-axis.

Appendix F. Evaluation of S_{mn} and T_{lm}

The orbit integrals S_{mn} and T_{lm} defined respectively by Eqs. (57) and (52) are unsuited for efficient numerical evaluation. Positions along a field line must be calculated as a function of time, and since the integrands have a sinusoidal position dependence, the appropriate time step for integration changes considerably as parallel velocity $v_{\parallel}$ approaches zero near the orbit turning point. Even though the numerical integration routine used[43] adjusts the step size automatically, extra integrand evaluations are needed.

It is convenient to replace t by a variable

$$x = \left[\chi - s(t;\chi,\mu)/s_{max}\right]^{1/2},$$

where χ is the dimensionless turning point $s_t(E,\mu)/s_{max}$ that is used instead of energy E in evaluating R^{e}_{mn}. In terms of x, the orbit integrals are written

$$S_{mn}(\chi,\mu) = -\frac{8\omega_b(\chi,\mu)s_{max}}{\pi}\int_0^{\chi^{1/2}} dx\, \frac{x}{|v_{\parallel}[s(x);\chi,\mu]|}\, sc\left[k_m s(x)\right] sc\left[k_n s(x)\right], \quad (F1)$$

and

$$T_{\ell m}(\chi,\mu) = -\frac{8\omega_b(\chi,\mu)s_{max}}{\pi}\int_0^{\chi^{1/2}} dx\, \frac{x}{|v_{\parallel}[s(x);\chi,\mu]|}\, sc\left[(2\ell+\sigma)\omega_b(\chi,\mu)t(x;\chi,\mu)\right] sc\left[k_m s(x)\right], \quad (F2)$$

where

$$t(x;\chi,\mu) = -2s_{max}\int_0^{x} dx'\, \frac{x'}{|v_{\parallel}[s(x');\chi,\mu]|}, \quad (F3)$$

$$s(x) = (\chi - x^2)s_{max}, \quad (F4)$$

and

$$v_{\parallel}^2(s;\chi,\mu) = \frac{2}{m_e}\left\{\mu\left[B(\chi s_{max}) - B(s)\right] + \psi(\chi s_{max}) - \psi(s)\right\}. \quad (F5)$$

The bounce frequency is calculated as a function of χ and μ using Eq. (F3):

$$\omega_b(\chi,\mu) = \frac{\pi}{2t(0;\chi,\mu)} \quad . \tag{F6}$$

Since both x^2 and $v_\parallel^2$ vanish linearly with position as $s \to s_t$, the $x/|v_\parallel|$ factor in Eqs. (F1), (F2), and (F3) approaches a finite value near the turning point. The integrands are consequently nonsingular as desired.

References

1. C. C. Damm, J. H. Foote, A. H. Futch, Jr., A. L. Hunt, K. G. Moses, and R. F. Post, *Phys. Rev. Lett.* 24, 495 (1970).
2. J. G. Cordey, G. Kuo-Petravic, E. G. Murphy, M. Petravic, D. R. Sweetman, and E. Thompson, "Ion Cyclotron Instabilities and the Effect of Microwave Heating in the Phoenix II Magnetic Well," in *Proc. Third IAEA Conf. Plasma Physics and Controlled Nuclear Fusion Research, Novosibirsk,* 1968 (IAEA, Vienna, 1969), Vol. II, p. 267.
3. J. H. Foote, *Instability-Threshold Data from the Baseball II Vacuum-Buildup Experiment,* Lawrence Livermore Laboratory, Rept. UCID-16664 (1974).
4. J. D. Jukes, *Rep. Prog. Phys.* 30, 333 (1967).
5. Yu B. Gott, M. S. Ioffe, and B. G. Telkovsky, *Sov. J. At. Energy* 14, 495 (1964).
6. J. D. Jukes, *Rep. Prog. Phys.* 32, 305 (1968).
7. M. N. Rosenbluth, "Microinstabilities," in *Plasma Physics* (IAEA, Trieste, 1964), p. 485.
8. A. J. Lichtenberg, *Phase Space Dynamics of Particles* (John Wiley & Sons, Inc., New York, 1969), p. 230.
9. A. J. Lichtenberg, op. cit., p. 33.
10. L. D. Landau, *Sov. Phys.-JETP* 16, 574 (1946).
11. I. B. Bernstein, *Phys. Rev.* 109, 10 (1958).
12. E. G. Harris, *Phys. Rev. Lett.* 2, 34 (1959).
13. E. G. Harris, *Plasma Phys.* 2, 138 (1961).
14. L. S. Hall, W. Heckrotte, and T. Kammash, *Phys. Rev.* 139, 1117 (1965).
15. R. F. Post and M. N. Rosenbluth, *Phys. Fluids* 9, 730 (1966).
16. G. E. Guest and R. A. Dory, *Phys. Fluids* 8, 1853 (1965); *Phys. Fluids* 11, 1775 (1968).
17. J. G. Cordey, *Phys. Lett.* 23, 228 (1966).
18. J. Heading, *An Introduction to Phase Integral Methods* (John Wiley & Sons, Inc., New York, 1962), p. 25.
19. H. L. Berk, *Phys. Fluids* 14, 1036 (1971).
20. M. N. Rosenbluth and R. F. Post, *Phys. Fluids* 8, 547 (1965).
21. H. L. Berk, C. W. Horton, M. N. Rosenbluth, and R. N. Sudan, *Phys. Fluids* 10, 2003 (1967).

22. G. W. Hamilton and R. W. Moir, *Conditions for Landau Damping and Wave Reflection in Open-Ended Magnetic Well Plasmas*, Lawrence Radiation Laboratory, Rept. UCRL-50900 (1970).
23. J. G. Cordey, *Phys. Fluids* 14, 1407 (1971).
24. D. E. Baldwin, *Phys. Rev. Lett.* 18, 1119 (1967).
25. H. L. Berk, C. W. Horton, and M. N. Rosenbluth, *Phys. Fluids* 11, 365 (1968).
26. H. L. Berk and D. L. Book, *Phys. Fluids* 12, 649 (1968).
27. J. G. Cordey, *Phys. Fluids* 12, 1506 (1969).
28. E. S. Weibel, *Phys. Fluids* 3, 399 (1960).
29. K. J. Harker, *Phys. Fluids* 8, 1846 (1965).
30. A. N. Kaufman, *Phys. Fluids* 13, 956 (1970).
31. A. N. Kaufman, *Phys. Fluids* 14, 387 (1971).
32. C. O. Beasley, Jr., W. M. Farr, and H. Grawe, *Phys. Fluids* 13, 2563 (1970).
33. J. E. McCune, *Landau Damping for Electrostatically Confined Electrons*, Oak Ridge National Laboratory, Rept. ORNL-TM-3970 (1972).
34. C. O. Beasley, Jr., H. R. Hicks, W. M. Farr, and J. E. McCune, *Nucl. Fusion* 14, 191 (1974).
35. N. A. Krall, in *Advances in Plasma Physics* (John Wiley & Sons, Inc., New York, 1968), Vol. 1, p. 153.
36. A. B. Mikhailovskii, *Sov. Phys.-Doklady* 11, 603 (1967).
37. D. E. Baldwin, C. O. Beasley, Jr., H. L. Berk, W. M. Farr, R. C. Harding, J. E. McCune, L. D. Pearlstein, and A. Sen, "Loss-Cone Modes in Inhomogeneous Mirror Machines," in *Proc. Fourth IAEA Conf. Plasma Physics and Controlled Nuclear Fusion Research, Madison, WI*, 1971 (IAEA, Vienna, 1971), Vol. II, p. 735.
38. D. E. Baldwin, *Phys. Fluids* 17, 1346 (1974).
39. G. N. Watson, *Theory of Bessel Functions, 2nd ed.* (University Press, Cambridge, 1952), p. 22.
40. Reference (39), p. 40.
41. H. L. Berk and L. D. Pearlstein, *Phys. Fluids* 14, 1810 (1971).
42. B. D. Fried and S. D. Conte, *The Plasma Dispersion Function* (Academic Press, New York, 1961), p. 1.
43. A. C. Hindmarsh, *GEAR: Ordinary Differential Equation System Solver*, Lawrence Livermore Laboratory, Rept. UCID-30001 (1974).
44. R. P. Dickinson, Jr., F. N. Fritsch, R. F. Hausman, Jr., and R. F. Sincovec, *Eispack User's Guide*, Lawrence Livermore Laboratory, Rept. UCID-30077 (1973).

45. C. C. Damm, J. H. Foote, A. H. Futch, Jr., R. K. Goodman, F. J. Gordon, A. L. Hunt, K. G. Moses, and J. E. Osher, "ALICE Plasma Experiments," in *Controlled Thermonuclear Research Report, July 1968 Through June 1969*, Lawrence Radiation Laboratory, Rept. UCRL-50002-69 (1969), p. 39.

46. C. C. Damm, J. H. Foote, A. H. Futch, Jr., R. K. Goodman, F. J. Gordon, A. L. Hunt, R. G. Mallon, K. G Moses, J. E. Osher, R. F. Post, and J. E. Steinhaus, "Dependence of Ion Cyclotron Instabilities on Particle Distribution Functions in the ALICE Experiment," in *Proc. Third IAEA Conference of Plasma Physics and Controlled Nuclear Fusion Research, Novosibirsk, 1968* (IAEA, Vienna, 1969), Vol. II, p. 253.

47. O. A. Anderson, D. H. Birdsall, C. C. Damm, J. H. Foote, A. H. Futch, Jr., R. K. Goodman, F. J. Gordon, G. W. Hamilton, E. B. Hooper. A. L. Hunt, J. E. Osher, and G. D. Porter, "Plasma Production and Confinement in the Baseball II Mirror Experiment," in *Proc. Fifth Conf. on Plasma Physics and Controlled Nuclear Fusion Research, Tokyo, 1974* (IAEA, Vienna, 1975), Vol. I, p. 379.

48. R. F. Post, *Phys. Fluids* 4, 902 (1961).

49. D. J. BenDaniel, *Plasma Phys.* 3, 235 (1961).

50. L. Spitzer, Jr., *Physics of Fully Ionized Gases, 2nd ed.* (John Wiley & Sons, Inc., New York, 1962), p. 135.

51. J. H. Foote, Lawrence Livermore Laboratory, private communication, 1975.

52. J. H. Foote, *Calculated Ion-Density Spatial Distribution in Alice Baseball I*, Lawrence Radiation Laboratory, Rept. UCID-15647 (1970).

53. H. L. Berk, L. D. Pearlstein, and J. G. Cordey, *Phys. Fluids* 15, 891 (1972).

54. F. H. Coensgen, J. F. Clauser, D. L. Correll, W. F. Cummins, C. Gormezano, B. G. Logan, A. W. Molvik, W. E. Nexsen, T. C. Simonen, B. W. Stallard, and W. C. Turner, *Status of 2XIIB Plasma Confinement Experiments*, Lawrence Livermore Laboratory, Rept. UCID-17037 (1976).

55. F. H. Coensgen, *MX Major Project Proposal*, Lawrence Livermore Laboratory, Rept. LLL-PROP-142 (1976).

56. D. E. Baldwin, *Low Frequency Electron Oscillations in Bounded Plasmas*, Lawrence Livermore Laboratory, Rept. UCID-15546 (1969).

57. B. B. Kadomstsev and O. P. Pogutse, *Nucl. Fusion* 11, 67 (1971).

58. M. Abramowitz and I. A. Stegun, Eds., *Handbook of Mathematical Functions* (National Bureau of Standards, Washington, D. C., 1967).

59. J. D. Jackson, *Classical Electrodynamics* (John Wiley & Sons, Inc., New York, 1967), pp. 611-621.
60. Reference (60), p. 260.
61. Reference (60), p. 360.
62. I. S. Gradshteyn and I. M. Ryzhik, *Table of Integrals, Series, and Products* (Academic Press, New York, 1965) pp. 717-718.
63. Reference (60), p. 228.
64. Reference (60), p. 258.

CKM/gw/vt